PHOSPHORYLATION-INDUCED CONFORMATIONAL CHANGES OF PTEN REVEALED BY PROTEIN SEMISYNTHESIS

by

David Michael Bolduc

A dissertation submitted to Johns Hopkins University in the conformity with the requirements for the degree of Doctor of Philosophy

Baltimore, Maryland

October 2013

Abstract

PTEN (phosphatase and tensin homolog deleted on chromosome 10) is a tumor suppressing lipid phosphatase that negatively regulates the PI3K/PTEN/AKT signaling pathway by dephosphorylating the lipid second messenger PIP_3. PTEN is one of the most frequently mutated genes in cancer and loss of PTEN function is found in many cancer types. There are a variety of mechanisms within cells by which PTEN is regulated. One mode of regulation is through a cluster of phosphorylations on PTEN's C-terminal regulatory tail at amino acids Ser380, Thr382, Thr383 and Ser385. Phosphorylation of this cluster has been proposed to reduce PTEN's ability to bind to membranes and access its substrate, though the exact mechanism by which this occurs is poorly understood. To study the regulatory affects of phosphorylation at this regulatory cluster we have employed expressed protein ligation to generate semisynthetic PTEN in its phosphorylated and unphosphorylated forms.

Using a variety of biochemical and biophysical techniques we have found that relative to its unphosphorylated form, phosphorylated PTEN binds to phospholipid membranes with lower affinity which results in a decrease in its catalytic activity. This decrease in membrane binding ability and catalytic activity is accomplished through a phosphorylation induced conformational change in the PTEN protein. When phosphorylated, the C-terminal tail of PTEN binds to the

membrane binding surface of the C2 domain, thereby reducing PTEN's ability to interact with membranes and access its substrate.

Thesis Readers: Philip A. Cole, M.D. Ph.D., Sandra B. Gabelli, Ph.D.

To my family, my friends and my advisor, without whom this never would have been possible.

Acknowledgements

Thesis Advisor: Phillip A. Cole, M.D. Ph.D.

Thesis Reader: Sandra B. Gabelli, Ph.D.

Thesis Committee Members: L. Mario Amzel, Ph.D., Peter N. Devreotes, Ph.D., Daniel M. Raben Ph.D.

Collaborators: Meghdad Rahdar, Ph.D., Becky Tu-Sekine, Ph.D., Sindu Carmen Sivakumarin

Colleagues: Mary-Katherine Tarrant Connacher, Ph.D., Kannan Karukurichi, Ph.D., David Meyers, Ph.D., Marc Holbert, Ph.D., Young-Hoon Ahn, Ph.D., You Sang Hwang, Ph.D., Rong Huang, Ph.D., Beverly Dancy, Ph.D., Blair Dancy, Ph.D., Isabel Ferrando, Ph.D., Zan Chen, Shonoi Ming, Ph.D., Zhihong Wang, Ph.D., Yun Wang, Ph.D., Robert Hsiao, Polina Prusevich, Meng-Jung Chang, Dominic Figueroa, Jay Kalin, Ph.D., Yan Sun Ph.D.

Support Staff: Robin Hart, Amy Paronto, Amy Forcier, Mimi Guercio, Brenda Figueroa, Paula Mattingly, Frank Williams

Table of Contents

List of Tables

List of Figures

Chapter 1: Introduction

Signal Transduction and Phosphorylation

Signal transduction is the process by which the cell relays signals and information from the exterior environment to the interior of the cell. These signaling events allow the cell to integrate and process a variety of complex external signals simultaneously[1]. The culmination of signaling events results in some response by the cell. Such responses include but are not limited to: cell growth, differentiation, death, migration, gene expression and the release of hormones and other signaling molecules[1,2]. Often times signal transduction is an extremely complex process, involving hundreds of proteins and multiple signaling pathways. One example of this complex signaling process is observed in the cell's response to growth factors. Growth factors bind to receptors on the cell surface where their signal must be transduced through the plasma membrane, relayed through the cytosol and eventually signal to the nucleus to affect gene expression[3]. Other times the signaling process is much simpler and only involves a small number of proteins. One such example is the response to lipid soluble hormones which can freely pass through the plasma membrane to bind nuclear receptors which directly bind their gene responsive elements to modulate gene expression[4].

Signal transduction within the cell can be mediated by a variety mechanisms including protein binding events, second messenger signaling (i.e.

Ca^{2+}, IP_3, PIP_3, ROS) and posttranslational modifications (i.e. phosphorylation, acetylation, ubiquitination)[1]. One of the most extensively studied posttranslational modifications in signal transduction is phosphorylation. Protein phosphorylation in eukaryotes is the attachment of a phosphate group to the hydroxyl of a serine, threonine or tyrosine amino acid[1,2,5,6]. Phosphorylation can also occur on molecules involved in signal transduction other than proteins such as lipids (i.e. phosphatidylinositols)[7]. Phosphorylation is dynamic and reversible. The attachment of a phosphate is catalyzed by kinases while its removal is catalyzed by phosphatases. There are over 500 protein kinases (~400 serine/threonine, ~100 tyrosine) and over 100 protein phosphatases[8–10]. Adding to the complexity of signaling events, many protein kinases and phosphatases are redundant. Different kinases can have the same substrate and different phosphatases can have the same substrate[5,6]. Additionally, many kinases and phosphatases also have more than one substrate[5,6,11].

Phosphorylation of proteins allows for signal transduction to proceed by causing changes in protein activity, cellular localization, stability or protein binding interactions[1,2,5]. Binding interactions altered by phosphorylation can be *in trans* (a binding event between two different proteins) or *in cis* (a binding event within a single protein)[12]. There are a number of phospho serine/threonine and phospho-tyrosine binding domains responsible for recruiting proteins to their phosphorylated binding partners. They include: WW, 14-3-3, FHA, BRCT and

PBD domains for phospho-serine and phospho-threonine[13] and SH2 and PTB for phospho-tyrosine[14,15].

Phosphoinositide Signaling

Phosphatidylinositol is a lipid signaling molecule that can be phosphorylated multiple times on the 3'-, 4'- and/or 5'-position of the inositol ring generating different phosphatidylinositol phosphates (PIPs)[7] (Figure 1). In all, there are 7 known phosphorylation variants of phosphatidylinositol modulated by ~20 phosphoinositide kinases and ~30 phosphoinositide phosphatases[16] (Figure 1). PIPs regulate a variety of different cellular events such as cellular migration, signaling, cytoskeletal rearrangements, adhesion and membrane trafficking[7,16,17]. The different signaling outcomes depend on which phospho-form of phosphatidylinositol is generated. The PIPs can recruit a variety of different proteins via their phosphatidylinositide phosphate sensing domains. Some of these domains include PH, ENTH, FYVE and PHOX domains[7]. PH domains can be specific for binding $PI(3,4)P_2$, $PI(4,5)P_2$ or $PI(3,4,5)P_2$[7].

Dysregulation of phosphotidylinositide phosphate signaling has been implicated in a number of pathologies including cancer, diabetes and several neurological disorders[7,16]. The two most well studied phosphatidylinositide regulators are the kinase PI3K and phosphatase PTEN due to their frequent

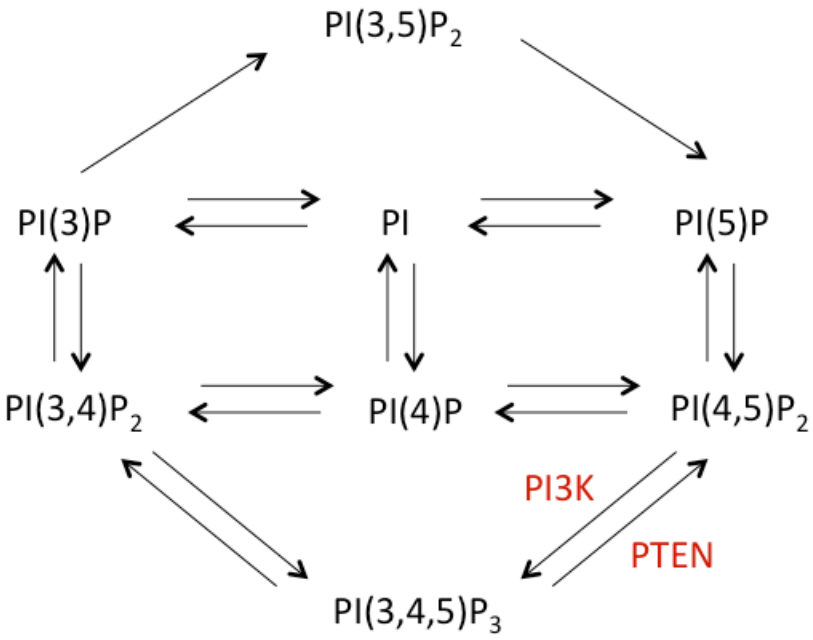

Figure 1: Phosphoinositide metabolism. There are a total of seven different phosphorylated forms of phosphotidylinositide phosphates (PIPs) generated from phosphotidylinositide (PI). There are approximately 20 phosphoinositide kinases and 30 phosphatases responsible for the maintenance of these PIPs. Two of the most well studied phosphoinositide enzymes are the kinase PI3K and the phosphatase PTEN shown in red.

mutation and regulatory roles in cancer. These two proteins oppose each other's actions. PI3K phosphorylates the 3'-position of $PI(4,5)P_2$ generating $PI(3,4,5)P_3$ while PTEN removes the 3'-phosphate from $PI(3,4,5)P_3$ generating $PI(4,5)P_2$[3].The generation of cellular $PI(3,4,5)P_3$ is essential for activating the PI3K/PTEN/AKT signaling pathway.

The PI3K/PTEN/AKT Signaling Pathway

One signaling pathway central to the subsequent chapters of this thesis is the PI3K/PTEN/AKT signaling pathway (Figure 2). This signaling pathway has been the subject of extensive study due to the high frequency of mutation of many of this pathway's proteins in cancer[3,18–21]. Initiation of this pathway occurs when a growth factor (i.e. EGF, IGF-1, PDGF) binds to a receptor tyrosine kinase (i.e. EGFR, IGF-1R, PDGFR) leading to its dimerization and activation. Dimerization and activation of the receptor tyrosine kinases cause autophosorylation of tyrosine residues on the intracellular domain of the protein. Phosphorylation of the tyrosine residues allows for the recruitment of SH2 domain containing proteins. PI3K is recruited to the receptor tyrosine kinase via its SH2 domain containing p85 regulatory subunit. This allows for the activation of PI3K and subsequent phosphorylation of its lipid substrate PIP_2, converting it to PIP_3. PIP_3 serves as a second messenger, recruiting the kinase AKT via its PH domain. Once recruited to the plasma membrane AKT is phosphorylated and activated by other kinases including PDK1 and the mTORC2 complex. Activated

AKT can then phosphorylate a variety of downstream substrates. Some of the downstream targets of AKT include: mTOR[22–24], MDM2[25,26], p27[27,28], p21[29,30] and FOXO[31,32]. The overall effects of AKT activation are increases in cell growth, proliferation, invasiveness and resistance to apoptosis[3,18–20]. The lipid phosphatase PTEN serves as a key negative regulator in this pathway. PTEN dephosphorylates PIP_3, thereby preventing the activation of AKT and downstream signaling to promote cell proliferation, growth and survival[33,34].

Due to the pro-growth, proliferation and invasiveness induced by the activation of the PI3K/PTEN/AKT signaling pathway, it is unsurprising that many of the components of this pathway are frequently targeted by mutations in cancer[3,18–20]. By accumulating gain of function mutations in positive regulators of the pathway and loss of function mutations in negative regulators of the pathway, the PI3K/PTEN/AKT signaling pathway can remain in the “on” state unchecked by normal cellular regulatory mechanisms. This gives cancer cells the selective advantage they need to grow, proliferate and infiltrate other tissues. Of all the proteins in this pathway the single most mutated gene is PTEN[35,36]. This will be discussed in detail in later sections. Several kinases are also targeted by gain of function mutations. Receptor tyrosine kinases (such as EGFR), PI3K and AKT have all been found to contain mutations that lead to constitutive activation of their enzymatic activity[3,18,20,37]. Additionally gene amplification has been found to increase protein levels of these oncogenic kinases[3,18].

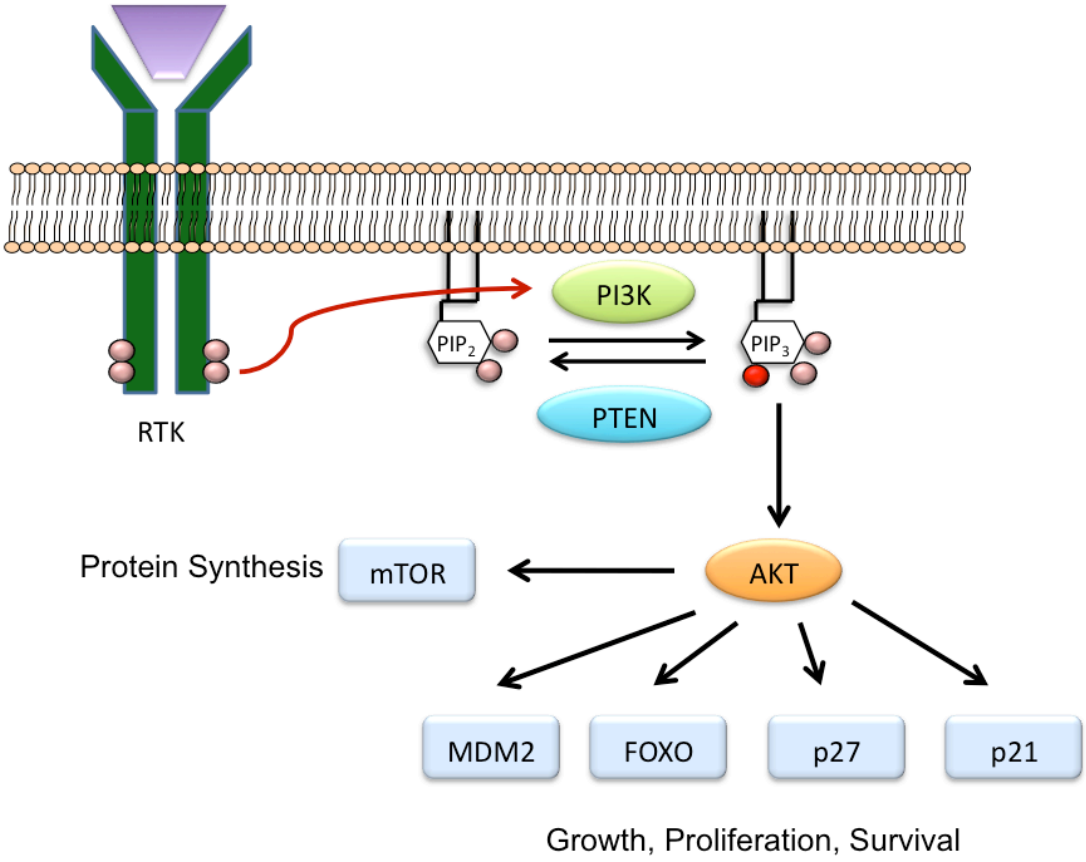

Figure 2: The PI3K/PTEN/AKT signaling pathway. In response to growth factor binding, receptor tyrosine kinases (RTKs) dimerize, leading to their activation and autophosphorylation at intracellular tyrosine residues. PI3-Kinase is recruited to the phospho-tyrosine residues of activated RTKs via its SH2 domain containing regulatory subunit p85 where is phosphorylates the lipid PIP_2, generating PIP_3. PIP_3 recruits the kinase AKT to the plasma membrane where it is activated and phosphorylates downstream targets which in turn promote cell growth, proliferation, invasiveness and resistance to apoptosis. PTEN turns off this pathway by dephosphorylating PIP_3.

Because of the high frequency of mutation of the PI3K/PTEN/AKT pathway in a number of different cancer types, billions of dollars have been funneled into developing drugs to inhibit this pathway by the pharmaceutical industry[37]. There are currently a number of FDA approved drugs targeting the receptor tyrosine kinase EGFR including trastuzumab, gefitinib and erlotinib that have prolonged the lives of cancer patients[38,39]. Although there are currently no FDA approved drugs targeting PI3K or AKT, there are dozens of drugs targeting these kinases currently being explored as potential therapeutics[40–47].

Phosphatases

There are approximately 150 known phosphatases[8,9]. They can be grouped into two main categories based on substrate recognition and mechanism of dephosphorylation. The first group is the family of serine/threonine protein phosphatases that are responsible for dephosphorylating serine/threonine residues of which there are about 40 members[9]. They will not be discussed further. The second group is the family of protein tyrosine phosphatases (PTPs) which dephosphorylate tyrosine residues[8]. There are just over 100 members of this family. The family of PTPs also contains a group of dual specificity protein tyrosine phosphatases (DUSPs) which can dephosphorylate serine/threonine and tyrosine residues[10].

Nearly all PTPs and DUSPs employ a similar mechanism of catalysis which involves a nucleophilic cysteine[8,48]. One exception to this rule is the Eya family of PTPs which use a nucleophilic aspartate[49]. In addition to the nucleophilic cysteine, PTPs and DUSPs also have a conserved arginine and aspartate. The cysteine and arginine are located on the P-loop within the active site of the phosphatase with a conserved CX_5RT/S motif[48]. The arginine and backbone N-H groups of the P-loop are responsible for binding and stabilizing the substrate phosphate group. The reaction mechanism acts through a phospho-enzyme intermediate. The nucleophilic cysteine attacks the phosphate group on the substrate, displacing the $^{-}O\text{-}R_1$ group as the aspartate acts as a general acid to protonate the leaving group. The aspartate then acts as a general base to deprotonate a water molecule as it hydrolyzes the phospho-enzyme intermediate and regenerates the free cysteine[48] (Figure 3).

Phosphatidylinositol Phosphatases

There are about ~30 phosphoinositide phosphatases capable of dephosphorylating the 3'-, 4'- or 5'- position of the inositol ring[7,16]. Some of these proteins can also dephosphorylate protein targets but have evolved primarily to modulate PIP signaling. 3'- and 4'- phosphoinositide phosphatases are all

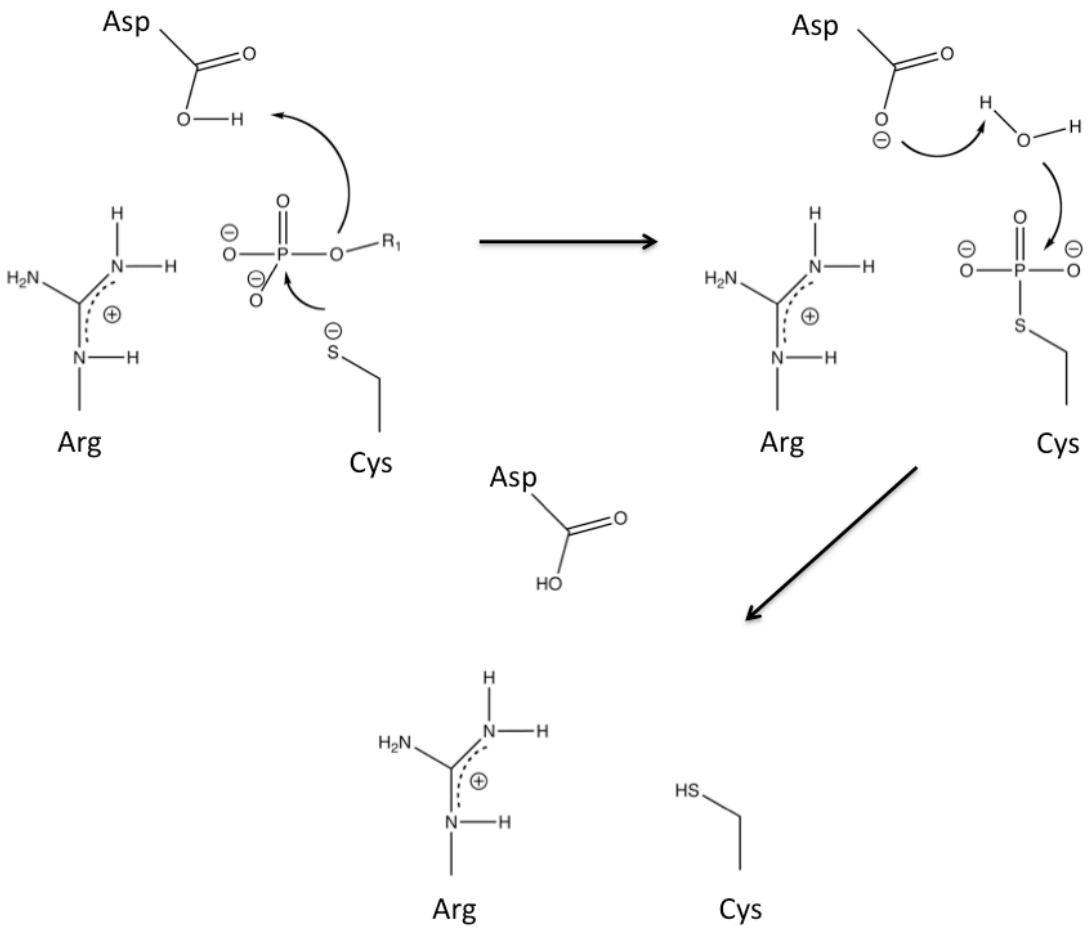

Figure 3: Protein tyrosine phosphatase reaction mechanism. The reaction mechanism acts through a phospho-enzyme intermediate where the nucleophilic cysteine attacks the phosphate group of the substrate, displacing the $^{-}O\text{-}R_1$ group as the aspartate acts as a general acid to protonate the leaving group. The aspartate then acts as a general base to deprotonate a water molecule as it hydrolyzes the phospho-enzyme intermediate and regenerates the free cysteine.

members of the DUSP family of phosphatases discussed in the previous section and all utilize a catalytic cysteine[7]. Well known members of this group include PTEN and myotubularins. 5'-phosphoinositide phosphatases have a mechanism distinct from DUSPs. Though the enzymatic mechanism is not completely understood, they contain two well conserved amino acid sequences: GD(L/F)N(F/Y)R and P(A/S)(W/Y)(C/T)DR(I/V)(L/I). These proteins also contain a fold similar to magnesium dependent endonucleases and require divalent cations for catalysis[7,16,50]. Well-known members of the 5' phosphoinositide phosphatase family are SHIP1 and SHIP2.

PTEN and Cancer

PTEN (phosphatase and tensin homolog deleted on chromosome 10) is a tumor suppressing lipid phosphatase that negatively regulates the PI3K/PTEN/AKT signaling pathway by dephosphorylating the lipid second messenger PIP_3[33,34]. PTEN was originally discovered in 1997 when deletion mapping of chromosome 10 identified a potential tumor suppressor at the 10q23 locus[36]. This gene was found to have sequence identity to a dual specificity protein tyrosine phosphatase and tensin, an actin filament binding protein[51]. This newly discovered gene was later named PTEN. The same year PTEN was discover it was found to be inactivated in a number of sporadic tumor types of the brain, breast and prostate[52]. It was also found to be targeted in germline mutations of individuals with cancer predisposition syndromes such as Cowden

disease[53,54]. PTEN knockout mice were found not to be viable[55]. Heterozygous deletion of PTEN in mice causes an increase in tumor formation[56,57]. In contrast to the “two-hit” model of cancer formation where two or more mutations must accumulate in proto-oncogenic or tumor suppressor genes in order tumors to form, PTEN’s ability to suppress tumor formation is thought to be dosage dependent[35,58]. In this continuum model of tumor suppression, the protein and/or activity level of PTEN is proportionately related to its ability to prevent a neoplastic transformation without the necessity of there being mutations in other key regulatory genes.

PTEN was found to be capable of dephosphorylating highly acidic synthetic peptide substrates *in vitro* though no physiologically relevant protein substrates could be identified[52]. It was later found to be able to efficiently dephosphorylate the phospholipid PIP_3 and that this activity was responsible for PTEN’s tumor suppressive ability *in vivo*[3,33,34,59]. By dephosphorylating PIP_3, PTEN prevents the activation of AKT and its downstream signaling to promote cell growth, proliferation and survival. Although the lipid phosphatase activity is the primary tumor suppressive function of PTEN, there is also a clear tumor suppressive function for nuclear localized PTEN that appears to be independent of its phosphatase activity[60–62]. The exact mechanism of this function is poorly understood though recent reports suggest that PTEN associates with CDH1 and the anaphase promoting complex (APC) causing an increase in genomic stability and chromosomal integrity[61]. Breast cancer patients with nuclear localized PTEN

have a much better prognosis that those without nuclear PTEN[35]. Additionally tumors lacking for nuclear PTEN are more aggressive than those containing nuclear PTEN[35,62].

Cancers target PTEN for inactivation by a variety of mechanisms including: allelic or complete gene deletion, gene silencing through promoter methylation and chromatin remodeling, miRNA mediated transcript reduction and loss of function point mutations[35,63–67]. Sequencing of the PTEN gene from patient tumors has demonstrated that point mutations are abundant at nearly every amino acid position other than its C-terminal tail (Figure 4). The highest frequency of mutation occurs within the catalytic pocket of PTEN with the mutation of catalytically essential arginine-130 being the most abundant. Other hotspots of mutation include proposed membrane binding surfaces and amino acids at the interface between the phosphatase and C2 domains. PTEN is one of the most frequently mutated genes in all cancers. Only the tumor suppressor p53 is thought to be mutated at a higher frequency[35]. Loss of PTEN function has been identified in cancers of the breast[52,68–71], endometrium[72–75], thyroid[76–78], prostate[79–82], brain[52,83,84], skin[85,86], lung[87,88], liver[89,90], bladder[91,92] and pancreas[75,93] demonstrating just how important PTEN's tumor suppressive ability is for normal cell and organism function.

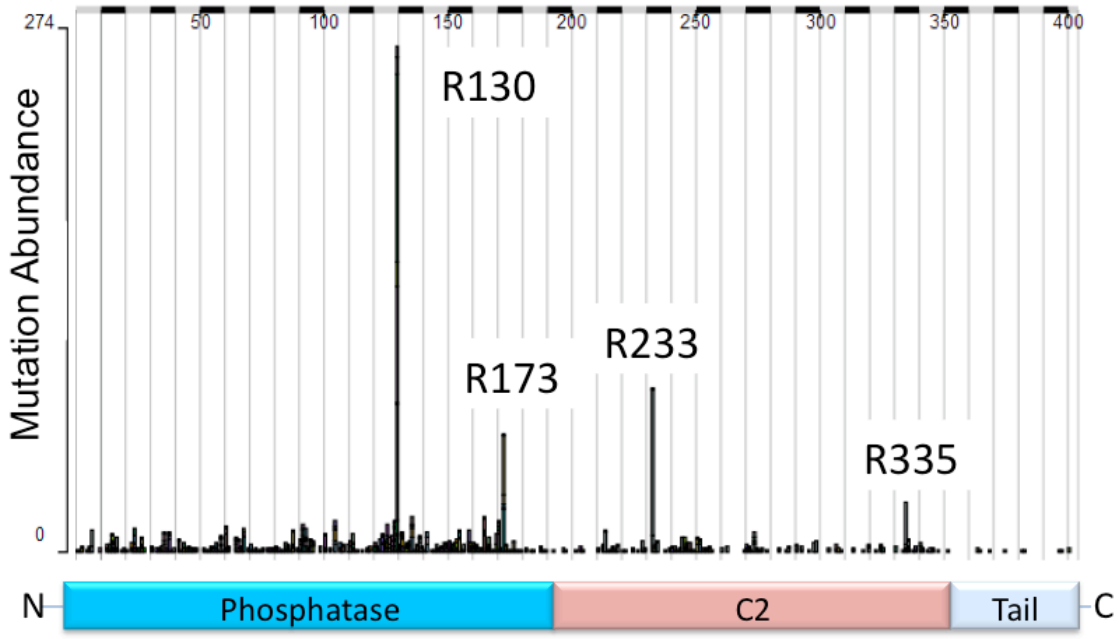

Figure 4: Common PTEN mutations. PTEN is frequently targeted by point mutations. Hotspot mutations are found within the catalytic pocket, on membrane binding surfaces and within the interface between the phosphatase and C2 domains. The histogram was taken from the COSMIC (catalog of somatic mutations in cancer) database (http://cancer.sanger.ac.uk/cancergenome/projects/cosmic, July 10, 2013).

The Structure of PTEN

PTEN is a 403 amino acid protein comprised of an N-terminal phosphatase domain, a C2 domain and a C-terminal 52 amino acid tail. A crystal structure of PTEN's core (phosphatase and C2 domains) was determined in 1999[51]. Three portions of the PTEN gene had to be omitted from the protein in order for crystals to form presumably due to their flexibility. The three segments that were deleted from the PTEN amino acid sequence, were a portion of the N-terminus (aa 1-6), an internal loop of the C2 domain termed the D-loop (aa 286-309) and the entire C-terminal tail (aa 352-403). The crystal structure with the approximate positioning of the deleted regions is shown in Figure 5.

The phosphatase domain of PTEN consists of six alpha helices surrounding a central beta sheet[51]. It shares structural similarity to the DUSP VHR. The active site of this domain contains the signature P-loop of DUSPs with the conserved CX_5RT/S sequence. The active site is deeper and larger than most DUSPs, presumably allowing it to accommodate the large head group of PIP_3. PTEN's mechanism of PIP_3 hydrolysis follows the same mechanism of all DUSPs. The nucleophilic cysteine-124 and substrate stabilizing arginine-130 of the P-loop are essential for catalysis[94]. Additionally, aspartate-92 of the adjacent WPD loop serves as a general acid to protonate the leaving group during hydrolysis of PIP_3[94]. Unique to PTEN and its homologs is the placement of lysine residues within the P-loop and on adjacent strands that serve to bind and stabilize the highly negatively charged substrate PIP_3[51].

The C2 domain of PTEN forms a beta sandwich composed of two antiparallel beta sheets. The C2 domain shares structural similarity to the C2 domains of PLCδ1, PKCδ, and phospholipase A2; though unlike the C2 domains of these proteins it does not bind calcium[51]. Two loops on what is thought to be the membrane binding surface of the C2 domain are highly positively charged with multiple lysine and arginine residues on each loop. These two loops are the Cα2 and the CBRIII loops[51].

Both the phosphatase domain and C2 domain have been proposed to be important for the membrane binding ability of PTEN. In particular, the amino acids 1-15 have been suggested to specifically recruit PTEN to the plasma membrane and bind the phospholipid PIP_2[95–98]. Deletion of these amino acids abrogates PTEN's ability to bind membranes. The CBRIII loop of the C2 domain is also a crucial membrane binding surface. It has been implicated in binding to phosphatidylserine and other lipids embedded in membranes[51,99].

The interface between the phosphatase and C2 domains of PTEN buries a total surface area of 1400 $Å^2$ and has many hydrophobic and hydrogen bonding interactions[51]. Mutations of several of the amino acids at the interface have been found in various cancers. In fact, two of the top eight PTEN mutations found in cancer are located at this interface[51]. This suggests that the structural integrity of interface between the two domains is necessary for proper PTEN function and its tumor suppressive ability. It also suggests that subtle perturbations in one of the domains may result in structural changes in the other.

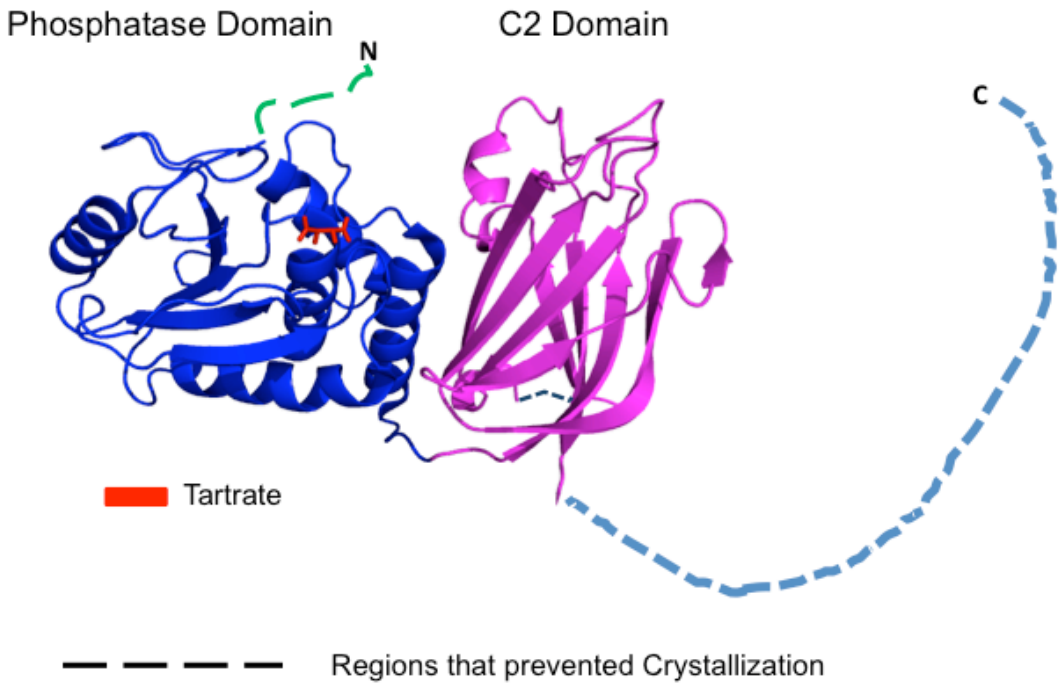

Figure 5: The partial crystal structure of PTEN. The crystal structure of PTEN contains a globular phosphatase (blue) and C2 (magenta) domain in tight junction with each other. Omitted from the crystal structure is the presumably flexible N-terminus (green, aa 1-6), internal D-loop (brown, aa 286-309) of the C2 domain and C-terminal tail (light blue, aa 352-403).

The C-terminal tail of PTEN is 52 amino acids in length and contains two PEST (proline, glutamate, serine and threonine) sequences and a PDZ interaction motif at amino acids 399-403. The tail is highly acidic, consisting of 15 aspartate and glutamate residues that are clustered mostly to the final 25 amino acids of the tail. The C-terminal tail can be phosphorylated at several positions by multiple kinases including casein kinase 2 (CK2) and glycogen synthase kinase 3 beta (GSK3β)[100,101]. These phosphorylations regulate a variety of PTEN functions that will be discussed in subsequent sections.

PTEN Regulation

PTEN function has been proposed to be regulated by a variety of mechanisms within cells. Gene expression is regulated at the level of transcription through promoter methylation[102–104] and by a number of transcription factors including SALL4[105], SNAIL[65], p53[66], CBF1[67] and c-JUN[106,107] amongst others. PTEN transcript levels are modulated by miRNA[64]. The PTEN protein is subject to a number of posttranslational modifications including phosphorylation[100,101,108–110], acetylation[111], sumoylation[112] and ubiquitiylation[113–117]. Like many members of the dual specificity protein tyrosine phosphatase family, PTEN can be inactivated by reactive oxygen species and disulfide bridge formation between its catalytic cysteine and another conserved cysteine residue

within its phosphatase domain[118]. As alluded to previously, PTEN is also acutely regulated by the lipid composition of membranes; it is particularly affected by the presence of the lipids PIP_2 and phosphatidylserine[95,96,119]. Additionally PTEN function can be modulated by other proteins. Some of the proteins PTEN has been proposed to interact with *in vivo* are p85[120–122], neutral endopeptidase[123], mysosin V[124] and MAGI2[125]. PTEN can also be regulated by its subcellular localization. There are at least three major subcellular areas where PTEN is located: the cytoplasm, the plasma membrane and the nucleus. PTEN's nuclear localization is promoted by monoubiquitylation while polyubiquitylation leads to its proteasome mediated degradation[113,114,116,117].

Phosphorylation of PTEN

Phosphorylation of PTEN is one of the most well characterized forms of PTEN regulation. PTEN can be phosphorylated at a number of different sites on its C2 domain and C-terminal tail (Figure 6). The C2 domain can be phosphorylated at amino acids Ser229, Thr232, Thr319 and Thr321 by the kinase RHOA associated protein kinase (ROCK)[126,127] and at Tyr336 by the protein kinase Rak[128]. The 52 amino acid C-terminal tail has been shown to be phosphorylated at amino acids Ser363, Thr366, Ser370, Ser380, Thr382, Thr383 and Ser385 by the kinases casein kinase 2 (CK2) and glycogen synthase kinase 3 beta (GSK3β)[100,101,108–110,129].

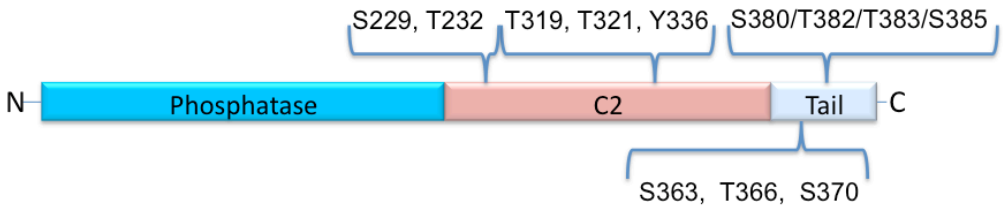

Figure 6: PTEN phosphorylation sites. PTEN can be phosphorylated on its C2 domain and C-terminal regulatory tail. The C2 domain can be phosphorylated at amino acids Ser229 and Thr321 by the kinase RHOA associated protein kinase (ROCK) and at Tyr336 by the protein kinase RAK. The C-terminal tail can be phosphorylated at Ser363, Thr366, Ser370, Ser380, Thr382, Thr383 and Ser385 by the kinases CK2 and GSK3β.

Phosphorylation at Ser229, Thr232, Thr319 and Thr321 by ROCK has been proposed to activate PTEN through unknown mechanisms[126,127]. In a predominantly cell biology based study, it was demonstrated that the GTPase RhoA may enhance PTEN membrane localization and phosphatase activity in leukocytes[127]. The ability of RhoA to regulate PTEN dependent reduction of AKT signaling was shown to be dependent on the kinase activity of ROCK (RhoA associated protein kinase) which is regulated by RhoA. ROCK is capable of phosphorylating PTEN *in vitro* and these phosphorylation sites were identified through mass spec analysis of cell lysates as being Ser229, Thr232, Thr319 and Thr321[127]. How these phosphorylation modifications might regulate PTEN activity remains to be determined. All four phosphorylation sites are located to non-membrane binding surfaces of the C2 domain of PTEN. Phosphorylation of these sites could alter PTEN's interaction with an unknown regulatory protein or could affect PTEN's catalytic activity directly. Given that these modifications are on the C2 domain it seems unlikely that could affect the activity of the phosphatase domain, though it is possible that subtle conformational changes in the C2 domain could be transmitted allosterically to the phosphatase domain. Alternatively these phosphorylation sites could promote an interaction between PTEN and a positive regulator of PTEN function or they could relieve some form of inhibition mediated by either a secondary protein or by PTEN itself. Certainly

additional biochemical work is necessary to elucidate the mechanism by which ROCK regulates PTEN by phosphorylation of its C2 domain.

Kim et al. has demonstrated that the protein tyrosine kinase Rak (a member of the Src family of kinases) co-immunoprecipitates with PTEN and is capable of phosphorylating PTEN at Tyr336[128]. This may lead to an increase in the cellular stability of PTEN as determined by comparing wild type PTEN to the unphosphorylatable Y336F mutant in pulse chase experiments. Here the mutant was significantly less stable than wild type. Additionally, Rak protein levels positively correlated with PTEN's stability and inhibitory affects on AKT signaling[128]. One confusing aspect about this study is that Tyr336 is located on the Cα2 loop of the C2 domain, which is known to be important for membrane binding. In the crystal structure of PTEN, Tyr336 juts out from the membrane binding surface of the C2 domain and would appear to be a key point of contact between PTEN and the plasma membrane. If phosphorylated, it seems likely that Tyr336 would interfere with membrane binding given that PTEN is known to selectively bind anionic membranes. This study did not examine the membrane binding ability or activity of PTEN. One of the E3 ubiquitin ligases for PTEN is NEDD4-1[62,113,114]. This protein is thought to be active at the plasma membrane. If phosphorylation of Tyr336 does prevent PTEN's membrane association, this may provide a mechanism by which the stability of PTEN is enhanced by Tyr336 phosphorylation by spatially separating PTEN from its E3 ligase within the cell.

Additional biochemical and cell based experiments would be necessary to determine this.

The most abundant sites of phosphorylation on PTEN are on its C-terminal tail[101,108]. Mass spectrometry and biochemical studies have demonstrated that PTEN is phosphorylated at amino acids Ser363, Thr366, Ser370, Ser380, Thr382, Thr383 and Ser385 by the kinases casein kinase 2 (CK2) and glycogen synthase kinase 3 beta (GSK3β)[100,101,108–110,129]. The physiological ramifications of phosphorylation at Ser363, Thr366 and Ser370 are poorly understood. Phosphorylation at the Ser380/Thr382/Thr383/Ser385 cluster has been the subject of much research and is likely a key regulator of PTEN function.

Using pulse chase experiments Maccario and coworkers demonstrated that phosphorylation of Thr366 by GSK3β may destabilize PTEN[130]. In this study they show that the unphosphorylatable T366A mutant is less stable than wild type. The mechanism by which phosphorylation of Thr366 leads to a decrease in PTEN stability remains unknown. Additionally, this study demonstrated that phosphorylation at S370 by CK2α primes for phosphorylation of Thr366 by GSK3β.

Phosphorylation at the Ser380/Thr382/Thr383/Ser385 cluster is mediated primarily by CK2 though GSK3β may also phosphorylate these amino acids to a minor extent[100,101,108,110,129]. These phosphorylation sites were identified primarily

by mass spectrometry. By using mutational analysis of PTEN constructs transfected into γ-[^{32}P] orthophosphate treated cells, Torres et al. found that mutation of Ser385 to Ala caused a large reduction in total phosphorylation of the tail of PTEN[131]. This suggests Ser385 may prime for phosphorylation of Ser380/Thr382/Thr383. This same study estimated that about four mol of phosphate where incorporated into one mol of PTEN protein following *in vitro* phosphorylation with CK2[131]. It is thought that the majority of cellular PTEN protein is constitutively phosphorylated at this cluster under most conditions, though the exact fraction of phospho-PTEN is unknown. There is a smaller pool of PTEN that is not phosphorylated at this cluster and the two pools of PTEN may have distinct cellular functions[110]. The ratio of phospho- to unphospho-PTEN may vary based on cell type with CK2 activity levels likely being a determining factor.

Few conditions have been discovered that modulate the level of phosphorylation at the Ser380/Thr382/Thr383/Ser385 cluster. To our knowledge only example of PTEN being rapidly phosphorylated in response to some signal is observed with the treatment of pancreatic beta cells with leptin[132–134]. In this example phosphorylation of the Ser380/Thr382/Thr383/Ser385 cluster increases several fold within five minutes and is reduced with near basal levels after 1 hour[134]. No conditions have been identified that lead to rapid dephosphorylation of PTEN. The tail of PTEN does not undergo dephosphorylation after the treatment of cells with growth factors[131]. Additionally no phosphatase has been

found to dephosphorylate PTEN though there are reports of PTEN possessing weak autophosphatase activity *in vitro*[135]. It is likely that there is a cellular phosphatase responsible for dephosphorylating PTEN given that levels of phosphorylated PTEN are reduced in less than half an hour in the leptin example discussed above and that the half of life of phosphorylated PTEN is thought to be roughly 24 hours (discussed below)[129,134]. Under most conditions it may be that CK2 and the unknown phosphatase are responsible for keeping some equilibrium level of phosphorylated PTEN. Identification of this phosphatase may lead to a better understanding of how PTEN is regulated within cells.

Mutation of the Ser380/Thr382/Thr383/Ser385 cluster to the tetra-alanine mutant which cannot be phosphorylated leads to changes in PTEN's cellular localization and stability[109,129,131]. WT PTEN is located predominantly to the cytoplasm while the tetra-alanine mutant is located primarily to the plasma membrane and to the nucleus (Figure 7). The mechanisms by which phosphorylation changes PTEN's cellular localization are poorly understood. Both changes in PTEN's conformation and ability to interact with different cellular proteins have been suggested to affect PTEN's interaction with the plasma membrane[109,110,136,137].

It has been proposed that phosphorylation of the Ser380/Thr382/Thr383/Ser385 cluster causes a conformational change in PTEN[109,137]. In this model PTEN exists in a "closed" conformation when phosphorylated that prevents it from binding to the plasma membrane and

accessing its substrate. When unphosphorylated, PTEN is in a more active "open" conformation where it can bind the plasma membrane. The evidence for this model has been provided by cell based co-immunoprecipitation experiments in which the PTEN molecule was expressed as two fragments that were shown to co-immunoprecipitate with each other only when the Ser380/Thr382/Thr383/Ser385 cluster was wild type and not mutated to the tetra-alanine S380A/T382A/T383A/S385A mutant[109]. While it is conceivable that what was occurring in these assays was a direct binding interaction between the two PTEN fragments, it is possible that the interaction was being mediated by another cellular protein that was also being immunoprecipitated as part of a complex with the two PTEN fragments. There are a number of proteins that have been proposed to bind to PTEN in a phosphorylation dependant manner including neutral endopeptidase[123], MAGI2[125], p85[120–122] and myosin V[124]. Neutral endopeptidase, MAGI2 and p85 are all found either embedded in the plasma membrane or associated with it[123,125,136]. Additionally, unphosphorylated PTEN has been shown to immunoprecipitate within a high molecular weight complex that contains p85 in addition to a number of unknown proteins[110,136].

In addition to increased plasma membrane localization, mutation of the Ser380/Thr382/Thr383/Ser385 cluster to alanine also causes increased PTEN localization in the nucleus[62,109]. The signal for PTEN's translocation from the cytosol to the nucleus is thought to be mono-ubiquitination[62,113,115,116]. The tetra-alanine mutant is also significantly less stable than WT[100,129], and is quickly

degraded by the proteasome. Taken together this suggests phosphorylation of the tail of PTEN prevents its ubiquitination though the exact mechanism is unknown. It is also unclear what determines whether PTEN is mono-ubiquitinated and targeted to the nucleus or poly-ubiquitinated and targeted for degradation by the proteasome.

The relative stability of the tetra alanine mutant compared to wild type was determined by pulse chase experiments[100,129,131]. Here, it was determined that wild type PTEN has a half live greater than 24 hours while the tetra alanine mutant has a half life of about 9 hours. While it is likely that the absence of phosphorylation is the primary cause of PTEN's reduced cellular stability, it is conceivable that mutation of the cluster rather than the absence of phosphorylation is the cause of destabilization of the PTEN protein. Phosphorylation of PTEN could influence its cellular stability by a number of different mechanisms including: causing a conformational change that prevents its interaction with an E3 ubiquitin ligase, changing PTEN's cellular localization and therefore its ability to interact with an E3 ubiquitin ligase localized specifically to a subcellular compartment or by influencing PTEN's ability to interact with other binding partners which indirectly affect PTEN's stability.

Several reports have suggested that PTEN can inhibit cell migration in a lipid phosphatase independent manner[138–140]. A mutation (G129E) has been identified in the catalytic pocket of PTEN that eliminates PTEN's lipid phosphatase activity but maintains its ability to dephosphorylate synthetic poly-

EpY peptides[34]. Published in 2004, Raftopoulou et al. found that microinjection of plasmids expressing wild type PTEN in cells was equally as effective at inhibition of cell migration in a scratch assay as plasmids expressing the G129E as well as the C2 domain of PTEN alone[138]. However, catalytically dead PTEN (C124S) could not inhibit cell migration. Interestingly mutation of Thr383 on the tail of PTEN to alanine allowed for the C124S mutant to inhibit cell migration equally as well as wild type, not only suggesting that the phosphorylated tail of PTEN is inhibiting its ability to prevent cell migration but also tying together the protein phosphatase activity of PTEN to the phosphorylation state of its tail[138]. There were two main conclusions from this study: 1) the C2 domain of PTEN contributes to its ability to inhibit cell migration in a lipid phosphatase independent manner; 2) the protein phosphatase activity of PTEN may be required for dephosphorylation of its tail. Interestingly only the mutation of Thr383 but not Ser380, Thr382 or Ser385 to alanine prevented that tail's autoinhibitory effects. Although this report suggests PTEN directly dephosphorylates pThr383, it is unclear if the catalytic activity of PTEN somehow influences another phosphatase that is directly responsible for dephosphorylating the tail of PTEN.

One recurring theme used to study PTEN phosphorylation has been comparing phosphorylatable, wild type PTEN to the tetra alanine unphosphorylatable PTEN mutant. The majority of the reports examining PTEN phosphorylation have been cell based; with no thorough biochemical studies of purified, site-specifically phosphorylated PTEN. The work of this thesis is

Figure 7: Localization of WT versus A4 PTEN. PTEN WT at the S380/T382/T383/S385 phospho cluster is located mostly to the cytoplasm. PTEN with the S380/T382/T383/S385 phospho cluster mutated to the tetra alanine S380A/T382A/T383A/S385A mutant (A4) is located predominantly to the plasma membrane and the nucleus.

concerned with obtaining a detailed understanding as to how phosphorylation of the Ser380/Thr382/Thr383/Ser385 cluster regulates PTEN's basic biophysical and biochemical properties in the context of an intact PTEN molecule containing a known phosphorylation state. To accomplish this we have employed expressed protein ligation to generate semisynthetic PTEN in its phosphorylated and unphosphorylated forms.

Expressed Protein Ligation

Expressed protein ligation (EPL) is a chemical ligation technique that allows for the native chemical ligation between the N-terminus of synthetically derived peptides and the C-terminus of recombinant proteins that contain an intein generated thioester[141]. EPL can be used for a variety of purposes including the labeling of proteins with flourophores and other tags, isotopic labeling of protein domains, synthesis of cytotoxic proteins, cyclization of proteins and of particular interest to the work of this thesis, the incorporation of peptides containing posttranslational modifications, replacing the natural C-termini of proteins[141–146].

This technique utilizes an intein to install a thioester at the C-terminus of the protein. Inteins are protein domains analogous to self splicing introns in that they splice themselves out from two flanking polypeptide chains while promoting the ligation of the two flanking chains together[147]. Inteins are found only in

prokaryotes and yeast. For the purposes of EPL, the intein has been engineered in such a way that it is stalled in the first step of the self splicing event[142]. For the EPL reaction, the protein of interest (PTEN in this case) is expressed recombinantly as an intein-CBD fusion protein with the intein at the C-terminus of the PTEN gene (Figure 8). The CBD (chitin binding domain) domain is used for purification purposes by binding the fusion protein to chitin beads. Here PTEN has been C-terminally truncated. The junction site between PTEN and the intein exists in an equilibrium between a native amide bond and an intein catalyzed thioester rearrangement (Figure 8). The thioester can be trapped and the truncated PTEN molecule cleaved from the intein with the use of a small molecule thiol such as sodium mercaptoethanesulfonate (MESNA). With a C-terminal thioester intact, a peptide with an N-terminal cysteine can then be ligated to the C-terminus of the PTEN protein. The cysteine on the peptide acts as a nucleophile to displace the MESNA thioester. Once the MESNA thioester is displaced, the peptide thioester undergoes an N-acyl shift to yield a native amide bond at the ligation site (Figure 8). In this way synthetic peptides containing any desired modification, natural or not, can be incorporated into a recombinant protein. The resulting ligated protein is thus termed a semisynthetic protein given that one part of the molecule is produced recombinantly and the other synthetically.

Expressed protein ligation is a powerful technique that is often used to study the effects of posttranslational modifications (PTMs). It allows for the exact

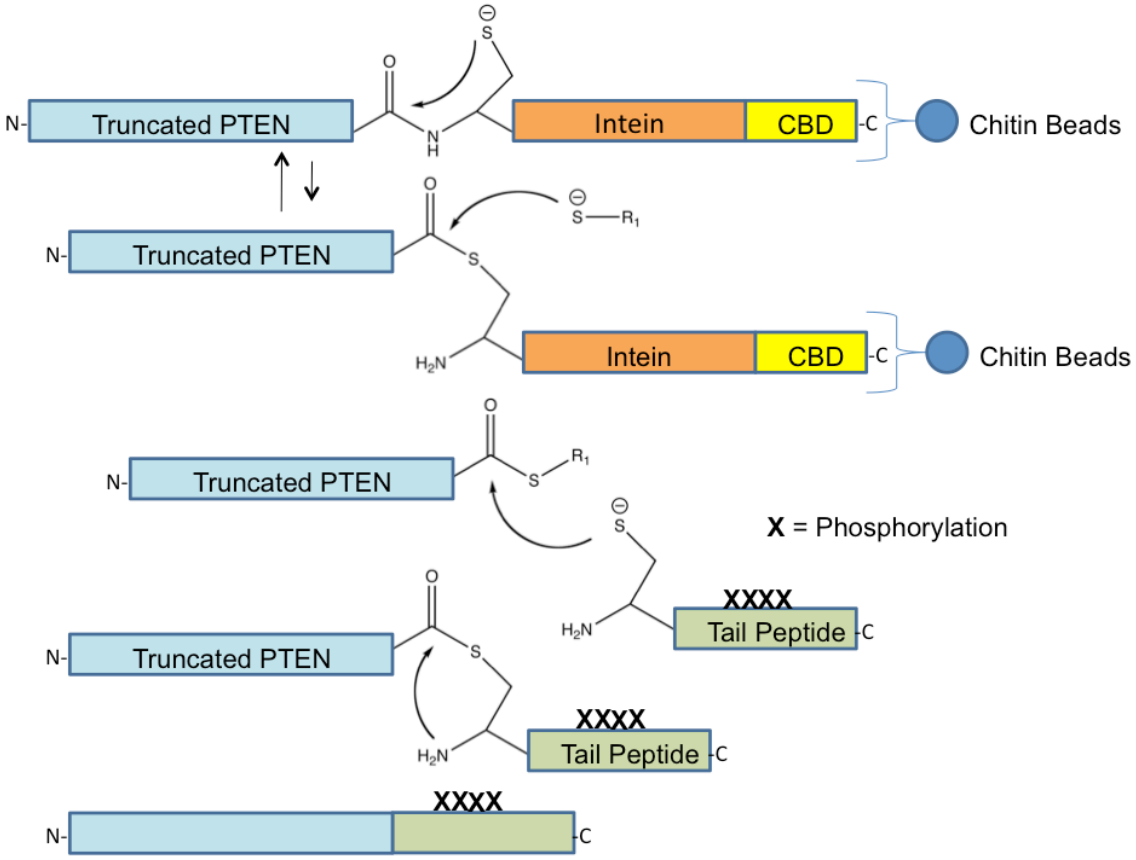

Figure 8: Mechanism of expressed protein ligation (EPL). The PTEN protein is expressed as an intein-cbd fusion protein that is purified over a column of chitin beads. The truncated PTEN protein is cleaved from the intein with a small molecule thiol such as MESNA (mercaptoethanesulfonate). A C-terminal tail peptide containing a cysteine at its N-terminus and posttranslational modifications is then ligated to the C-terminus of the thioester containing PTEN. This process generates full length semisynthetic PTEN containing posttranslational modifications at its C-terminus.

positioning and stoichiometry of PTMs to be known. Other methods of PTM incorporation, such as enzymatic addition of PTMs, are often promiscuous and incomplete. As powerful as EPL is, the major weaknesses of this technique are the requirements for a cysteine at the ligation site and the restriction of its applicability to the C-terminus of a protein. If a cysteine doesn't naturally occur on the C-terminus of a protein then mutating an amino acid to cysteine is required. EPL can only be used when studying PTMs on the C-terminus of a protein due to the fact that the upper limit of the lengths of peptides that can be synthesized is approximately 50 amino acids.

Interfacial Enzyme Kinetics

Interfacial enzymes such as PTEN act at the interface between the cytosol and a cellular membrane such as the plasma membrane. These enzymes are often located predominately in the cytosol, and can translocate to the cellular membrane in which their cognate substrate is located. Interfacial enzymes almost always act on lipid substrates. The different types of enzymes in this class include: kinases, phosphatases, lipases, oxygenases and lipid biosynthetic enzymes[148]. Prominent members of this enzyme class include: PTEN[34,109,119], PI3K[3,149], COX1/2[150,151] and PLC[152,153]. Interfacial enzymes are subject to the same types of regulation as soluble enzymes; namely transcriptional and translational control, posttranslational modifications and protein-protein interactions. Additionally, the activity and localization of interfacial enzymes can

be dramatically affected by the lipid composition of the membranes containing their substrate[119,148,154]. Consequently the lipid composition of membranes is a major regulator of interfacial enzyme function.

When considering enzyme kinetics, water soluble enzymes that act on water soluble substrates depend only on the bulk concentration of substrate. Under these conditions, enzymes with soluble substrates follow standard Michaelis-Menten kinetics in which the rate of the reaction depends only on the bulk or total substrate concentration. Because the substrate of an interfacial enzyme is not water soluble, but rather embedded and dispersed in a lipid bilayer, the rate of the reaction depends both on the bulk and the surface concentration of substrate within the lipid bilayer[119,148,154–158]. Interfacial enzymes therefore do not follow standard Michaelis-Menten kinetics. The reaction follows the scheme below which is also displayed in Figure 9.

$$E + M \underset{k_{-1}}{\overset{k_1}{\rightleftharpoons}} EM + S \underset{k_{-2}}{\overset{k_2}{\rightleftharpoons}} EMS \xrightarrow{k_3} EM + P \qquad 1.1$$

Here M is the membrane and S is the lipid substrate dispersed within the membrane surface. The enzyme must first bind to the membrane surface forming the EM complex before it can access its substrate. After processing its substrate the interfacial enzyme can either dissociate from the membrane or undergo another round of catalysis. Some interfacial enzymes bind only transiently to membranes and quickly dissociate from the membrane after turning over only a

small number of substrate molecules. These enzymes are thus termed “hopping” enzymes. Contrary to “hopping” enzymes, “scooting” enzymes remain associated with the membrane, processing all of the substrate within the membrane prior to dissociation[148].

Like all enzymes, it is of interest to study the kinetic parameters of interfacial enzymes to better understand their mechanism of action and how they are regulated. To accomplish this, lipid substrates are often dispersed in vesicles *in vitro* where the reaction progress of an interfacial enzyme can easily be monitored. The initial rate of the reaction follows the equation:

$$V_o = (V_{max} * X_s * [S_o])/(i\mathit{k}_m * K_s + i\mathit{k}_m * [S_o] + X_s * [S_o])^{119} \quad 1.2$$

Here X_s refers to the surface concentration of substrate expressed as the mol fraction of total lipid. S_o is the bulk concentration of substrate. K_s is the dissociation constant of enzyme for vesicle where $K_s = k_{-1}/k_1$. It is equivalent to K_d. $i\mathit{k}_m$ is the interfacial K_m. Here $i\mathit{k}_m = (k_{-2} + k_3)/k_2$. Just as with the K_m determined from the Michaelis-Menten equation, $i\mathit{k}_m$ can be used as an approximation of the enzyme’s affinity for substrate within the lipid bilayer[119,148,154,159].

The vesicles used in these assays often contain more than one type of lipid; the substrate lipid and at least one carrier lipid. The carrier lipid can be any type of lipid that has no stimulatory or inhibitory effects on the enzyme of interest. Thus, any effects of varying the concentration of carrier lipid should be due solely

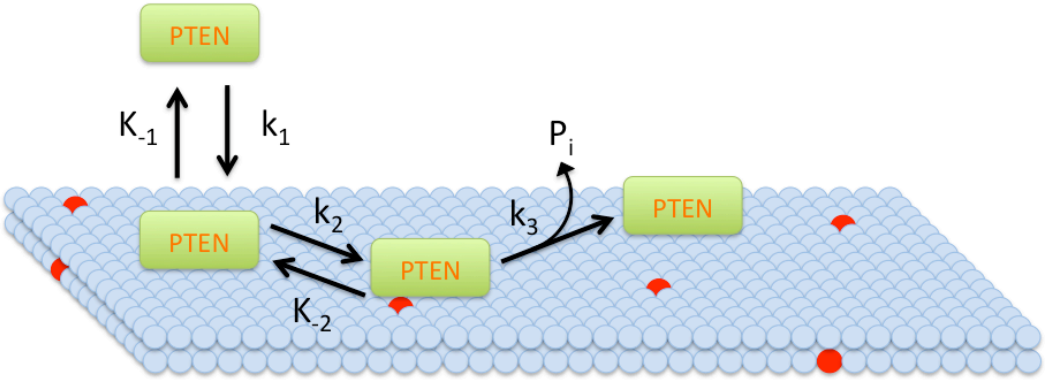

Figure 9: The kinetic mechanism of an interfacial enzyme such as PTEN. Prior to accessing its lipid substrate an interfacial enzyme must first bind to the membrane which its substrate is embedded in. The enzyme can then act on its substrate, turning over a few or many substrate molecules before dissociating from the membrane.

to the accompanied varying surface concentrations of substrate lipid. Given that interfacial enzymes depend on both the bulk and surface concentrations of substrates, two types of experiments must be performed in order to calculate the kinetic parameters for the enzyme. The first type of experiment is a bulk dilution experiment in which the surface concentration of substrate is held constant while varying the bulk concentrations of the substrate and carrier lipid proportionately. A plot of the reaction rate versus the bulk concentration of substrate yields a rectangular hyperbola with apparent V_{max} and K_m values according to the following equations:

$$app V_{max} = V_{max}(i k_m / X_s + 1)^{119,148} \qquad 1.3$$

$$app K_m = K_s(X_s / i k_m + 1)^{119,148} \qquad 1.4$$

The second type of experiment is a surface dilution experiment in which the bulk concentration of substrate is held constant while the surface concentration is varied by varying the amount of carrier lipid. A plot of the reaction rate versus the surface concentration of substrate yields a rectangular hyperbola that defines the true V_{max} and where the apparent K_m follows the equation:

$$app K_m = i k_m(K_s / [S_0] + 1)^{119,148} \qquad 1.5$$

One important technical consideration when performing a surface dilution kinetic analysis on an interfacial enzyme is the ratio of the number of vesicles to the number of enzyme molecules in the reaction. The ratio must always be 3:1 vesicles:enzyme or greater. This ensures that on average, no more than one

molecule of enzyme is present on a single vesicle at one time[148,154,159]. This is necessary to keep the percent turnover of lipid substrate within an individual vesicle under 10% where the rate of the reaction should still be linear. In order to calculate the number of vesicles within a reaction one must know three things: the number of lipids in the reaction, the size of the vesicles and the average surface area of the head groups of the lipids used. Using the equation for the surface area of a sphere ($4\pi r^2$) along with the radius of the vesicles, it is possible to calculate how many lipids are incorporated into one vesicle of that given size. Knowing the total number of lipids in the reaction it is then possible to calculate the total number of vesicles, with the understanding that each vesicle is a lipid bilayer composed of two leaflets of lipids.

There are many different ways to generate vesicles for use in interfacial kinetic assays. One method to ensure vesicles are of uniform size is by the extrusion of lipid solutions through a polycarbonate filter[119,160,161]. Vesicles extruded through a filter will be the same diameter as the pore size of the filter. For example, vesicles generated with a 100 nm pore size filter will have a diameter of 100 nm. Extruded vesicles of this size are unilamellar, meaning they are one contiguous membrane with only water and buffer molecules in the hollow center. Vesicles can also be made by sonication of dried lipid films in the presence of buffered solutions. These types of vesicles are called small unilamellar vesicles (SULs) and typically have diameters of 30-60 nm[160,161]. Another type of vesicle are called large multilamellar vesicles (LMVs). These

vesicles are composed of vesicles within vesicles. The diameter of LMVs can vary greatly and be upwards of 1 μm. LMVs can be generated by repeated freeze thawing of dried lipid films in the presence of buffer or by the vigorous vortexing of a lipid/buffer solution[160,161].

Small Angle X-ray Scattering

Small Angle X-ray Scattering (SAXS) is a technique that utilizes X-ray scattering of macromolecules at very low angles. The data obtained from scattering at these low angles can be used to obtain information about the shape and size of the macromolecule responsible for scattering the X-rays[162–167]. The advantage SAXS has over the more traditional method of structural analysis X-ray crystallography is that no crystals need to be obtained for data collection. The structural determination of proteins by NMR doesn't require crystals but is limited to proteins of molecular weights of less than 30-40 kDa. SAXS is performed on concentrated proteins in solution with no limit to the molecular weight of the proteins or protein complexes being studied. Data collection is quick (less than 2 minutes) and only requires the protein sample to be pure and monodispersed in solution[168]. The major disadvantages relative to crystallography and NMR is its low resolution and that the SAXS data is spatially averaged to account for the different orientations of protein macromolecules in solution[163,164,167]. The exact position of atoms in the macromolecule can therefore not be determined. Instead, molecular envelopes of the macromolecule are calculated *ab initio* using

modeling programs with a limit to the resolution of ~12-60 Å depending on the quality of the sample[166,167,169–173]. The relative structural resolution obtainable by SAXS compared to other structural determination techniques is shown in Figure 10. Nevertheless SAXS has many important applications, especially for large macromolecules and macromolecular complexes in addition to studying protein dynamics. Small angle X-ray scattering is a complex and expansive field of study. Only the basics as they pertain to this thesis work will be discussed.

Protein samples should be greater than 95% pure based on coomassie staining[167]. They must also be monodispersed in solution at the protein concentrations at which data is collected. This must be verified by size exclusion chromatography[167]. The only other requirement before data collection is initiated is that the buffer solution that the protein sample is stored in must match exactly the buffer solution of the background buffer solution (blank) which will also be exposed to X-rays[167–169]. When the protein sample is bombarded with X-rays, every molecule in the solution will give rise to elastic X-ray scattering, including buffer molecules. It is therefore imperative to collect scattering data on the buffered protein sample and the buffer in the absence of the protein sample. Scattering data from the buffer is then subtracted from the protein sample to give only signal from the protein macromolecules in solution. Buffer matching is achieved by dialysis or gel filtration.

The protein samples are exposed to high energy X-rays and the scattering data is collected using a detector (Figure 11). The buffer subtracted, raw

scattering data yields all of the information necessary to obtain information about the size and shape of the protein molecules in solution. The raw scattering data is intuitively informative after an indirect Fourier transform[171,172]. This yields a p(r) plot as seen in Figure 11. The p(r) plot is the pair distance distribution plot. It is a histogram of electron pair distances (distances between atoms) within the macromolecule. Therefore the shape of the plot gives information about the shape and overall size of the molecule. It is used to calculate the radius of gyration (R_g) and maximum particle dimension (D_{max}) of the protein[167,168,172].

SAXS data can be used to generate molecular envelopes of the proteins in solution. This is done using molecular modeling programs. There are several different modeling programs that can be used for this which use different constraints during the modeling process[167,168]. One program called DAMMIN assumes the protein is initially a perfect sphere containing much smaller balls within the sphere's interior[167,170]. DAMMIN will then remove these smaller balls one at a time and generate the theoretical scattering curve for the resulting shape (Figure 12). It will repeat this process until the scattering data of the modeled shape fits to the experimental scattering data obtained from the protein sample. There is more than one three-dimensional structure for every scattering curve generated. This is the inherent challenge of generating three-dimensional structures from one-dimensional data. Because of this, modeling programs such as DAMMIN are typically run at least 10 times. The output of each DAMMIN run is then averaged using a program such as DAMAVER to converge on the most

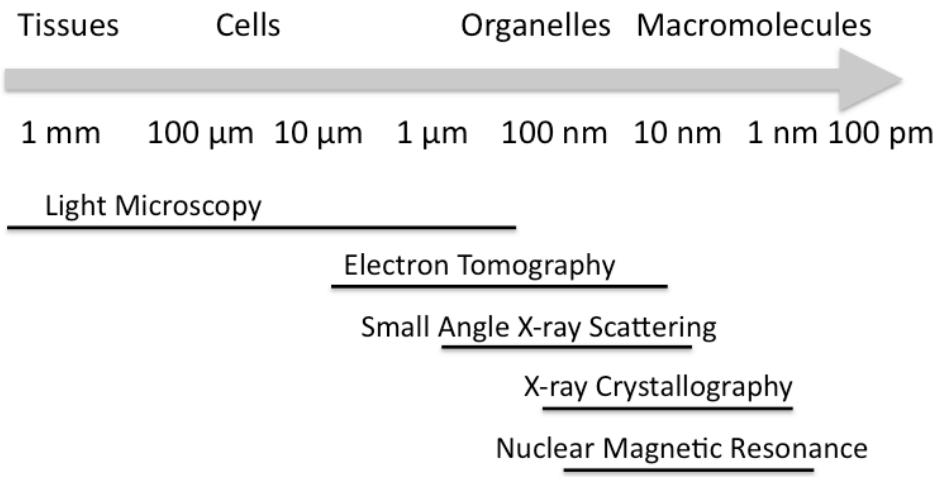

Figure 10: The resolution of small angel X-ray scattering (SAXS). The resolution achievable using small angel X-ray scattering compared to the resolution of other frequently used methods for the structural analysis of macromolecules.

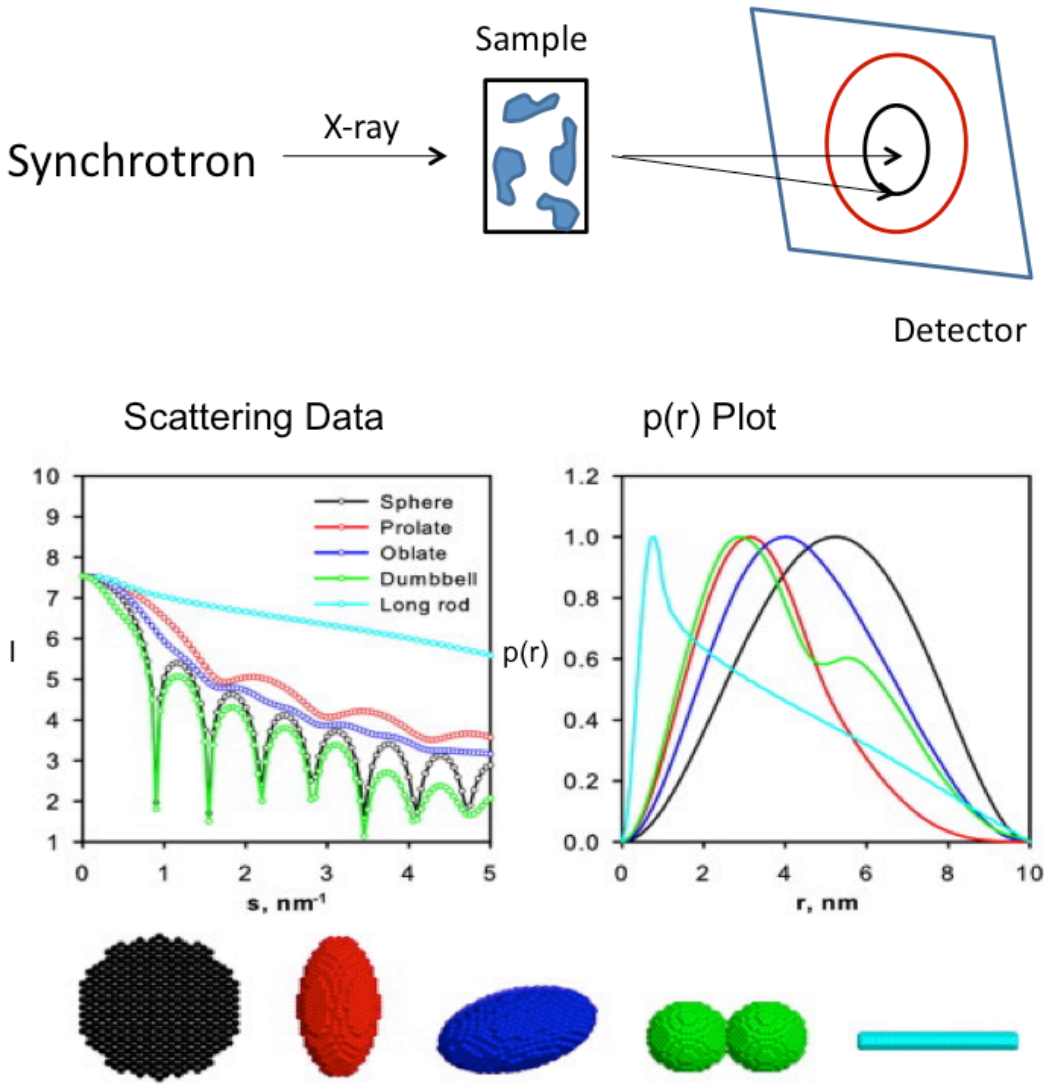

Figure 11: Small angle X-ray scattering (SAXS). (Top) Protein samples in solution are irradiated with X-rays produced from a synchrotron. Scattering data from the protein sample is collected with a detector. (Bottom) Differently shaped molecules give rise to different scattering profiles and pair distance distribution p(r) functions. Scattering and p(r) plots taken from Svergun et al. 2010.

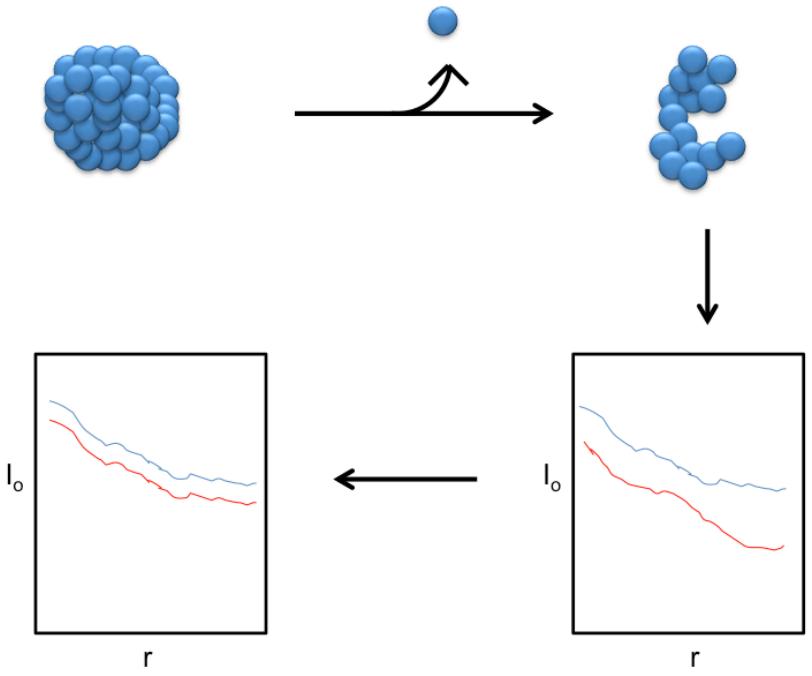

Figure 12: Molecular envelope modeling using DAMMIN. DAMMIN generates molecular envelopes *ab initio* by simulated annealing of a dummy atom model. Theoretical scattering data from generated envelopes are then compared to experimental scattering data and the process is repeated until the theoretical matches the experimental.

likely structural conformation[163,167,168,170]. Because of this, SAXS is not as robust as X-ray crystallography or NMR. There is always the possibility that the structures obtained from the modeling programs are incorrect or misleading. Nevertheless molecular envelopes obtained from SAXS analysis have often proven to be in close agreement with X-ray crystal structures in the literature[173]. Proper sample preparation and data processing is required to reduce the chances for error in molecular envelope modeling.

Summary

The importance of PTEN as a tumor suppressor is demonstrated by its high frequency of inactivation in many different types of somatic cancers and cancer predisposition syndromes. PTEN's ability to turn off the PI3K/PTEN/AKT signaling pathway by dephosphorylating PIP_3 is central to its tumor suppressive ability. Although much research has gone into studying PTEN and its functions, important questions still remain about the most basic forms of PTEN regulation including phosphorylation of the S380/T382/T383/S385 cluster on its C-terminal regulatory tail. We aim to answer some of these questions by studying the biochemical and biophysical properties of phosphorylated and unphosphorylated semisynthetic PTEN.

Chapter 2: Generation of Semisynthetic PTEN

Introduction

As discussed in Chapter 1, phosphorylation of PTEN has been given considerable attention in the literature[100,101,108–110,126,129,133]. PTEN has been shown to be phosphorylated at multiple positions on its C2 domain as well as its C-terminal tail (Figure). The C2 domain of PTEN can be phosphorylated at amino acids Thr223, Ser229, Thr319 and Thr321 by the kinase Rock[126] while the tail can be phosphorylated at amino acids Ser363, Thr366, Ser370, Ser380, Thr382, Thr383 and Ser385 by the kinases GSK3β, CK2 and perhaps others[100,101,108,129]. Phosphorylation of PTEN has been proposed to affect the membrane localization[109], nuclear localization[62], stability[100,110,113], activity[109] and protein binding partners[124,136,174] of PTEN. PTEN is thought to be phosphorylated on its C-terminal tail at positions Ser380, Thr382, Thr383 and Ser385 most of the time, with only a few conditions being known to modulate the phosphorylation state of this phospho cluster[132–134]. There has yet to be a rigorous characterization of purified, tail phosphorylated PTEN.

Mutation of the S380/T382/T383/S385 cluster to alanines has been shown to change the sub-cellular localization PTEN[109,175]. In cellular experiments, PTEN that contains the wild type S380/T382/T383/S385 cluster and tagged with a GFP fluorophore at its C-terminus is located predominantly in the cytosol. When the cluster is mutated to the tetra-alanine form, the transfected

PTEN molecules accumulate at the plasma membrane and within the nucleus of the cell[109,175]. The observed effect has been assumed to be due to the presence of phosphorylation at the S380/T382/T383/S385 cluster in wild type PTEN and the absence of the phosphorylation in the tetra-alanine mutant. The mechanism by which this occurs is poorly understood. It has been proposed that a conformational change in the PTEN protein induced by phosphorylation could be the cause of the changes in cellular localization[109,137]. In this model phosphorylated PTEN would undergo a conformational change in which the phospho-tail binds somewhere on the PTEN molecule, preventing it from binding to the plasma membrane. When dephosphorylated, PTEN would adopt a conformation that is free to associate with the plasma membrane. In another model, phosphorylation of PTEN could affect its binding interactions with other proteins which would then dictate its subcellular localization. There are several proposed examples of the binding of PTEN to other proteins being affected by the tetra-alanine mutated state of the S380/T382/T383/S385 cluster of the tail[124,136,174].

In prior studies of PTEN phosphorylation, the effects of phosphorylation have been deduced by comparing wild type, phosphorylatable PTEN and the tetra-alanine, unphosphorylatable PTEN mutant. This can cause misleading results since the introduction of mutations into a protein can lead to unintended consequences in addition to the intended lack of phosphorylation. In the case of PTEN, analysis of the tetra-alanine mutant has led to conflicting results when

studying the stability of PTEN conferred by tail phosphorylation[100,131]. Additionally, the phosphorylation state of proteins can change under different conditions within the cell. It is not possible to know what percentage of wild type PTEN molecules are phosphorylated or to what stoichiometry. Some studies have attempted to phosphorylate PTEN *in vitro* with CK2 kinase. In these cases, it is still not possible to determine to what extent PTEN is phosphorylated, and it is likely that excessive phosphorylation with large quantities of CK2 could phosphorylate other unintended sites in addition to the S380/T382/T383/S385 cluster. This could lead to ambiguity as to whether the observed affects if any are due to phosphorylation of the S380/T382/T383/S385 cluster or to other sites that are inadvertently phosphorylated by the kinase.

In studies pertaining to PTEN conformational changes associated with tail phosphorylation, potential conformational changes have been looked at indirectly through *in trans* co-immunoprecipitation experiments[109,137]. In these experiments, two segments of the protein containing artificial tags were expressed within cells and the binding of one segment to another was determined by western blot analysis after immunoprecipitation. Because these proteins were expressed within cells and not purified, the possibility that the binding interaction is being mediated by a third protein remains plausible. Again mutations of the S380/T382/T383/S385 cluster to alanine were used to simulate the unphosphorylated tail state.

To circumvent the issues discussed above we have employed expressed protein ligation to generate semisynthetic PTEN in its phosphorylated and unphosphorylated forms. In doing so it is possible to study the direct effects of PTEN phosphorylation in a purified system *in vitro* without having to mutate the S380/T382/T383/S385 cluster to alanines and with known stoichiometry of phosphorylation. Any conformational changes associated with tail phosphorylation can be studied *in cis* with the natural polypeptide intact and without having to engineer unnatural tags (GFP, FLAG) onto the protein. As discussed in Chapter 1 the utilization of this technique requires a cysteine at the ligation site. Given that PTEN does not contain any cysteines on its C-terminal tail, Tyr379 was mutated to a cysteine to facilitate the native chemical ligation reaction.

Methods

Peptide Synthesis:

All peptides were synthesized on a PS3 peptide synthesizer from Protein Technologies using standard Fmoc based solid phase peptide synthesis[176–179]. The unmodified (unphosphorylated) peptide pertaining to amino acids 379-403 of the PTEN tail was synthesized by double coupling every amino acid. Tyr379 was replaced with a Cys for the purposes of expressed protein ligation (EPL). Fmoc amino acids were deprotected for 10 minutes a total of 5 times with 20%

piperidine in DMF. Coupling times were 1.5 hours. The phosphorylated tail peptide was synthesized using Fmoc-phospho-serine and Fmoc-phospho-threonine from EMD. The phosphate groups were mono-protected by O-benzyl groups during the synthesis. Phospho-serine was used at amino acids 380 and 385. Phospho-threonine was used at amino acids 382 and 383. Phospho-amino acids were double coupled for 3 hours each. Asp381, Asp384 and Cys379 were triple coupled for 3 hours each. All peptides ending in amino acid number 403 were synthesized on Wang resin to yield a carboxylic acid at the C-terminus of the peptide after peptide cleavage from the resin. Peptides ending in amino acid number 395 were synthesized on Rink amide resin but otherwise synthesized identically to the full length 25mer tail peptide. All peptides were cleaved from the resin and deprotected using reagent K (trifluoroacetic acid:ethane dithiol:water: thioanisole, phenol – 82.5%:2.5%:5%:5%:5%) then purified by reversed phase C18 HPLC and lyophilized.

Generation and Purification of Semisynthetic PTEN:

PTEN C-terminally truncated at residue 378 was first subcloned into the pTXB1 vector from NEB which contains the GyrA intein from the organism *Mycobacterium xenopi*[180,181]. Tyr379 was mutated to a Cys to facilitate the intein mediated cleavage reaction. The PTEN-intein-CBD DNA sequence was then subcloned into the pFastBac1 baculovirus entry vector and the subsequent

bacmid was generated in DH10Bac *E.coli* according to the protocols outlined in the Bac-to-bac insect cell expression system from Invitrogen (10359-016)[182]. Baculovirus was generated in SF21 insect cells. Second generation (P2) virus was used to infect 1 L of High Five insect cells for protein expression at a multiplicity of infection of 1. High Five cells were grown in shaking flasks in the presence of 10 U/mL of heparin. Flasks were allowed to shake at 115 rpm for 48 hours.

After 48 hours the High Five insect cells were pelleted by centrifugation and resuspended in lysis buffer (50 mM Hepes pH 8.0, 150 mM NaCl, 1 mM EDTA, 10% glycerol and 0.1% triton X-100). Cells were lysed by 40 passes of a Dounce homogenizer. The lysate was the pelleted at 27,000 X g for 40 minutes. The supernatant from the cell lysate which contained the PTEN-intein-cbd fusion protein was first passed over a 5 mL bed of fibrous cellulose (Whatman) to remove viral chitinase, then bound to chitin beads (5 mL bed volume) from NEB by gravity flow. Full length semisynthetic PTEN was then generated on the chitin column by adding 400 mM MESNA and 2 mM of C-terminal peptide buffered with 50 mM HEPES (pH 7.2), 150 mM NaCl. C-terminally truncated PTEN (t-PTEN) was purified the same way but cleaved from the intein with 50 mM DTT buffered with 50 mM HEPES (pH 7.2), 150 mM NaCl. The ligation reactions were carried out for 48-72 hrs at room temperature. Upon completion of the ligation reaction the ligation mixture was eluted from the chromatography column with 15 mL of dialysis buffer (50 mM Tris pH 8.0, 150 mM NaCl, 10 mM DTT) and subsequently

dialyzed into 4 L of dialysis buffer for a period of 48 hrs with multiple buffer exchanges in a dialysis cassette (Slidealyzer) with a 12 K MWCO in order to remove excess unreacted peptide. Proteins were then concentrated following dialysis to >5 mg/mL (>100 μM). We estimate that there is less than 10 μM of residual unligated peptides at this stage. Due to large dilutions (>1000-fold) of the semisynthetic enzyme for enzymatic and other biochemical assays, small amounts of residual contaminating peptide remaining after dialysis would not be expected to interfere with any assays. Semisynthetic PTEN proteins produced in this way yields 8-10 mg of protein per liter of insect cell culture with the desired modifications on the C-terminus at purities of greater than 90% based on Coomassie stained SDS-PAGE.

The semisynthetic PTEN protein was further purified for SAXS and other biochemical experiments by anion exchange chromatography (mono Q) using an AKTA FPLC from GE Healthcare. Proteins were purified with a gradient of 0-50% Buffer B over 250 mL at a flow rate of 1.0 mL/min. (Buffer A: 50 mM Tris pH 8.0, 10 mM DTT; Buffer B: 50 mM Tris pH 8.0, 1.0 M NaCl, 10 mM DTT). Size-exclusion chromatography was carried out with a Superdex 200 column in the following buffer: 50 mM Tris pH 8.0, 150 mM NaCl, 10 mM DTT. After FPLC purification PTEN protein was concentrated to between 1 and 14 mg/mL in 50 mM Tris pH 8.0, 150 mM NaCl and 0-10% glycerol. The PTEN protein was then aliquoted and stored at -80 ºC. Semisynthetic PTEN protein made and stored in this way was stable for at least 12 months. Semisynthetic PTENs produced in

this way yields ~2-3 milligrams of protein per liter of insect cell culture with the desired modifications on the C-terminus at purities of greater than 90%.

Results

Using expressed protein ligation (EPL) to generate semisynthetic proteins requires the protein to first be made in two segments prior to ligating the two together to yield the full length semisynthetic protein (Figure 13A). The N-terminal segment must be expressed recombinantly as an intein fusion protein. The C-terminal segment is synthesized by standard peptide synthetic techniques then ligated to the intein generated thioester at the C-terminus of the N-terminal segment.

Initial attempts to produce large quantities of PTEN-intein-CBD fusion protein in *E. coli* proved fruitless. The majority of the fusion protein was expressed insolubly in inclusion bodies. Many different techniques and protocol modifications were used in attempt to increase protein production. Two different intein fusion protein constructs from NEB (pTXB1 and pTYB2) were used but yielded comparable amounts of fusion protein (~50 µg/L of culture). Several different commonly used *E. coli* expression strains were employed along with low expression temperatures but did not increase soluble protein yield. GST fusion proteins often increase the amount of soluble protein being expressed from various expression systems. However GST-PTEN-intein-CBD fusion proteins

proved to be completely insoluble. Oftentimes the position of the ligation site at the C-terminus of the EPL protein (PTEN) and the N-terminus of the intein can affect the yield and solubility of the fusion protein. However changing the truncation site and therefore the ligation site on the C-terminus of PTEN also did not increase fusion protein yield but did cause the thioester generated at the ligation site of a large percentage of the protein to be cleaved within the *E. coli* cells. Lastly molecular chaperone proteins were co-transformed into the *E. coli* cells to aid in the proper folding of the PTEN-intein-CBD fusion protein. This final effort did increase yields moderately, up to 200 μg/L of culture, however these yields would still be too low for the quantities of proteins needed for biophysical experiments in the future. Additionally this caused large quantities of chaperone to co-purify with PTEN such that PTEN could only be purified to approximately 60% purity. This could possibly be due to the fusion protein not being completely folded properly even in the presence of co-expressed chaperone, causing the chaperone to stick to the semisynthetic PTEN molecule when it was eluted from the chitin affinity column.

Due to the difficulties of expressing PTEN-intein-CBD fusion protein in an *E. coli* expression system, we decided to attempt to produce the fusion protein in insect cells using baculovirus. Historically, the expression of such intein-cbd fusion proteins in insect cells has proven quite difficult to researchers working with expressed protein ligation. One potential reason for this is that baculovirus encodes and expresses chitinase. Chitinase is an enzyme that hydrolyzes chitin.

Intein-CBD fusion proteins are affinity purified with chitin covalently linked to a solid support of beads. Chitinase competes with CBD (chitin binding domain) for the chitin beads. Chitinase also hydrolyzes the chitin, eliminating binding sites for intein-CBD fusion proteins. Intein fusion proteins may also have the propensity to cleave the intein generated thioester within insect cells prior to purification of the fusion protein. This could be due to high levels of endogenous thiol within insect cells. These factors may lead to decreased yields of the desired intein fusion protein when using baculovirus/insect cell expression systems.

Despite the historical difficulties of expressing intein fusion proteins in insect cells, we were able to produce large quantities of PTEN-intein fusion protein in insect cells after optimizing a few expression and purification conditions. Initial attempts to express the protein in SF9 and SF21 insect cells produced low amounts of protein that could only be visualized by western blot with an anti-CBD antibody. However High Five insect cells produced massive amounts of the fusion protein. Even though about 50% of the fusion protein remained insoluble or had its thioester cleaved within the insect cells, the yield of soluble C-terminally truncated PTEN protein from 1 L of culture was approximately 10 mg after DTT cleavage of the thioester. Viral chitinase was removed by passing the lysate over a bed of fibrous cellulose prior to binding the fusion protein to chitin beads. Cellulose selectively binds to chitinase while having minimal affinity for the intein-cbd fusion protein.

With the PTEN-intein fusion protein being expressed in ample quantities, all that was need to generate semisynthetic PTEN was the C-terminal tail peptide that would be ligated to the intein generated thioester on the C-terminus of the recombinant PTEN protein. The tail peptide was needed in its phosphorylated and unphosphorylated form. Synthesis of these tail peptides proved to be just as difficult as expressing the N-terminal PTEN-intein fusion protein. Initially, the ligation site at the C-terminus of PTEN was chosen to be at amino acid position 362. This would have required the synthesis of a 42 amino acid peptide and the mutation of Ser362 to a Cys to facilitate the native chemical ligation reaction. Using standard solid phase Fmoc based peptide synthesis, the 42mer unphosphorylated PTEN tail was readily synthesized with decent yields on a PS3 peptide synthesizer from Protein Technologies. Unfortunately, the 42mer phosphorylated peptide with amino acids Ser380, Thr382, Thr383 and Ser385 phosphorylated proved impossible for us synthesize. It is widely accepted that phosphorylated peptides are significantly more difficult to synthesize than their unphosphorylated counterparts. This is at least partially because phosphates and their protecting groups used during peptide synthesis are large and bulky, leading to steric hindrance during the chemical coupling reaction of the phospho-amino acid and of subsequent amino acids. The phosphates are typically mono-protected, meaning only one of the negative charges on the phosphate is masked by a protecting group. Therefore, if the phospho-peptide requires there to be multiple phospho-amino acids in close proximity to each other, there could be repulsion of negative charges in addition to steric hindrance leading to lower

coupling efficiency. The phosphorylated PTEN tail peptide may be particularly difficult to make given that there are four phosphorylated amino acids clustered within six amino acids. There is likely both steric hindrance and repulsion of negative charges leading to a decrease in coupling efficiency and therefore final yields.

Adding to the difficulty of synthesizing the phosphorylated PTEN tail peptide is that phosphorylated peptides do not give large ionization/detection signals in mass spectrometry[183,184]. Multi-phosphorylated peptides give lower signals than singly phosphorylated peptides, further decreasing the signal. This made it difficult to ascertain whether or not the peptide was being synthesized or not. To surmount this problem MALDI matrix containing ammonium citrate was used with the mass spectrometer set to negative mode. Ammonium citrate is known to increase the signal obtained from a phosphorylated peptide in MALDI mass spectrometry[185]. Negative mode also enriches the signal from negatively charged species, further enhancing the low signal[186]. After the addition of each amino acid a small portion of the growing peptide chain was cleaved from the resin and monitored by MALDI-TOF to determine if the previous reaction occurred or not.

Several different approaches were taken in attempt to successfully synthesize the phospho-42mer. Because the unphosphorylated 42mer was easily made, it was likely that the addition of phospho-amino acids was responsible for our problems. We therefore focused on optimizing the addition of

the phospho-amino acids and the amino acids added after the phospho amino acids. Longer reaction/coupling times of the phospho amino acids did appear to increase yields. Typical coupling times in Fmoc based peptide synthesis are 1.5 - 2 hrs. Coupling times for the phospho-amino acids were increased to 6 - 12 hrs and were coupled by hand to ensure adequate washing in between deprotection and coupling steps. After coupling all of the phospho amino acids manually, the peptide was put on the PS3 synthesizer to complete the remainder of the peptide, however this never lead to any of the desired complete 42mer phospho peptide after purification.

The correct synthesis of the desired peptide can be blocked by the buildup of side products that sterically hinder the desired reaction. To prevent this and to more easily purify the final product, free amines at the growing N-terminus can by capped by acetic anhydride which effectively terminates the extension of incompletely coupled peptide chains. This approach eliminated any desired product after the addition of the phospho amino acids even before attempting to complete the full 42mer. This could be due to the fact that the phosphates are only mono protected, leaving one hydroxyl to react with the acetic anhydride. This could form an asymmetric anhydride on the growing peptide that could then cap the N-terminal amine after deprotection, thereby preventing the addition of the next amino acid.

After many unsuccessful attempts to synthesize the 42mer phospho-peptide, we decided to shorten the length of the peptide to just after the phospho-

cluster given that we could successfully synthsize the phosphorylated peptide up to amino acid 378, albeit at significantly lower yields than the unphosphorylated peptide. We thus decided to mutate Tyr379 to a Cys to facilitate the native chemical ligation reaction and synthesize a phospho-peptide 25 amino acids in length (Figure 14A). Ideally, we would have liked to mutate a Ser, Ala or Met to a Cys which would have been a more conservative mutation. However, given the constraints of the length of peptide that could be synthesized, Tyr379 was the best option. Cys is not similar to Tyr in terms of bulk and hydrophobicity but the two amino acids do have similar pK_a values (Cys ~9; Tyr ~10). The unphosphorylated and phosphorylated 25mer PTEN tail peptides were successfully synthesized and purified (Figure 14B, C). Changing the ligation site to Tyr 379 of course required changing the truncation site on the C-terminus of PTEN in the PTEN-intein fusion protein. Fortunately this did not change the expression yield of the fusion protein in the High Five insect cells.

With the two components required for expressed protein ligation in hand, semisynthetic PTEN was generated in its unphosphorylated and its fully phosphorylated (pSer380/pT382/pT383/pS385) form (Figure 13B). Unphosphorylated PTEN and phosphorylated PTEN will be referred to as n-PTEN and 4p-PTEN respectively for the remainder of this thesis. Additionally C-terminally truncated PTEN (t-PTEN) at amino acid 378 was made to compare the affects of removing a portion of the tail on various PTEN activities (Figure 15). The ligation reaction proceeded to near completion over 48 – 72 hrs with the

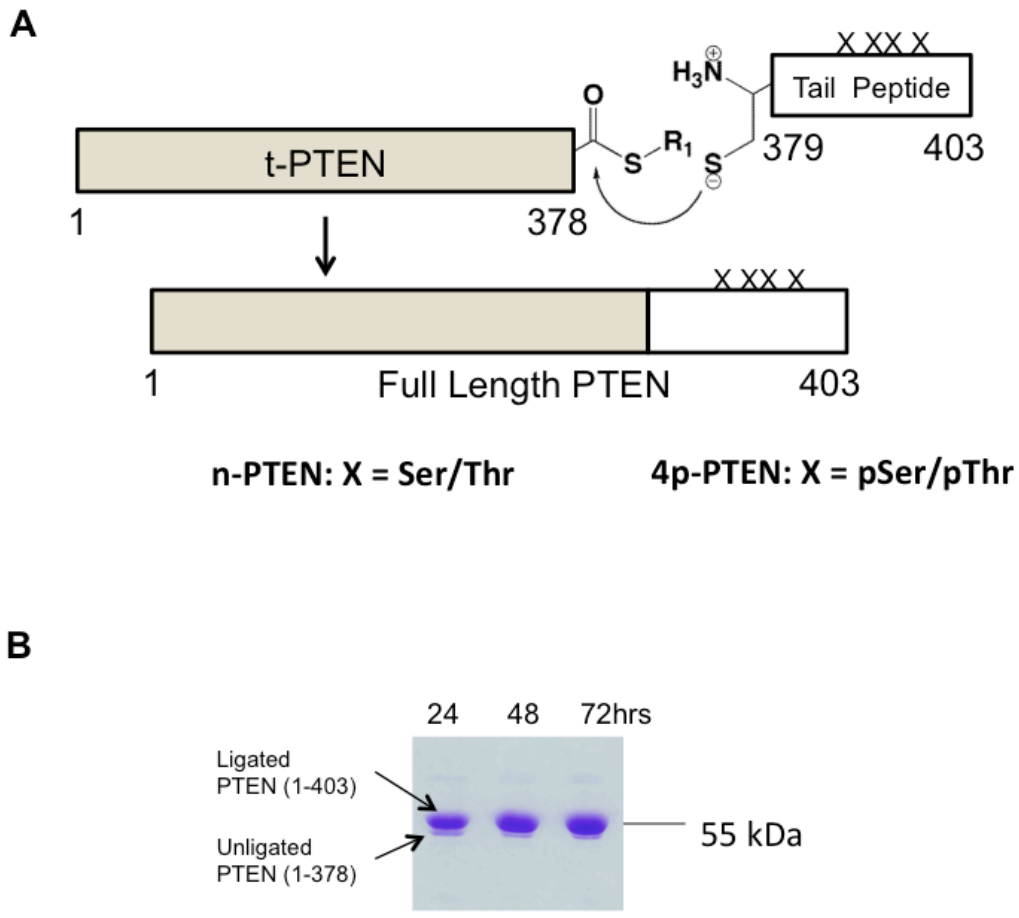

Figure 13: Generation of semisynthetic PTEN proteins. (A) C-terminal PTEN tail peptides (aa 379 – 403) are ligated to the C-terminal thioester containing body of PTEN (aa 1 – 378). (B) The reaction proceeds over 72 hrs yielding full length PTEN.

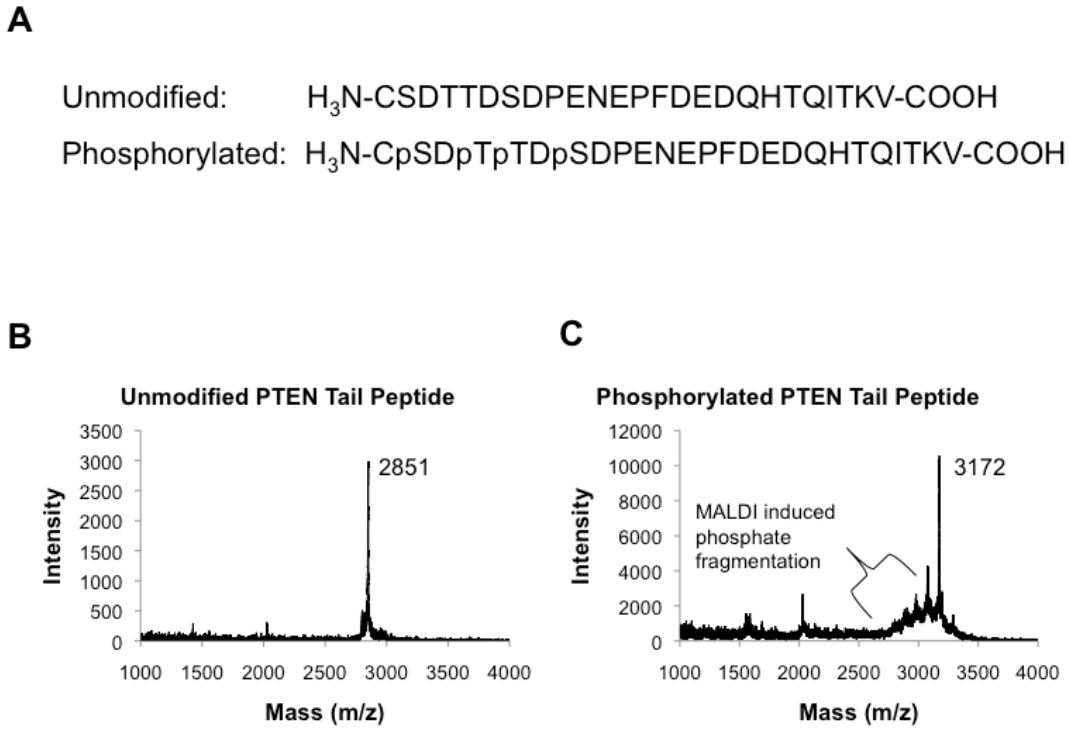

Figure 14: Synthesis of PTEN C-terminal tail peptides. (A) The amino acid sequences of the unmodified and phosphorylated tail of PTEN with amino acids Ser380, T382, T383 and S385 either unphosphorylated or phosphorylated. (B) MALDI-TOF mass spectrum of the unmodified tail peptide. Expected mass: 2852 (m/z). (C) MALDI-TOF mass spectrum of the phosphorylated tail peptide. Expected mass: 3172 (m/z). MALDI induced fragmentation of phosphates results in the loss of 95 mass units for each phosphate which is seen in the series of four peaks preceding the major peak of the desired mass at 3172.

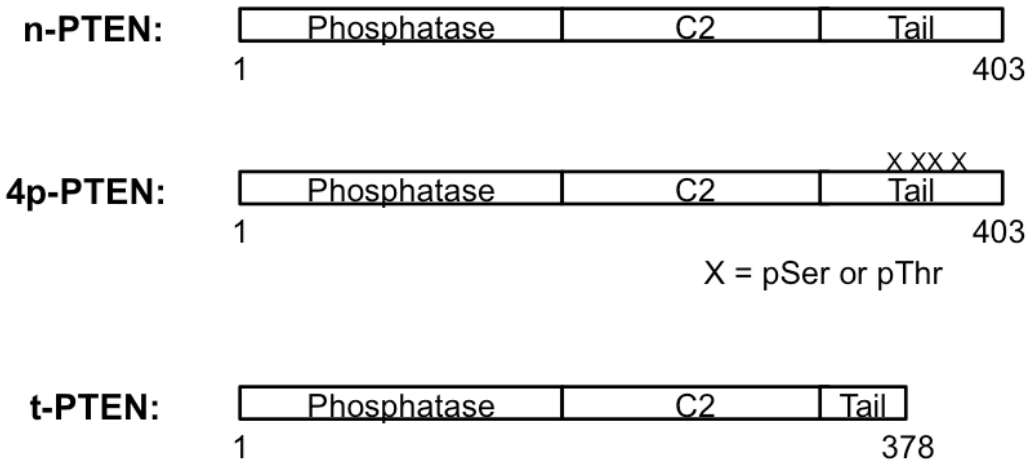

Figure 15: Schematic view of semisynthetic PTEN proteins. n-PTEN and 4p-PTEN are full length (aa 1 – 403) and contain the Tyr379 to Cys mutation. t-PTEN contains amino acids 1 – 378.

upper band corresponding to the mass of full length PTEN (Figure 13B). The correct theoretical masses of the semisynthetic proteins were verified by MALDI-TOF with the expected 320 mass unit increase for 4p-PTEN (Figure 16A, B). The presence of the phosphorylated cluster in 4p-PTEN was also verified using a commercially available antibody to the phospho cluster. With this antibody, intact phospho cluster in 4p-PTEN is detected by western blot while n-PTEN is not (Figure 17). Both n-PTEN and 4p-PTEN eluted as monomers on a size exclusion column (Figure 18).

There have been reports of PTEN possessing auto-phosphatase activity, meaning it can remove its tail phosphates. However semisynthetic 4p-PTEN generated in the presence of a PTEN inhibitor (VO-OHpic) showed identical tail phosphorylation status compared to 4p-PTEN generated in the absence of this inhibitor (Figure 19A). Additionally 4p-PTEN incubated with n-PTEN for a period of up to 24 hrs showed little to no appreciable removal of tail phosphates while alkaline phosphatase readily removed tail phosphates as measured by western blot (Figure 19B).

There was some concern that the Tyr379 to Cys mutation could affect the activity of PTEN. We therefore expressed and purified WT GST-PTEN and Y379C GST-PTEN from *E. coli* and tested their enzymatic activity *in vitro*. Phosphatase activity with a soluble PIP_3 substrate was nearly the same for the pair (Figure 20). Phosphate release was monitored by malachite green detection[187,188].

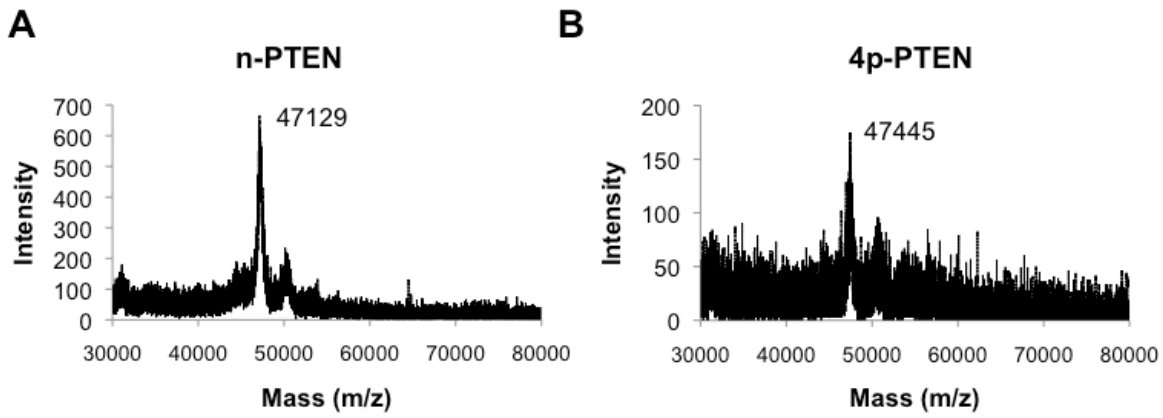

Figure 16: MALDI-TOF of semisynthetic PTEN proteins. (A) Unphosphorylated semisynthetic PTEN (n-PTEN) (expected mass: m/z 47106.2). (B) Phosphorylated semisynthetic PTEN (4p-PTEN) (expected mass: m/z 47426.2). The spectra for A and B were normalized to the external reference bovine serum albumin. The approximate accuracy for the mass spectrometric measurements of these protein masses is +/- 50 Da.

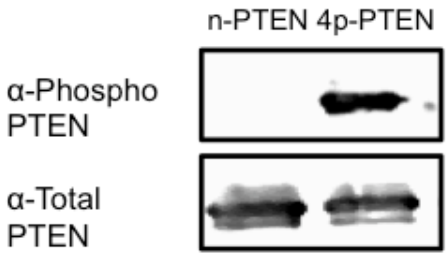

Figure 17: 4p-PTEN contains the phospho S380/T382/T383/S385 cluster intact. Western blot with an antibody to the phospho cluster shows 4p-PTEN but not n-PTEN is phosphorylated. Phosphorylated PTEN was detected using a 1:1000 dilution of anti phospho-S380/T382/T383 from Novus Biological. Total PTEN was detected using a 1:1000 dilution of an antibody recognizing the phosphatase domain of PTEN form Santa Cruz Biotechnologies.

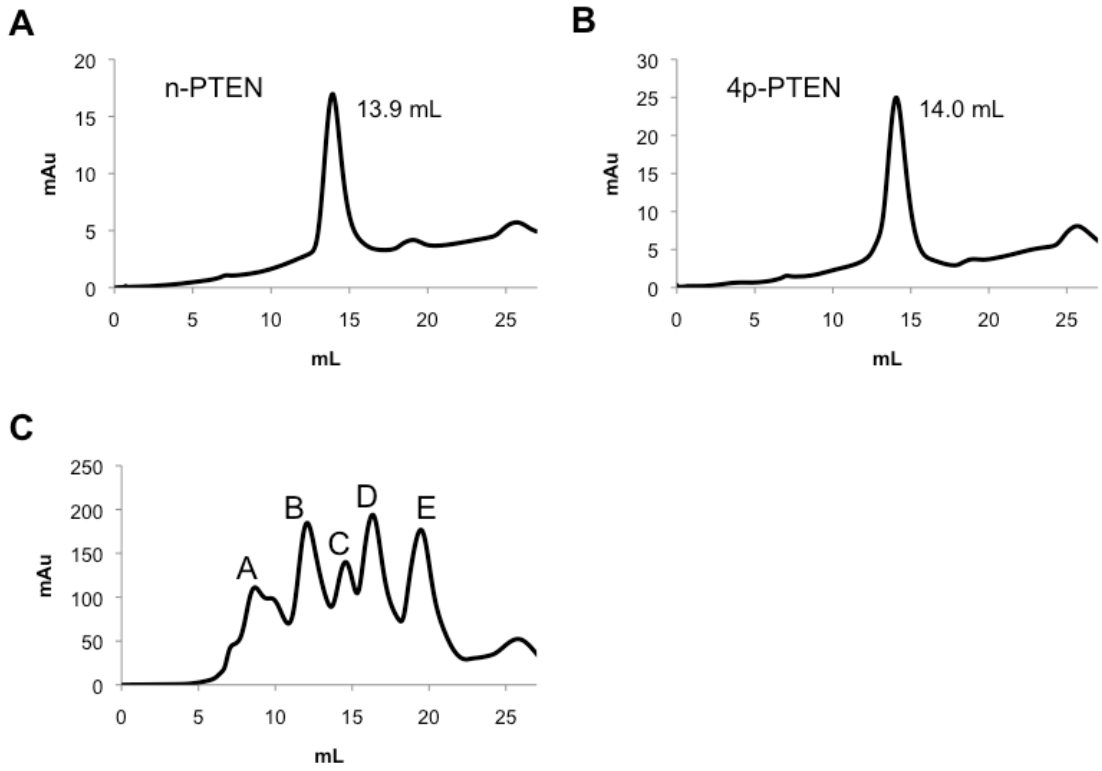

Figure 18: Size exclusion chromatography of n-PTEN and 4p-PTEN. The chromatograms and elution volumes of (A) n-PTEN and (B) 4p-PTEN purified by FPLC on a size exclusion column (Superdex 200). (C) The chromatogram of protein standards on a size exclusion column (Peak A: thyroglobulin, MW=670,000, elution vol. = 8.7 mL; Peak B: gamma globulin, MW=158,000, elution vol. = 9.7 mL; Peak C: ovalbumin, MW=44,000, elution vol. = 14.6 mL; Peak D: myoglobin, MW=17,000, elution vol. = 16.3 mL; Peak E: vitamin B12, MW=1350, elution vol. = 19.5 mL).

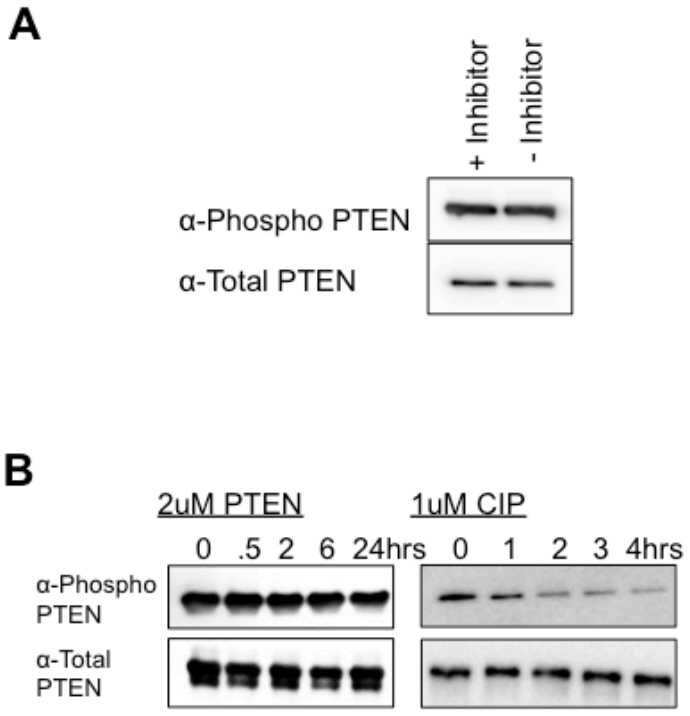

Figure 19: Determination of autophosphatase activity of PTEN. (A) Generation of 4p-PTEN by expressed protein ligation in the presence or absence of 25 μM VO-OHpic, a potent PTEN inhibitor monitored by western blot. (B) 50 ng of 4p-PTEN treated with 2 μM n-PTEN (left) or 1 μM calf intestinal phosphatase (right). Dephosphorylation of the phospho tail is monitored by western blot.

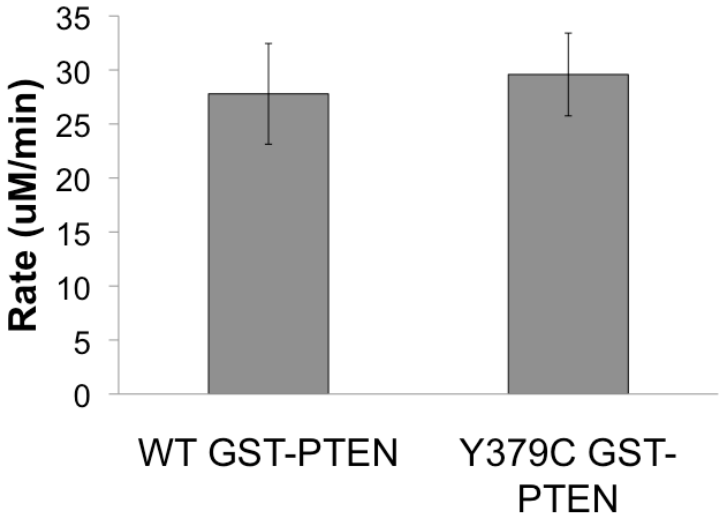

Figure 20: Activity of Y379C PTEN mutant. Phosphatase assays using diC6 PIP_3 for WT GST-PTEN and Y379C GST-PTEN purified from *E. coli*. Data are reported as the mean +/- the SEM of three experiments performed in duplicate.

Discussion

The generation of semisynthetic PTEN in its unphosphorylated and fully phosphorylated forms allow for the characterization of phosphorylated PTEN for the first time. PTEN is thought to be phosphorylated most of the time *in vivo* though the extent and stoichiometry of phosphorylation is unknown. Only a few conditions in specialized cell lines have been found to modulate the phosphorylation level of PTEN[132–134]. Previous studies have relied exclusively on mutations to study PTEN phosphorylation at the Ser380, Thr382, Thr383 and Ser385 cluster. Using semisynthetic 4p-PTEN, PTEN phosphorylation can be studied without mutating the phosphorylation sites to Ala and without having to assume that WT PTEN expressed in eukaryotic cells is phosphorylated. Any conformational changes associated with PTEN phosphorylation can be studied *in cis* rather than *in trans* using 4p-PTEN. 4p-PTEN and n-PTEN could potentially be used to study other affects of PTEN phosphorylation that are not examined in this thesis such as protein-protein interactions, ubquitinylation and PTEN stability among others.

Although we do not detect any autophosphatase activity for PTEN *in vitro*, it is possible that PTEN may possess autophosphatase activity *in vivo*. There may be other proteins responsible for binding to PTEN's tail and presenting it in such a way that allows for PTEN to hydrolyze its tail phosphates. It is important to note that the detection of any autophosphatase activity in this thesis was monitored with a polyclonal antibody raised to the phospho cluster

phosphorylated three times at Ser380, Thr382 and Thr383. Therefore the removal of pSer385 may not be detectable with this antibody. Also, it is unknown if the removal of a single phosphate at either of the other three sites could be detectable with this antibody. Though no dephosphorylation was detected during the ligation reaction in the absence of PTEN inhibitor VO-OHpic, it is possible that the conditions of the ligation reaction are not suitable for PTEN phosphatase activity (400 mM MESNA, 2 mM phospho-peptide). It is also possible that 4p-PTEN which is phosphorylated four times is in a conformational state that is closed off to dephosphorylation by itself. PTEN is thought to be phosphorylated most of the time *in vivo* but it is unknown what percentage of the protein is phosphorylated four times on the S380/T382/T383/S385 cluster.

No difference in the activity between WT GST-PTEN and Y379C GST-PTEN was detected against a soluble PIP_3 substrate with the malachite green detection assay. While this is encouraging it is not conclusive evidence that the Tyr to Cys mutation required for expressed protein ligation does not alter PTEN activity in some way. It may be that the Y379C mutation is only relevant with respect to vesicle based substrate. The Y379C mutation was not examined in the context of the phospho PTEN protein. If there is a conformational change that affects PTEN activity when PTEN is phosphorylated, the mutation may only affect PTEN's various activities when PTEN is phosphorylated. There is no easily testable experiment to determine this. Even if the Y379C mutation has no affect

on 4p-PTEN activities by itself, it could alter reported protein-protein interactions requiring the tail phospho cluster to be intact.

Chapter 3: The Effects of Phosphorylation on PTEN Function

Introduction

Phosphorylation of PTEN has been proposed to modulate many different PTEN functions including but not limited to: protein stability[100,129,131], plasma membrane recruitment[109,175], nuclear localization[62], modulating other posttranslational modifications (including ubiquitinylation[113,116,117], acetylation[189] and sumoylation[112]), altered catalytic activity[109,137], conformational changes[109,137] and altered protein-protein interactions[124,136,174]. Though it would be nice to examine all of these proposed phosphorylation dependent activities and functions with semisynthetic 4p-PTEN, the time required to do so would be prohibitive during the time span of a graduate student's thesis work. We instead decided to examine the most basic effects of PTEN phosphorylation on PTEN enzymatic activity, membrane binding ability and structural conformation. This work is outlined in the next three chapters of this thesis.

PTEN has been shown to possess phosphatase activity against both peptide and lipid substrates[34,94,119,135]. PTEN's activity to peptide substrates *in vitro* is very low and concrete evidence that these peptide substrates are legitimate PTEN substrates *in vivo* is weak[94]. On the other hand, PTEN activity to its lipid substrate PIP_3 is much higher *in vitro* and its lipid phosphatase activity has been linked to its tumor suppressor ability *in vivo*[18,34,119]. The majority of

studies involving PTEN catalytic activity have used soluble lipid PIP_3 substrates due to their ease of use. Soluble lipid substrates contain short aliphatic chains linked to the glycerol backbone of the lipid causing them to be monodispersed in aqueous solutions. While PTEN activity with soluble substrates is easier to study, these substrates may not capture functions of membrane embedded PIP_3. We therefore decided to examine PTEN enzymatic activity with long chain PIP_3 embedded in vesicles in addition to soluble substrates to get a better understanding of how phosphorylation affects PTEN functions when bound to membranes versus when it is in solution. One of the added advantages of performing an interfacial kinetic analysis for an interfacial enzyme such as PTEN is that the membrane binding affinity of the protein can be determined using steady state kinetic measurements.

There are several methods that can be used to directly measure a protein's ability to bind to phospholipid membranes including surface plasmon resonance (SPR)[190,191], fluorescence anisotropy[192,193], nuclear magnetic resonance (NMR)[194,195] and vesicle sedimentation experiments[51]. Several of these methods can be used to precisely determine the equilibrium binding constants of the protein of interest to the phospholipid membrane. Low technology techniques such as vesicle sedimentation assays are used to estimate the relative amount of protein bound to lipid membranes.

A very influential regulator of PTEN function *in vivo* has been shown to be the lipid composition of membranes[95,96,99,109,125,175,196]. The phospholipids PIP_2

and phosphatidylserine (PS) are particularly important[95,96,119,175]. PTEN localization at the plasma membrane is dependent on the amount of PIP_2 within the membrane[96,96]. PIP_2 also targets PTEN to vesicle membranes *in vitro*[51]. PTEN enzymatic activity is allostercially activated by PIP_2 as well[119]. The effects of PIP_2 are dependent on a native, structurally intact N-terminus of PTEN, corresponding to the first 15 amino acids of the protein[96,109]. PS also enhances PTEN's membrane binding ability and has been suggested to bind the C2 domain of PTEN specifically[99,119]. A number of point mutations on the membrane binding surfaces of both the phosphatase and C2 domain that disrupt PTEN's ability to bind membranes have been identified in tumors with increased signaling through the PI3K/PTEN/AKT signaling pathway[51,119].

In this chapter we characterize the enzymatic activity of the semisynthetic phosphorylated and unphosphorylated PTEN proteins discussed in the previous chapter with both soluble and membrane embedded PIP_3 substrates. Differences in membrane binding ability were examined using a vesicle sedimentation assay.

Methods

Soluble Substrate Activity Assay:

PTEN activity with a water soluble substrate (diC6-PIP_3) was determined by measuring the release of inorganic phosphate with a malachite green detection kit from R and D Biosystems[187,188]. 25 µL reactions were allowed to

proceed for 5-10 minutes at 30 ºC in assay buffer (50 mM Tris pH 8.0, 10 mM BME) before being quenched by malachite green reagent A according to the manufacture's protocol. Amounts of PTEN used per data point ranged from 0.5 to 20 µg. Reactions were shown to be linear with respect to time and enzyme concentration in the ranges used.

Generation of Radiolabed PIP_3:

Radiolabeled PIP_3 was generated as previously described[119]. PIP_3 labeled with $^{32}P_i$ at the 3'-position of the inositol ring was generated by incubating PI3K (Echlon) and PIP_2:PS (1:1) vesicles in the presence of 250 µCi γ-^{32}P-ATP, 1 mM ATP and 2.5 mM $MgCl_2$ in PI3K assay buffer (25 mM HEPES pH 7.6, 120 mM NaCl and 1 mM EGTA) for 1 hour. The total reaction volume was 500 µL. The reaction was stopped by the addition of 50 µL 3 M HCl. The radiolabeled PIP_3 was then isolated by performing a Bligh-Dyer extraction with chloroform:methanol:3 M HCl (1:2:1) in a 1 mL volumn[197]. Preparatory thin-layer chromatography (TLC) (Analtech) showed radiolabeled PIP_3 to be the major product by comparison to an unlabeled standard. The radiolabeled PIP_3 was visualized by exposure of the TLC plate to autoradiography film. The unlabeled PIP_3 was visualized by iodine staining. TLC plates were run in the following solvent conditions: [$CHCl_3$:Acetone:MeOH:Acetic Acid:H_2O]; [70:20:50:20:20].

Radiolabeled PIP_3 was stored in 95:5 chloroform:methanol at -20 °C for up to three weeks at a concentration of 4 mg/mL total lipid.

Vesicle Based Phosphatase Assays:

Lipid phosphatase assays were modified from those already described in the literature[119]. 3'-^{32}P-PIP_3 was incorporated into vesicles containing unlabeled PIP_3, Phosphatidylcholine (PC), and/or Phosphatidylserine (PS) and/or PIP_2 by sonication of dried lipids hydrated in the presence of 100 – 300 µL PTEN assay buffer (50mM Tris pH 8.0, 150 mM NaCl, 10 mM DTT, 1 mM EGTA). The specific activity of ^{32}P-PIP_3 ranged from 3 – 10 mCi/nmol PIP_3. Lipids were first dried under a stream of nitrogen in glass test tubes. The lipid film was then hydrated in assay buffer at 50ºC for 20 minutes. Lipids were sonicated in 100 µL volumes in glass test tubes at room temperature until the solution clarified. Depending on the amount of lipid in the tube this could take anywhere from 20 minutes to 2 hours. Vesicles made in this way are 30-50 nm in diameter[160,161]. Vesicles were used in assays within 15 min of being made. In assay reactions, the ratio of the number of vesicles to the number of PTEN molecules was maintained at 4:1 or greater. Ovalbumin (0.05 mg/mL) from Sigma-Aldrich was used to stabilize the PTEN protein in the assays. 25 µL reactions were initiated by the addition of vesicle substrate and incubated at 30ºC for 3 minutes. The reaction was quenched with 5 µL 3 M perchloric acid. Hydrolyzed $^{32}P_i$ was then separated from ^{32}P-PIP_3 by

using a Bligh-Dyer[197] extraction with $CHCl_3$, methanol and 3 M perchloric acid. The aqueous phase was then treated with 400 µL of 1% ammonium molybdate and the resulting phosphate-molybdate complex was extracted with 500 µL toluene:isobutanol (1:1). This organic phase was then counted using a Beckman scintillation counter.

Interfacial Kinetic Analysis:

Analysis of the kinetic parameters of the semisynthetic PTEN proteins were determined in accordance with the procedures pioneered by Dennis and coworkers and previously performed for recombinant PTEN produced in *E. coli*[119,154,156,159]. With this type of analysis, the initial velocity of an interfacial enzyme follows the equation below:

$$V_0 = (V_{max}*X_s*[S_0])/(i\mathit{K}_m*K_s + i\mathit{K}_m*[S_0] + X_s*[S_0])^{119,154} \quad 3.1$$

Here, X_s represents the mol percent of substrate within the lipid bilayer, $[S_0]$ is the total amount of substrate in the reaction, $i\mathit{K}_m$ is the interfacial K_m (expressed as a mol percent) and K_s is the dissociation constant of enzyme for vesicle membrane. Two types of experiments were performed, bulk dilution (BD) and surface dilution (SD). In BD experiments, the surface concentration of PIP_3 was held constant and the bulk concentration of PIP_3 was varied by adjusting the concentration of PIP_3 and the carrier lipid PC proportionately. In SD experiments, the bulk concentration of PIP_3 was held constant and the surface concentration

was varied by adjusting the amount of PC. In both types of experiments rectangular hyperbolas were obtained with apparent V_{max} and apparent K_m values. Apparent V_{max} and apparent K_m values were then fit to the equations below to determine the kinetic variables for each PTEN protein.

$$iK_m = (V_{max\ SD}/V_{max\ BD} - 1)X_s^{119,154} \qquad 3.2$$

$$K_s = K_{m\ BD}(Xs/ik_m + 1)^{119,154} \qquad 3.3$$

$$k_{cat} = V_{max\ SD}*[E_T]^{119,154} \qquad 3.4$$

Vesicle Pulldowns:

Large Multilamillar Vesicles (LMVs) containing various amounts of PC, PS and/or PIP_2 were generated by vigorously vortexing dried lipids that were hydrated in the presence of PTEN buffer for 5 minutes in 1 mL volumes. Lipids were dried under a stream of nitrogen in glass test tubes. The lipid film was then hydrated in assay buffer at 50ºC for 20 minutes. The LMVs were then incubated with 50 ng of the different forms of PTEN protein for 30 minutes at 25ºC. The vesicles and bound protein in 50 µL volumes were then pelleted at 180,000g using a Beckman ultracentrifuge for 2 hours at 4 °C. The supernatant was removed from the vesicle pellet and the pellet washed with buffer, then boiled in 10% SDS loading dye and run on a 10% SDS-PAGE gel. The amount of PTEN protein that bound to the LMVs was then visualized by Western blot using an

anti-PTEN antibody from Santa Cruz Biotechnologies (SC-6818). The primary antibody was diluted 1:1000 in 1% BSA (Sigma-Aldrich) in TBS/T and incubated overnight at 4 °C. The anti-goat secondary antibody (Santa Cruz) was diluted 1:10000 in 1% BSA in TBS/T and incubated for 1 hour at room temperature. The amount of PTEN bound was quantified using Carestream Media image quantification software.

Results

With phosphorylated 4p-PTEN and unphosphorylated n-PTEN successfully generated, we characterized the enzymatic activity of each semisynthetic protein to determine what effects tail phosphorylation may have on PTEN regulation. PTEN activity is most easily tested using water soluble PIP_3 substrates such as the diC6-PIP_3 (containing hexanoyl side chains) used in this study. The release of inorganic phosphate was monitored by the colorimetric malachite green assay. The progress of the reaction was determined to be linear with respect to time for both n-PTEN and 4p-PTEN (Figure 21A). The rate of the reaction was determined to be linear with respect to enzyme concentration for both proteins as well (Figure 21B). The K_m of n-PTEN for diC6-PIP_3 was determined to be 67 μM (Figures 22, 23A). The K_m of 4p-PTEN could not be determined as the plot of rate versus substrate concentration was linear up to 160 μM substrate (Figures 22, 23B). Comparing k_{cat}/K_m for each enzyme reveals about a 6-fold decrease in catalytic efficiency when the tail is phosphorylated.

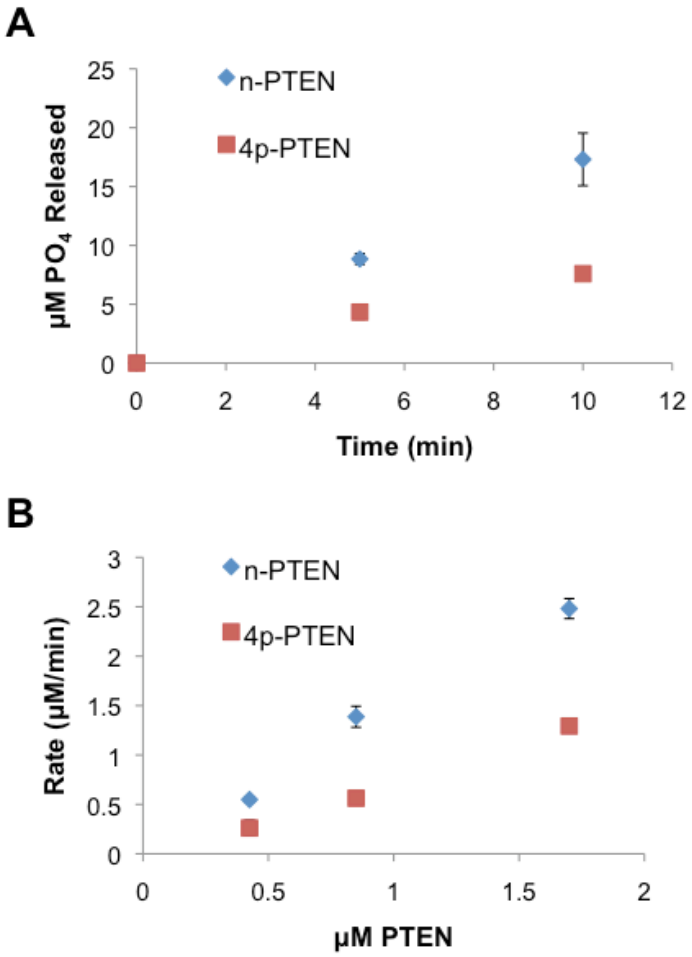

Figure 21. Semisynthetic PTEN phosphatase activity with diC6-PIP_3 substrate. The rate of the reaction is linear with respect to (A) time (750 nM PTEN) and (B) PTEN concentration. Phosphate release was measured using the Malachite green detection assay. The substrate concentration was 160 µM diC6-PIP_3. Data is represented as the mean +/- the SEM of three experiments performed in duplicate.

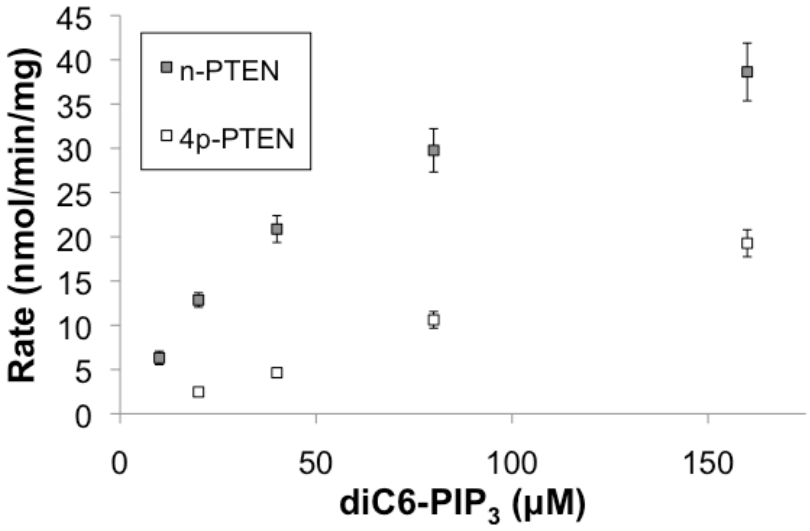

Figure 22. n-PTEN and 4p-PTEN K_m curves with diC6-PIP_3 substrate. PTEN concentrations ranges from 300 – 750 nM. Reaction times were 10 minutes. Data are reported as the mean +/- the SEM from three experiments performed in duplicate.

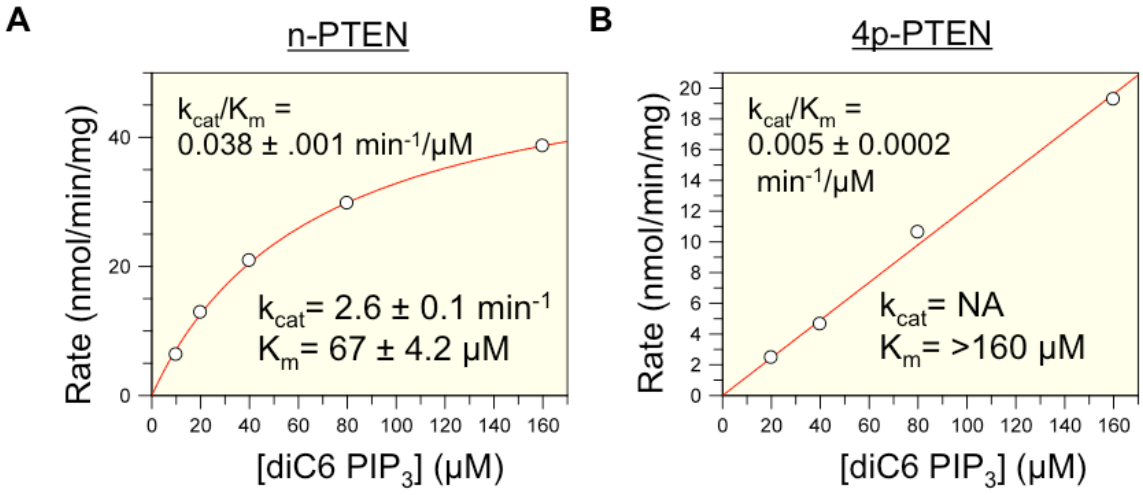

Figure 23. Non-linear regression analysis for n-PTEN and 4p-PTEN with diC6-PIP_3 substrate. (A) Steady-state kinetic analysis of n-PTEN. k_{cat} and K_m values were obtained by non-linear regression. (B) Steady-state kinetic analysis of 4p-PTEN. k_{cat}/K_m was determined from the slope of the line of rate versus substrate concentration as saturating substrate conditions were not achieved. Data is represented as the mean +/- the SEM of three experiments performed in duplicate.

While it was interesting to observe changes in enzymatic activity caused by tail phosphorylation with respect to a soluble substrate, soluble PIP_3 is not a natural PTEN substrate as PIP_3 *in vivo* contains long aliphatic side chains (C-18) and is embedded in cellular membranes. We therefore decided to study PTEN activity to PIP_3 (containing palmitoyl side chains) integrated into lipid vesicles containing a carrier lipid. As described in Chapter 1 and the methods section, interfacial enzymes such as PTEN do not follow standard Michaelis-Menten kinetics given that they do not act on soluble substrates. Instead the initial rate of interfacial enzymes follows the equation below:

$$V_0 = (V_{max}*X_s*[S_0])/(i\mathit{K}_m*K_s + i\mathit{K}_m*[S_0] + X_s*[S_0])^{119,154} \quad 3.1$$

Here X_s is the mol fraction of lipid substrate in the lipid bilayer, S_0 is the bulk or total substrate concentration, K_s is the dissociation binding constant of enzyme for vesicle and $i\mathit{K}_m$ is the interfacial K_m[119,148,154,155]. X_s and $i\mathit{K}_m$ are expressed in terms of the mol % of substrate while S_o and K_s are expressed as μM concentrations. Interfacial enzymes are dependent on both the total concentration of substrate in a reaction and the surface concentration of substrate within the lipid bilayer[119,148,154,155]. Therefore two types of experiments must be performed to determine the steady state constants outlined above. The first is a bulk dilution experiment in which the surface concentration of substrate is held constant while the bulk concentration is varied by adjusting the amount of substrate and carrier lipid proportionately. The second is a surface dilution experiment in which the bulk concentration of substrate is held constant at

saturating levels while the surface concentration is varied by adjusting the amount of carrier lipid. Both bulk dilution and surface dilution experiments yield rectangular hyperbola with apparent V_{max} and apparent K_m values that are then fit to a series of equations outlined in the methods section to calculate the steady state constants outlined above.

The correct determination of initial rates for interfacial enzymes depends on finding a carrier lipid into which the substrate lipid is incorporated that has neither inhibitory or stimulatory affects on the enzyme. Therefore, any changes in rate can be attributed directly to changes in substrate concentration when varying the amount of carrier lipid for bulk and surface dilution experiments. Fortunately, this type of interfacial, surface dilution kinetic analysis had been performed previously for PTEN produced as an N-terminal GST tagged protein in *E. coli* by McConnachie et al[119]. This study identified phosphatidylcholine (PC) as an appropriate carrier lipid for studying PTEN interfacial kinetic activity. These authors also identified that PTEN operates in the “hopping” mode of interfacial catalysis; meaning PTEN binds transiently to vesicles rather than binding essentially irreversibly (at least for the duration of the reaction) to vesicles as “scooting” enzymes do. A “hopping” enzyme will bind briefly to a vesicle, turning over one or several molecules of substrate, then detach from the vesicle before every molecule on that vesicle is converted to product. Conversely, “scooting” enzymes will remain bound to a vesicle, converting every molecule of substrate to product.

The malachite green detection assay proved to be incompatible with the high concentrations of lipid required for an interfacial kinetic analysis of PTEN. We therefore decided to use a radioactive assay that had been previously used in the literature[119]. Radiolabeled PIP_3 was generated by phosphorylating PIP_2 with γ−[^{32}P]-ATP using PI3-Kinase. [^{32}P]-PIP_3 was purified by Bligh-Dyer extraction and incorporated in the PC vesicles along with unlabeled PIP_3 by sonication of dried lipids in the presence of assay buffer. [^{32}P]-PIP_3 was the major product as determined by thin layer chromatography (Figure 24). Sonicated vesicles are typically 25 – 50 nm in diameter. By considering the diameter of the vesicles and the amount of lipid in each reaction, the approximate total number of vesicles in each reaction can be calculated. In every reaction the vesicle to enzyme ratio was kept equal to or greater than 3 to 1. The rate of the reaction was linear with respect to enzyme concentration for n-PTEN, 4p-PTEN and t-PTEN (Figure 25). Allowing the reaction to go to completion reveals that ~60% of the substrate could be hydrolyzed (Figure 26A). The percent turnover of the reaction could be pushed to nearly 100% by forcing the fusion of vesicles with BSA (Figure 26B). This established that the [^{32}P]-PIP_3 substrate was properly incorporated into vesicles with only about 50% of the substrate being available for hydrolysis in the outer membrane of the bilayer. It is expected that for small sonicated vesicles the amount of substrate in the outer layer of the vesicle would be slightly larger than 50% given that the diameter of the outer layer is larger than that of the inner layer of the vesicle membrane[119,160]. These experiments also ensure that n-PTEN, 4p-PTEN and t-PTEN are operating in the “hopping”

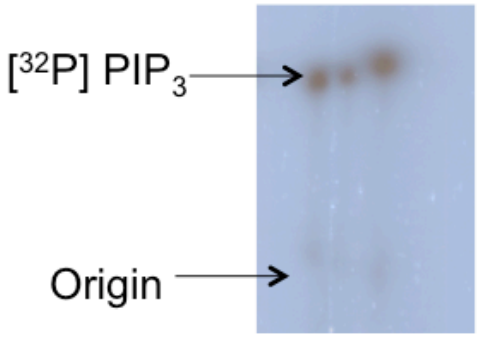

Figure 24. Generation of [^{32}P]-PIP_3. ^{32}P labeled PIP_3 was the major product generated by phosphorylating PIP_2 with ^{32}P-ATP using PI3-Kinase as visualized by autoradiography after running the radiolabeled lipid on thin layer chromatography. [$CHCl_3$:Acetone:MeOH:Acetic Acid:H_2O]; [70:20:50:20:20].

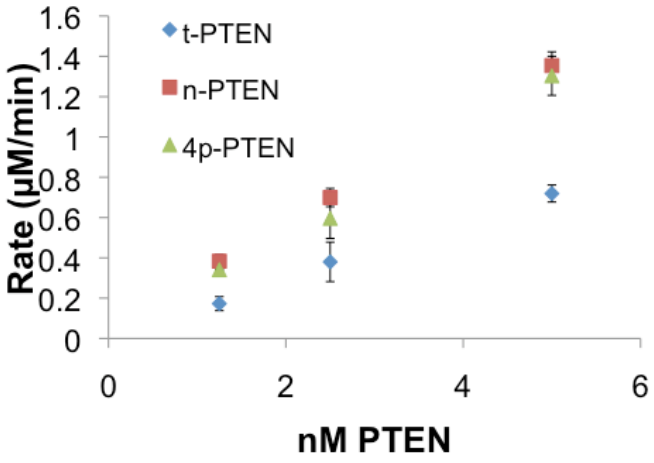

Figure 25. PTEN phosphatase activity with radiolabled palmitoyl PIP_3 substrate incorporated into phosphatidylcholine vesicles. Velocity is linear with respect to enzyme concentration. Vesicle substrate contained 1% (50 μM) PIP_3. Reactions proceeded for 3 minutes. Data are reported as the mean +/- the S.D. of three experiments preformed in duplicate.

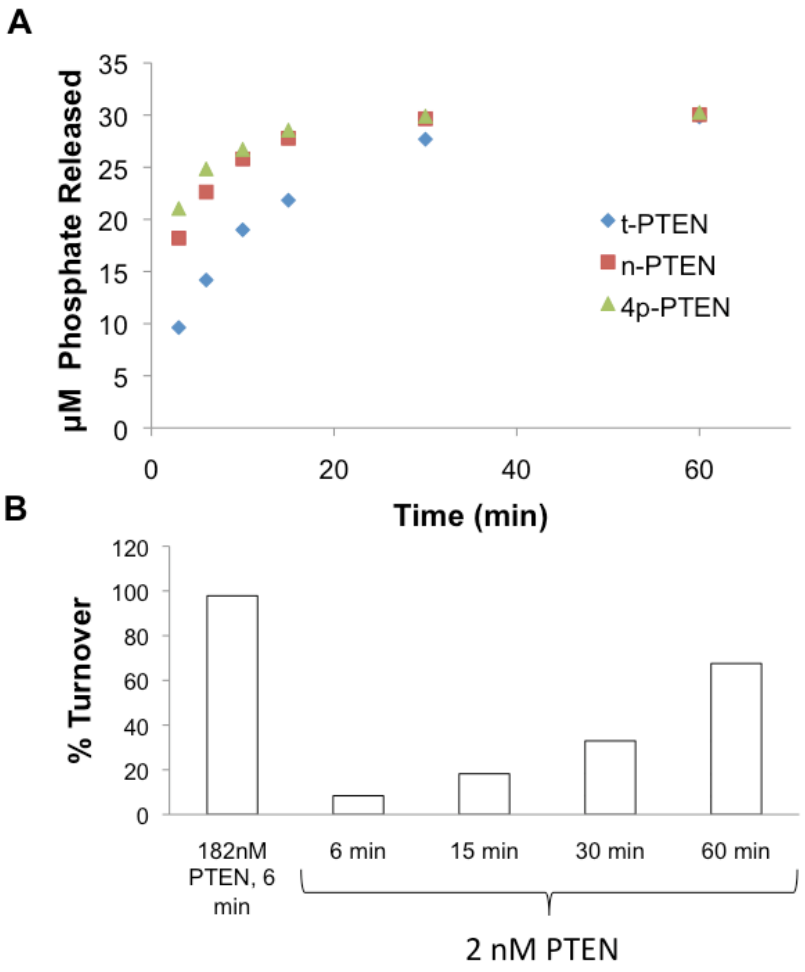

Figure 26. PTEN is acting on PIP_3 incorporated into vesicle substrates. (A) 2.5 nM n-PTEN, 4p-PTEN and t-PTEN consume up to ~30 μM PIP_3 in vesicles generated by sonication containing a total of 50 μM PIP_3. (B) The percent of the reaction that can be consumed can be pushed to ~100% by the addition of 0.15 mg/mL BSA to each reaction. BSA causes the fusion of vesicles and the exchange of lipid between vesicles.

mode of catalysis given that the number of vesicles always out numbers the number of PTEN molecules. If any of the different forms of PTEN were not operating the hopping mode, the reaction progress should have stopped prior to reaching ~50% turnover.

Bulk dilution curves, holding the concentration of PIP_3 constant at 1 mol %, yield expected rectangular hyperbolas for n-PTEN and 4p-PTEN (Figure 27A). From these plots it was determined that 50 μM bulk concentrations of PIP_3 was nearly saturating. 50 μM PIP_3 was therefore used as the constant bulk concentration of PIP_3 while the surface concentration was varied in surface dilution experiments. Plots of the surface dilution experiments show apparent substrate inhibition at higher surface concentrations of PIP_3 (>1 mol %) for both n-PTEN and 4p-PTEN (Figure 27B). This made it difficult to directly measure V_{max} for these conditions. Nevertheless, apparent V_{max} values were extrapolated from fitting the first four data points of the surface dilution curves to a nonlinear regression curve fitting program (Figure 28). Using the apparent V_{max} and apparent K_m values from both bulk and surface dilution experiments (Figure 28), the kinetic constants from equation 3.1 above were determined and are displayed in Table 1. The interfacial kinetic analysis reveals that there is no change in the iK_m with little difference in k_{cat} conferred by PTEN tail phosphorylation. There is however about a 3-fold increase in the K_s for 4p-PTEN, suggesting the binding affinity to vesicle is decreased when PTEN is

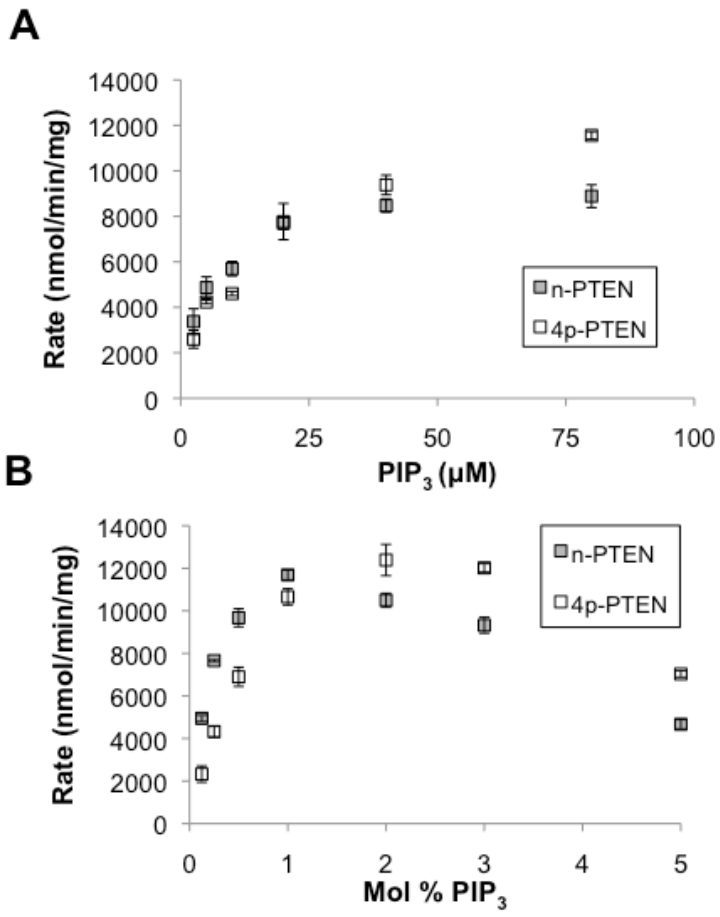

Figure 27. Interfacial kinetic analysis of n-PTEN and 4p-PTEN. (A) In the bulk dilution experiment enzymatic activity for n-PTEN and 4p-PTEN was measured at a fixed surface concentration of 1% PIP_3 while the bulk concentration was varied. (B) In the surface dilution experiment activity was measured at a fixed bulk concentration of 50 μM PIP_3 while the surface concentration was varied. Data are reported as the mean +/- the SEM from three experiments performed in duplicate.

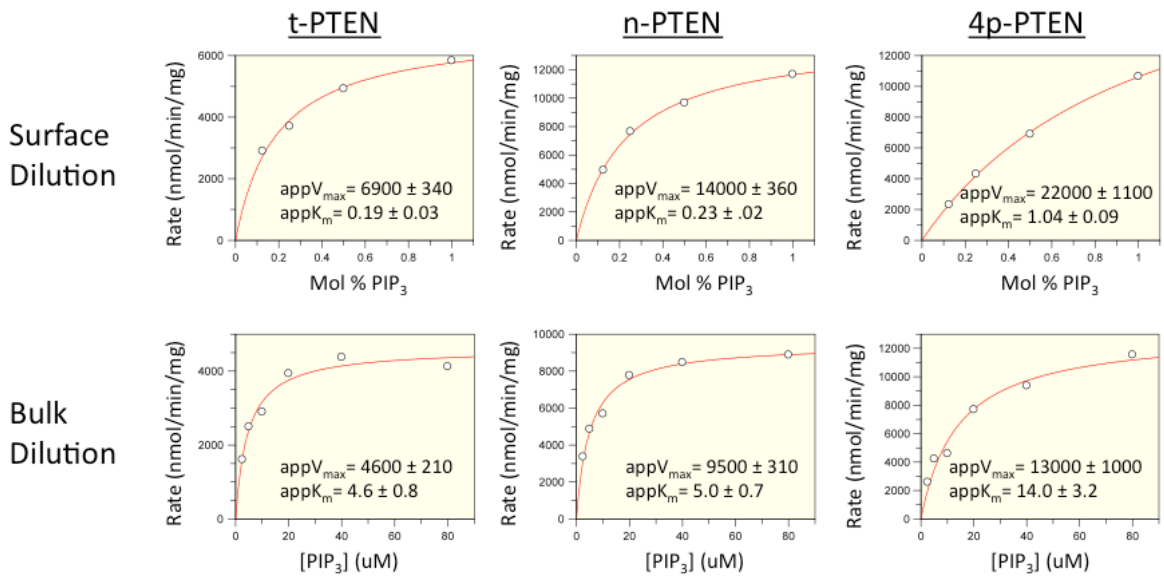

Figure 28. Interfacial kinetic data for semisynthetic PTENs obtained by non-linear regression analysis. Apparent k_{cat} and apparent K_m values were obtained by non-linear regression analysis for each form of PTEN for surface dilution experiments (top row) and bulk dilution experiments (bottom row). Apparent k_{cat} and apparent K_m values were then fit to the equations in the methods section to obtain the interfacial kinetic parameters in tabulated in Tables 1 and 2.

	iK_m (mol %)	K_s (mM Lipid) (1 mol % PIP_3)	k_{cat} (s^{-1})
n-PTEN	0.52 ± 0.04	1.49 ± 0.14	11.22 ± 0.3
4p-PTEN	0.59 ± 0.10	4.06 ± 0.75	16.96 ± 0.9

Table 1. Summary of the interfacial kinetic analysis of n-PTEN and 4p-PTEN. Data are reported as the mean +/- the SEM from three experiments performed in duplicate. Apparent V_{max} values were obtained from the best fit curves from the first four points of the surface dilution experiments.

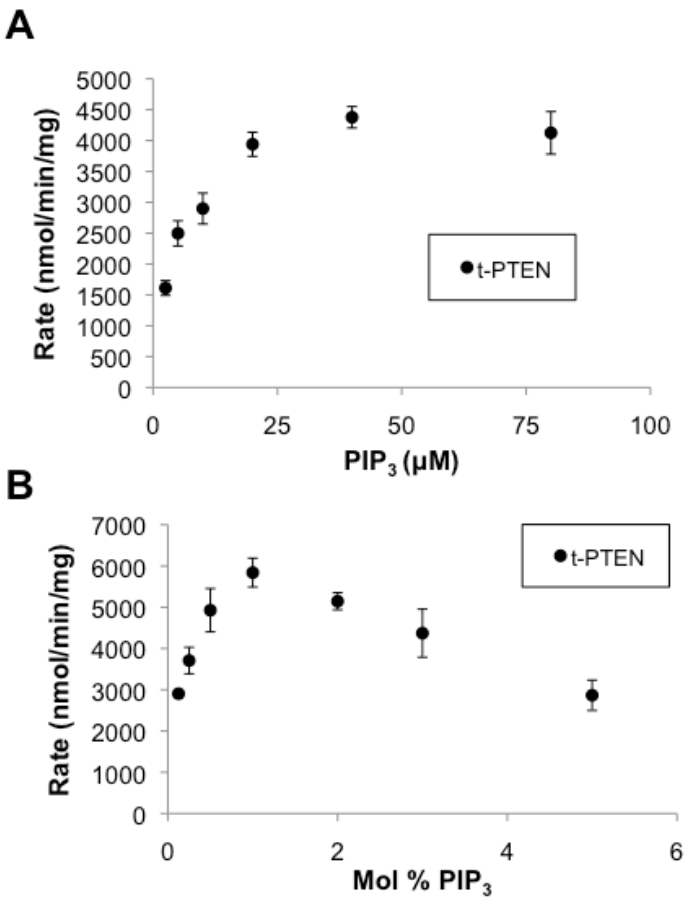

Figure 29. Interfacial kinetic analysis of t-PTEN. (A) In the bulk dilution experiment, enzymatic activity for t-PTEN was measured at a fixed surface concentration of 1% PIP_3 while the bulk concentration was varied. (B) In the surface dilution experiment, activity was measured at a fixed bulk concentration of 50 μM PIP_3 while the surface concentration was varied. Data a represented as the mean +/- the SEM of three experiments performed in duplicate.

	$i\mathit{K}_m$ (mol %)	K_s (mM Lipid) (1 mol % PIP_3)	k_{cat} (s^{-1})
t-PTEN	0.49 ± 0.06	1.45 ± 0.21	5.03 ± 0.3

Table 2. Summary of the interfacial kinetic analysis of t-PTEN. Data are reported as the mean +/- the SEM from three experiments performed in duplicate. Apparent V_{max} values were obtained from the best fit curves from the first four points of the surface dilution experiments.

phosphorylated (Table 1). This same analysis was performed for t-PTEN (Figure 29). The iK_m for t-PTEN was similar to that of n-PTEN and 4p-PTEN while the K_s is similar to that of n-PTEN and lower than that of 4p-PTEN (Table 2). This would suggest that the unphosphorylated tail doesn't play a significant role affecting PTEN activity in the context of vesicle embedded substrate. It is important to note that the activity of 4p-PTEN is lower than that of n-PTEN at low surface concentrations of PIP_3 (Figure 30). At higher surface concentrations, 4p-PTEN has activity equal to or greater than n-PTEN at PIP_3 levels greater than 1% (Figure 30).

Given that the major differences between n-PTEN and 4p-PTEN were observed in the values of K_s in the interfacial kinetic analysis, we wanted to corroborate these differences using a more direct measurement of membrane binding ability using a vesicle sedimentation assay. This assay uses western blot analysis to determine the amount of PTEN protein that binds to and sediments with phospholipid vesicles upon centrifugation. The anionic phospholipids PIP_2 and phosphatidylserine (PS) have been shown to enhance PTEN recruitment and binding to membranes[95,96,99,119]. Phosphatidylcholine vesicles incorporated with increasing amounts of PIP_2 and PS enhanced the amount of both n-PTEN and 4p-PTEN that bound to and sedimented with the vesicles (Figures 31, 32). In all conditions tested, the amount of 4p-PTEN that bound the vesicles was significantly less than the amount of n-PTEN for the same amount of PIP_2 or PS, thus corroborating the membrane affinity differences deduced from the interfacial

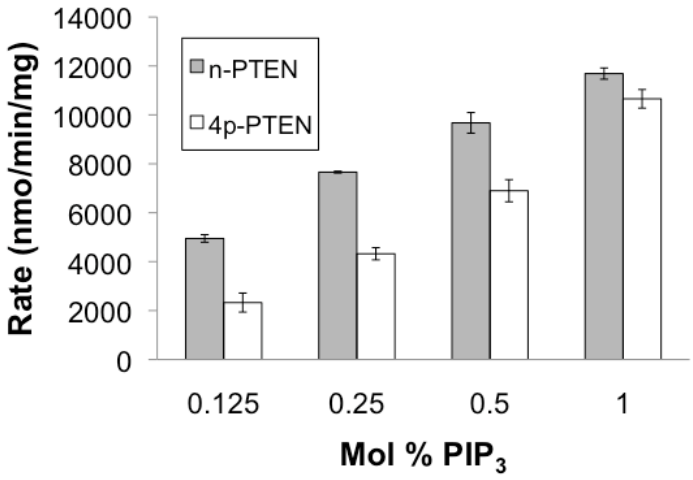

Figure 30. Relative activity of n-PTEN and 4p-PTEN at low PIP_3 concentrations. PTEN activity was measured against a fixed bulk PIP_3 concentration of 50 μM while varying the surface concentration of PIP_3 and PC. Data are reported as the mean +/- the SEM from three experiments performed in duplicate.

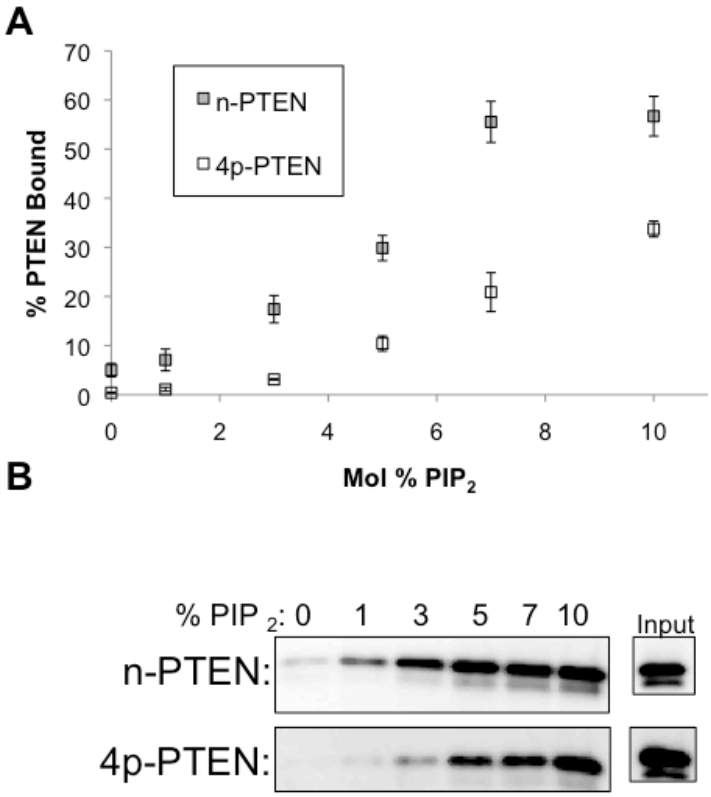

Figure 31. n-PTEN and 4p-PTEN binding to large multilamellar vesicles (LMVs) containing PIP_2. (A) The percent of n-PTEN and 4p-PTEN bound to sedimented phosphatidylcholine LMVs incorporated with PIP_2 was determined by quantification of western blot bands using an anti-PTEN antibody (SC-6818, Santa Cruz). Data are reported as the mean +/- the SEM of three separate experiments. (B) Representative blots of the percent of n-PTEN and 4p-PTEN bound to sedimented phosphatidylcholine LMVs incorporated with PIP_2.

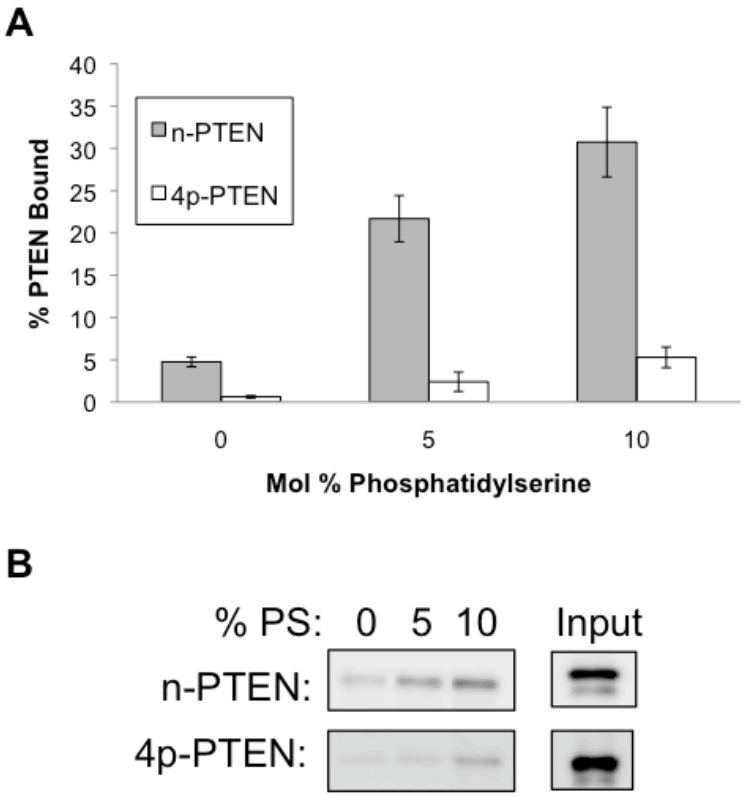

Figure 32. n-PTEN and 4p-PTEN binding to large multilamellar vesicles (LMVs) containing PS. (A) The percent of n-PTEN and 4p-PTEN bound to sedimented phosphatidylcholine LMVs incorporated with PS was determined by quantification of western blot bands using an anti-PTEN antibody (SC-6818, Santa Cruz). Data are reported as the mean +/- the SEM of three separate experiments. (B) Representative blots of the percent of n-PTEN and 4p-PTEN bound to sedimented phosphatidylcholine LMVs incorporated with PS.

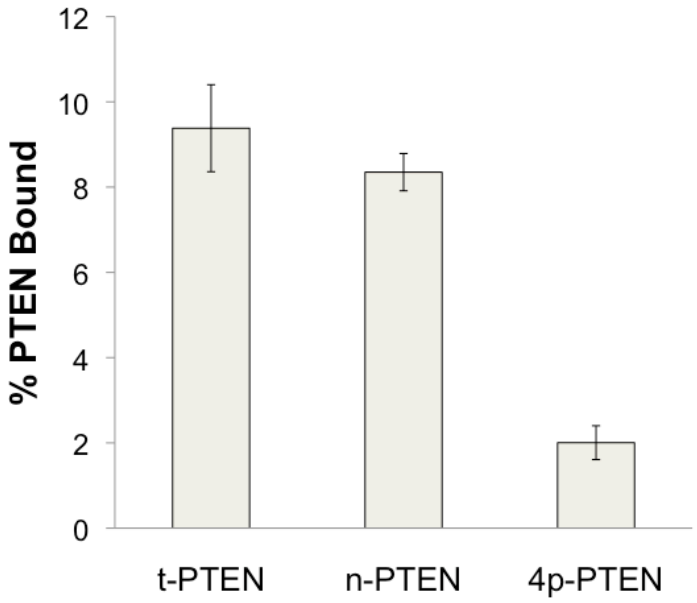

Figure 33. t-PTEN, n-PTEN and 4p-PTEN binding to LMVs. PTEN binding to phosphatidylcholine LMVs containing 2% PIP_2. Data are reported as the mean +/- the S.D.

enzyme kinetic activity analysis. t-PTEN behaved similarly to n-PTEN (Figure 33).

At this point it was clear that the phosphorylated tail of PTEN was having an inhibitory effect on the ability of PTEN to bind membranes and therefore access its substrate, causing a reduction in enzymatic activity. It has been reported that the phospho-tail may able to exert its mode of regulation *in trans*; meaning if it were detached from the PTEN molecule it may still be able to inhibit PTEN enzymatic and membrane binding activities. We thus tested the ability of the detached PTEN tail peptides (phosphorylated and unphosphorylated) to inhibit the activity of t-PTEN against a soluble substrate. We identified that the phosphorylated 25mer tail peptide is a potent inhibitor of t-PTEN *in trans* with an IC_{50} of about 1 μM (Figure 34A).The unphosphorylated tail peptide demonstrated less than 20% inhibition at 10 μM (Figure 34A, B). Characterization of t-PTEN reveals that it possesses similar catalytic activity to n-PTEN with a slightly lower K_m of about 33 μM (Figure 35). In the presence of 1 μM of the phosphorylated 4p-25mer tail, the k_{cat}/K_m of t-PTEN for diC6-PIP_3 is elevated to about the same level as 4p-PTEN (Figures 23, 35) (4p-PTEN: k_{cat}/K_m = 0.005 min^{-1}/μM; t-PTEN + 1 μM 4p-25mer: k_{cat}/K_m = 0.006 min^{-1}/μM). The phosphate release in the presence of phosphopeptide inhibitor was linear with respect to time and enzyme concentration (Figure 36). Additionally, the 4p-25mer phosphopeptide was also able to reduce the amount of t-PTEN that sedimented with 1% PIP_2 vesicles. The amount of t-PTEN that pelleted with the vesicles was reduced to about 50% in

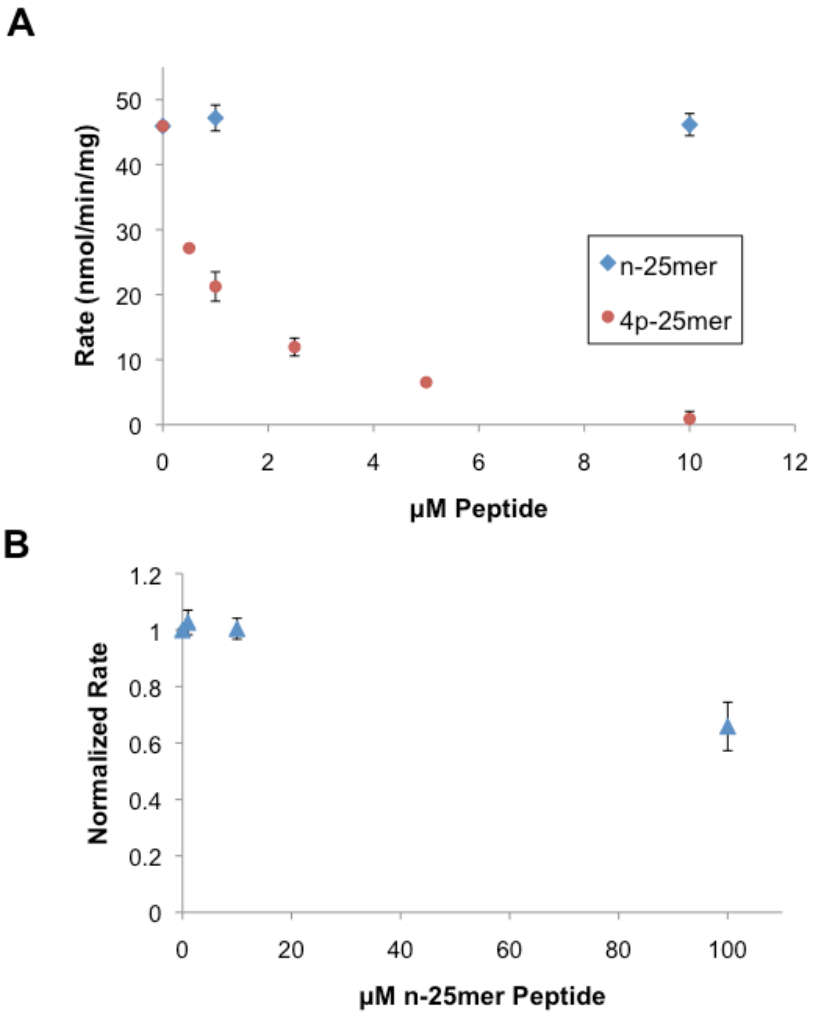

Figure 34. *In trans* inhibition of t-PTEN activity with tail peptides. Activity is measured with 160 μM diC6-PIP_3 substrate. (A) IC_{50} curve of t-PTEN treated with phosphorylated 25mer or unphosphorylated 25mer tail peptide. (B) IC_{50} curve of t-PTEN treated with higher concentrations of unphosphorylated 25mer tail peptide. Data points are represented as the mean +/- the S.D. of three experiments in duplicate.

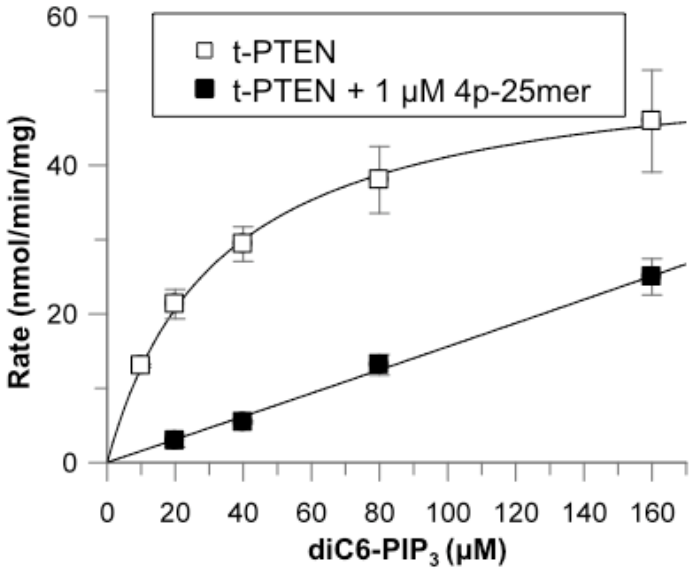

Figure 35. Characterization of t-PTEN with diC6-PIP_3 substrate in the absence and presence of 1 µM 4p-25mer phosphopeptide. K_m curve for t-PTEN with k_{cat} (2.9 +/- 0.1 min-1) and K_m (33 +/- 2 µM) values determined from nonlinear regression analysis. In the presence of 1 µM 4p-25mer phosphopeptide k_{cat}/K_m = 0.006 min^{-1}/µM for t-PTEN, similar to 4p-PTEN (k_{cat}/K_m = 0.005 min^{-1}/µM). Data are represented as the mean +/- the S.D. of three experiments performed in duplicate.

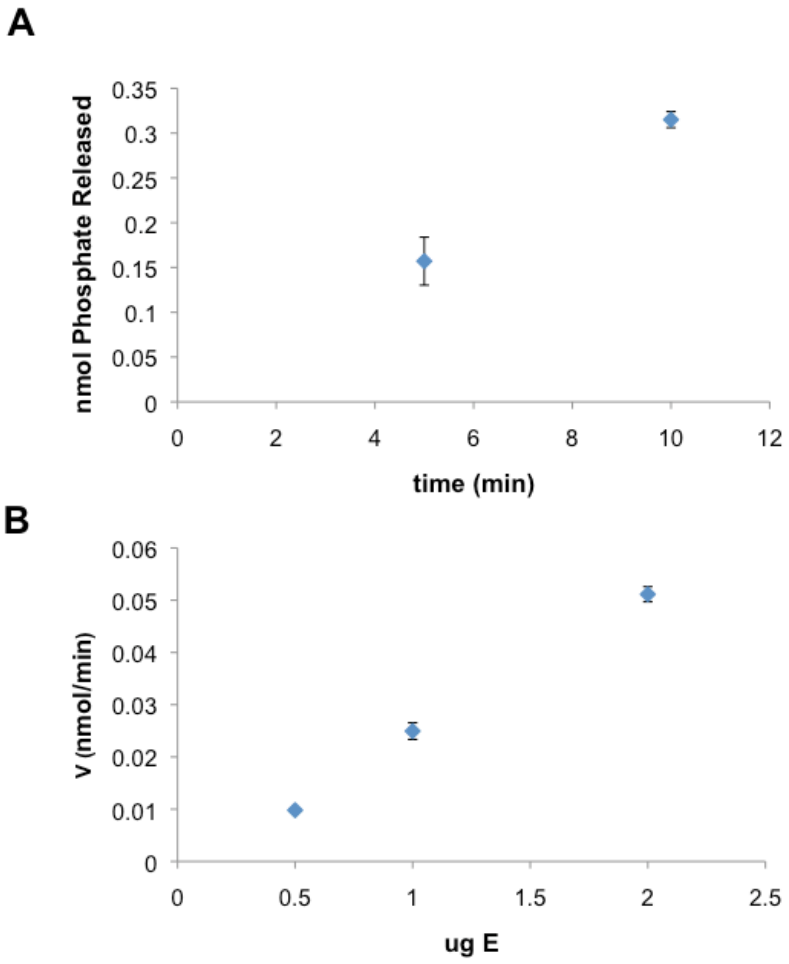

Figure 36. Characterization of t-PTEN in the presence of phospho-peptide. (A) Product vs time and (B) velocity vs enzyme concentration plots of t-PTEN in the presence of 1 μM 25mer phospho-peptide. Data are represented as the mean +/- the S.D. of two experiments performed in duplicate.

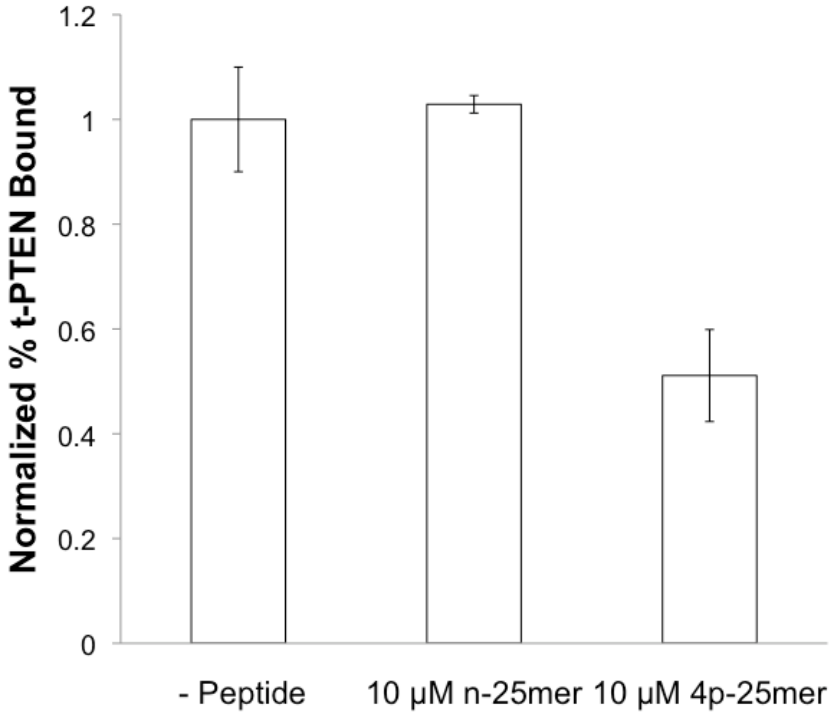

Figure 37. Vesicle sedimentation of t-PTEN in the presence of n- and 4p-25mer tail peptides. Data are represented as the mean +/- the S.D. of at least three replicates.

the presence of 10 μM phosphopeptide (Figure 37). The fact that the same 4p-25mer phosphopeptide is not as potent an inhibitor in the vesicle binding assay compared to the soluble substrate assay suggests that the phosphopeptide may be competing with membrane binding surfaces on the body of PTEN.

PIP_2 and PS have been reported to activate the enzymatic activity of recombinant, unphosphorylated PTEN produced in *E. coli* when incorporated into phospholipid vesicles[119]. It is unknown what effect if any these anionic lipids would have on phosphorylated PTEN. These lipids are reported to activate PTEN only at low surface concentrations of PIP_3. At higher surface concentrations there is less of a stimulatory effect suggesting that the anionic nature of the PIP_3 substrate itself is activating. At 0.01% PIP_3 in PC vesicles very low amounts of PIP_2 are needed to have large activating affects on PTEN with the maximal effect being approximately 100-fold at 1% PIP_2 (Figure 38A). Both 4p-PTEN and n-PTEN are equally activated by PIP_2 with the activation plot closely resembling the surface dilution plots of PIP_3 discussed previously (Figure 27B). Just like the surface dilution plot, the PIP_2 activation plot shows 4p-PTEN being less active than n-PTEN at lower PIP_2 concentrations (<1%) but having equal to or greater activity at higher PIP_2 concentrations (>1%) (Figure 38A). Similarly, there is also apparent inhibition of enzymatic activity at PIP_2 concentrations greater than 1% for both enzymes (Figure 38A). This suggests a similar mechanism of inhibition. PS also activated both n-PTEN and 4p-PTEN to an equal extent though it was much less potent and efficacious than PIP_2 (Figure 38B). PS only stimulated

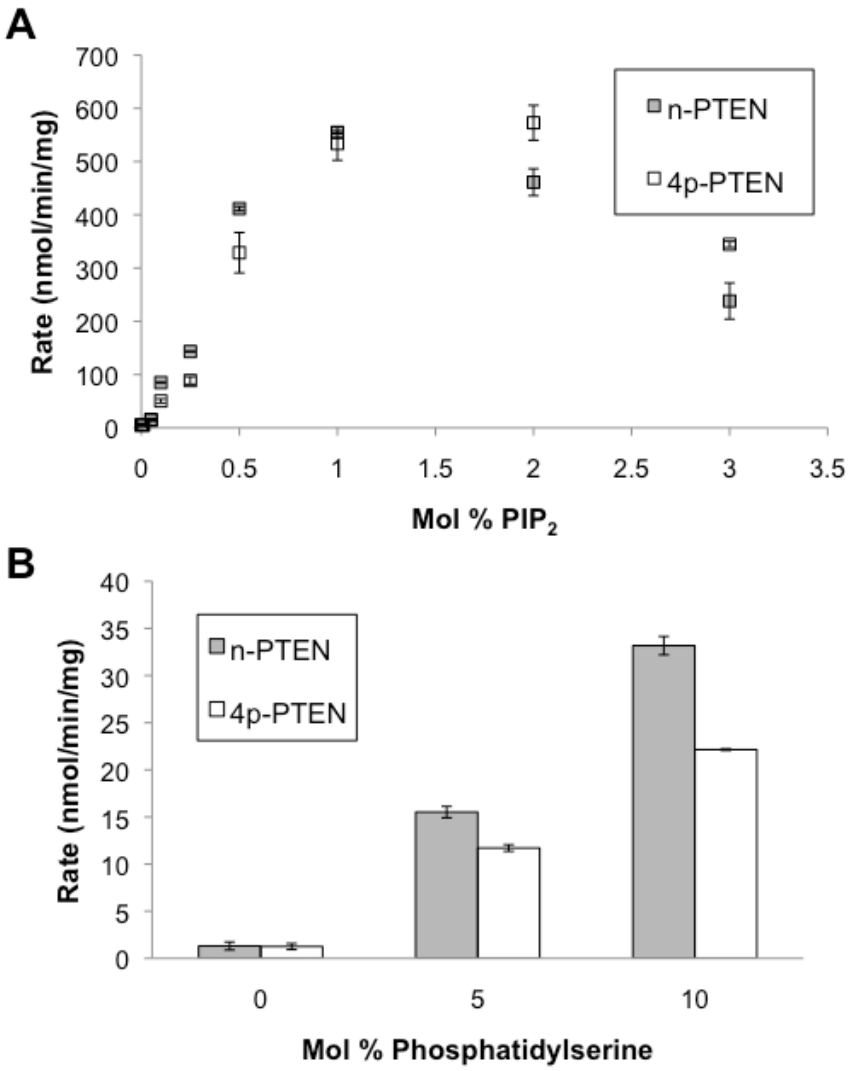

Figure 38. Anionic lipid stimulation of n-PTEN and 4p-PTEN. At a low surface concentration of PIP_3 (0.01%) incorporated vesicles, (A) PIP_2 and (B) Phosphatidylserine stimulate the enzymatic activity of n-PTEN and 4p-PTEN. Data are reported as the mean +/- the SEM of three experiments performed in duplicate.

PTEN activity about 15-fold at 10% PS (Figure 38B). There was no observed activity inhibition at the PS levels tested.

It is interesting that at the very low PIP_3 concentrations (0.01%) in the absence of PIP_2 or PS, the activity of n-PTEN and 4p-PTEN are approximately equal. Figure 30 shows that the difference in activity between the two increases as the surface concentration of PIP_3 decreased. It would therefore be expected that 4p-PTEN should still have lower activity than n-PTEN at 0.01% PIP_3 but that is not what is observed. We think this is likely an artifact of the assay. At these very low substrate concentrations there would be a significant number of vesicles containing no substrate at all. Given that n-PTEN binds to all vesicles more tightly than 4p-PTEN (Figures 31, 32), 4p-PTEN would be able to "hop" from vesicle to vesicle more easily while n-PTEN remains bound to vesicles containing no substrate for longer periods of time. 4p-PTEN would therefore be able to access more substrate than n-PTEN, resulting in the apparent equal activity seen here. This shouldn't be relevant *in vivo* given that the plasma membrane is one contiguous membrane and PTEN is not known to bind to any other cellular membrane.

Discussion

The differences in membrane binding affinity between n-PTEN and 4p-PTEN, calculated in the surface dilution kinetic analysis and corroborated with

the vesicle sedimentation assay, demonstrate clearly for the first time that phosphorylation of the S380/T382/T383/S385 tail cluster results in a direct loss of membrane binding affinity without involvment of any other protein. Exactly how tail phosphorylation achieves this effect remains to be determined. It is intriguing that with respect to soluble substrates, the K_m for n-PTEN is much lower than it is for 4p-PTEN but the interfacial K_m is identical for both proteins when PIP_3 is incorporated into lipid membranes. This suggests that the conformation of both proteins is the same when PTEN is bound to the vesicle membrane but that phosphorylation causes a conformational change when the enzyme is in solution. Conformational changes associated with PTEN tail phosphorylation are examined in the next chapter of this thesis.

The cause of the apparent substrate inhibition observed in the surface dilution experiments is unknown. Given that the percent turnover of the reactions was kept under 10% and that the product of the reaction PIP_2 activates rather than inhibits PTEN it is unlikely that the decreased rates are due to product inhibition. Similar patterns of inhibition are observed in the PIP_2 activation curves at levels greater than 1%. This effect is not due to decreased membrane binding given that increasing amounts of PIP_2 cause increased binding of PTEN up to 10% PIP_2 in the vesicle sedimentation assay. It is possible that the inhibition is due to the increase in vesicle binding of PTEN. If the apparent substrate inhibition is due to increased vesicle binding it would be expected that 4p-PTEN would be less affected than n-PTEN given that it has lower membrane binding

affinity. Supporting this hypothesis are the observations that inhibition of catalytic activity is observed for n-PTEN at lower PIP_3/PIP_2 concentrations than it is observed for 4p-PTEN. At greater than 1% PIP_3/PIP_2, there is increased 4p-PTEN activity compared to n-PTEN where substrate inhibition is observed. Also, there was no observable substrate inhibition for soluble PIP_3 at the concentrations tested suggesting this phenomena is vesicle dependent. PTEN may bind to membranes in a conformation that has lower enzymatic activity at very high substrate and PIP_2 concentrations. This apparent substrate inhibition is likely not relevant *in vivo* since the cellular levels of PIP_3 probably don't approach the higher levels used in this *in vitro* assay.

Enzymatic activity decreases for 4p-PTEN at a faster rate than n-PTEN as the surface concentration of PIP_3 decreases, therefore increasing the rate differential between the two as the concentration of PIP_3 drops. This is important because cellular concentrations of PIP_3 are thought to be at levels less than 0.001%[119]. It would therefore be expected that phosphorylated PTEN should be less active than unphosphorylated PTEN *in vivo* under physiologically relevant conditions. Conversely, this also suggests that phosphorylated PTEN can be more quickly activated as needed by the cell when PIP_3 concentrations increase. Phosphorylation may therefore allow the cell to keep PTEN in a less active state most of the time, only to activate it with increasing substrate concentrations as needed. At 1% PIP_3 both n-PTEN and 4p-PTEN appear to have the same activity. While total levels of PIP_3 don't reach anywhere near 1% of the total

plasma membrane composition, it may be that localized PIP_3 concentrations in lipid rafts and other membrane signaling clusters do approach this level. If this is the case, phosphorylation may have little effect on PTEN activity in these membrane regions.

We find that PIP_2 stimulates PTEN activity about 100-fold over basal levels. This is more than 10-fold higher than was previously reported[119]. This inconsistency may be due to the fact that in the previous study recombinant PTEN was produced in *E. coli* with an N-terminal GST tag. This tag was later cleaved off with a protease leaving a non-native N-terminus on the PTEN protein. The N-terminus of PTEN has been implicated in PIP_2 binding[95,96,119]. Having additional amino acids at the N-terminus of PTEN may therefore prevent optimal PIP_2 binding and subsequent activation. Because the semisynthetic PTEN proteins generated in this study posses a native N-terminus, the ~100-fold activation measured here may be more accurate than the ~8-fold activation measured in the previous study.

It is intriguing that PIP_2 activates both n-PTEN and 4p-PTEN about 100-fold over basal levels while phosphorylation of PTEN appears to inhibit activity more modestly. This raises interesting questions. Is phosphorylation the major regulator of PTEN activity as many research studies have suggested? Or does the lipid composition of the plasma membrane play a more important role in PTEN regulation? Certainly if phosphorylated and unphosphorylated PTEN behave similarly *in vivo* as they do in these *in vitro* studies, one could argue that

lipids play a more important role than phosphorylation. As mentioned previously, PTEN is thought to be phosphorylated under most conditions with few examples of its phosphorylation state being regulated. The phosphorylation state of PTEN has not been found to be modulated during signaling events through the PI3K/PTEN/AKT signaling pathway. Yet there must be a way PTEN is recruited to signaling domains at the plasma membrane. Our data and others would suggest that lipids likely play an important role in this. There have been several studies on the importance of the N-terminal PIP_2 binding motif as well as the membrane binding surface of the C2 domain[51,95,96]. Without these regions, PTEN appears to be unable to bind to the plasma membrane. Gao et al. recently found that PTEN preferentially associates with non-lipid raft regions of the plasma membrane[198]. It has also been shown that PTEN associates preferably with the lagging edge of chemotaxing cells[95,96]. It is likely that lipids play a major role in these examples.

But if phosphorylation plays only a minor role in regulating PTEN enzymatic activity, why is PTEN phosphorylated at all? It is possible that phosphorylation plays a more important role in regulating PTEN functions other than enzymatic activity. Phosphorylated PTEN has been proposed to be more stable than its unphosphorylated counterpart. The A4 phosphocluster mutant appears to be degraded by the proteasome faster than wild type[129,131]. Interestingly, NEDD4-1, one E3 ubiquitin ligase responsible for ubiquinating PTEN, is located at the plasma membrane[199–201]. It may be that tail

phosphorylation serves to keep PTEN off of the plasma membrane when it is not needed to prevent it from being ubiquitinated and subsequently degraded. Additionally there are several proteins that have been proposed to interact with PTEN in a manner that is dependent on the phosphorylation state of PTEN. These proteins include p85[122,136], Myosin V[124], MAGI[174], neutral endopeptidase[123] and p-rex2a[202,203].

While the 100-fold activation of PTEN caused by PIP_2 is larger than the difference in activity conferred by tail phosphorylation *in vitro*, these values could be different *in vivo*. It is possible that the presence of other proteins and/or lipids could either exaggerate or decrease the activation caused by PIP_2 or the deactivation caused by tail phosphorylation.

Chapter 4: The Effects of Phosphorylation on PTEN Structure

Introduction

One of the mechanisms by which phosphorylation by a kinase relays an intracellular signaling event is by inducing a conformational change in the phosphorylated target protein that modulates its function in some manner. The majority of these conformational changes involve minor structural changes such as the phosphorylation of the flexible activation loop of a kinase leading to its activation. However, there are several examples of proteins that undergo major conformational changes upon phosphorylation by a kinase. Several examples include: Src[204–206], CrkL[207] and SHP-1/2[208,209]. In the case of the Src kinase, C-terminal phosphorylation at Tyr527 causes an intramolecular conformational change in which the phosphorylated Tyr527 binds to Src's SH2 domain, leading to inactivation of the protein[204–206].

The cellular localization and stability changes associated with PTEN phosphorylation have been proposed to be due to a change in PTEN's conformation caused by phosphorylation on its C-terminal tail[109,137]. The best evidence to date of a phosphorylation induced conformational change for PTEN has been demonstrated by the co-immunoprecipitation of the body of PTEN with the wild type phosphorylatable C-terminal tail. In these experiments, the body of PTEN (aa 1-352) and the wild type C-terminal tail (aa 353-403) were co-

expressed in eukaryotic cells and shown to immunoprecipitate with one another[109,137]. PTEN tail peptides with four alanine mutations at the S380/T382/T383/S385 phosphorylated cluster did not immunoprecipitate the body. While this did raise the possibility of a phosphorylation induced conformational change in PTEN, it did not rule out that the interaction between the body and tail of PTEN was being mediated by a secondary cellular protein. It also did not definitively demonstrate that phosphorylation was necessary for this intermolecular interaction. It is possible that the mutation of the C-terminal tail tetra alanine mutant rather than the absence of phosphorylation was the cause of the loss of co-immunoprecipitation between the two segments.

As discussed in the previous chapter, purified unphosphorylated n-PTEN and phosphorylated 4p-PTEN were determined to have several distinct kinetic and biochemical characteristics such as significantly different K_m values for soluble PIP_3 substrates as well as different membrane binding affinities. Taken together, this may suggest that PTEN undergoes a conformational change when its tail is phosphorylated. In the present chapter we use a variety of techniques to better characterize this conformational change including partial trypsin proteolysis, anion exchange chromatography, sensitivity to alkaline phosphatase and small angle X-ray scattering (SAXS). We demonstrate that relative to n-PTEN, phosphorylated 4p-PTEN is in a more compact state that is caused by the phosphorylated tail binding to the main body of PTEN.

Methods

Anion Exchange Chromatography:

The semisynthetic PTEN protein was further purified for SAXS and other biochemical experiments by anion exchange chromatography (monoQ) using an ACTA FPLC from GE Healthcare. Proteins were purified with a gradient of 0-50% Buffer B over 250 mL at a flow rate of 1.0 mL/min. (Buffer A: 50 mM Tris pH 8.0, 10 mM DTT; Buffer B: 50 mM Tris pH 8.0, 1.0 M NaCl, 10 mM DTT).

Trypsin Digests:

2 µg of semisynthetic PTEN in 20 µL reactions volumes was digested with varying amounts of trypsin (Promega, V511A) for 10 minutes at 37ºC in PTEN assay buffer. Reactions were quenched with SDS loading dye and run on 10% SDS-PAGE gel. The digestion fragments were visualized by Colloidal Blue stain from Invitrogen (LC6025) or by western blot analysis (antibodies SC-6818 or NBP1-44412). Primary antibodies were diluted 1:1000 in 1% BSA in TBS/T and incubated with the membrane overnight at 4 °C. Secondary antibodies were diluted 1:10000 in 1% BSA in TBS/T and incubated with the membrane for 1 hour at room temperature.

Sequencing of Trypsin Digest Fragments:

Trypsin digestion products were run on a 10% SDS PAGE gel and transferred to a PVDF membrane. The membrane was then stained with Coomassie stain for 30 seconds. The bands of interest were cut out of the membrane and analyzed by N-terminal Edman degradation sequencing[210,211] at the JHMI Synthesis and Sequencing Facility.

Phosphatase Sensitivity Assay:

50 ng of semisynthetic phosphorylated PTEN and its mutants were dephosphorylated in the presence of 1 μM alkaline phosphatase from NEB (CIP) for varying periods of time in phosphatase assay buffer (50 mM Tris pH 8.0, 20 mM NaCl, 25 μM $MgCl_2$ and 10 mM DTT) at room temperature in 20 μL reactions. Reactions were quenched with SDS loading dye and run on SDS-PAGE. Dephosphorylation of PTEN was monitored by western blot with an antibody to the phospho-tail cluster (NBP1-4136). The fraction of phospho-PTEN remaining was determined using Carestream Media image quantification software.

Small-Angle X-ray Scattering (SAXS):

SAXS experiments were performed at Brookhaven National Laboratories at the National Synchrotron Light Scource (NSLS), beamline X9 using a MarCCD

detector, located 3.4 m from the sample. Data for each protein sample was collected in triplicate. All samples were in PTEN assay buffer. 20 µL of each sample was continuously passed through a capillary tube exposed to a 400 x 200 µm X-ray beam and data recorded for 30 s. Normalization for beamline intensity, buffer subtraction and merging of data were carried out using proc.py software developed by the beamline staff[212].

SAXS data analysis was carried out using software from the ATSAS program suite. The radius of gyration (R_g) was calculated using a Guinier approximation with the program PRIMUS[171]. The pair distribution function P(r) and the maximun particle dimension (D_{max}) were determined using GNOM[169]. Ten *ab initio* models were generated for each protein using DAMMIF, then averaged using DAMAVER[167,168,170]. The resulting molecular envelopes were fit with the tailless crystal structure in PyMOL. Figures of the models were made using PyMOL[213].

Results

Though it had been proposed that PTEN undergoes a conformational change upon phosphorylation, phosphorylation induced changes in structure had yet to be analyzed with an intact PTEN molecule as prior to our work here. The first evidence we observed for an intramolecular PTEN conformational change came from the FPLC purification of the semisynthetic proteins by anion exchange

chromatography. Contrary to expectations, 4p-PTEN eluted at an earlier volume (~70 mL) on anion exchange chromatography than n-PTEN (~105 mL) (Figure 39). This is unexpected since the more negatively charged species 4p-PTEN, compared with n-PTEN, should have higher affinity for the positively charged anion exchange resin. The most likely explanation for this is that the four phosphates on the S380/T382/T383/S385 cluster are concealed from the anion exchange resin in a binding interaction with the body of PTEN (Figure 40). In the case of n-PTEN, the tail contains about twenty negative charges (due mostly to a high number of Asp and Glu residues) with only two positive charges, likely allowing the tail to interact with the positively charged resin. When the tail is phosphorylated PTEN presumably undergoes a conformational change in which the phospho cluster is concealed, burying many of the other negative charges on the tail as well. It has been established in the literature that clusters of charges on a protein can be more important than the net charge in dictating the elution volume of the protein with respect to ion exchange chromatography[214,215].

n-PTEN elutes from the anion exchange column initially at ~105 mL in one large peak followed by several smaller peaks (Figures 39, 41A, B). This is likely due to the presence of heterogeneous phosphorylation of the portion of the PTEN protein expressed within High Five insect cells. Two of these phosphorylation sites are Thr366 and Ser370 as determined by western blot with an antibody to these two sites (Figure 42). This antibody reveals that the later elution peaks for n-PTEN are more heavily phosphorylated at these sites than

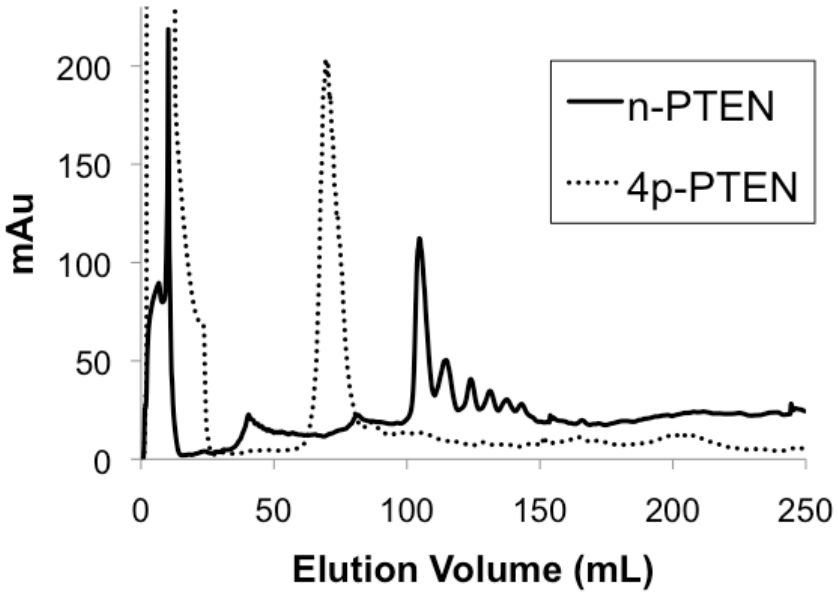

Figure 39: FPLC purification of n-PTEN and 4p-PTEN by anion exchange chromatography. Proteins were purified using a mono-Q column. With a gradient of 0-50% Buffer B over 250 mL on an anion exchange column, 4p-PTEN elutes in one peak at ~70 mL while n-PTEN elutes at ~100 mL in a series of peaks at 280 nm. Buffer A: 50 mM Tris pH 8.0, 5 mM NaCl, 5 mM DTT. Buffer B: 50 mM Tris pH 8.0, 1 M NaCl, 5 mM DTT.

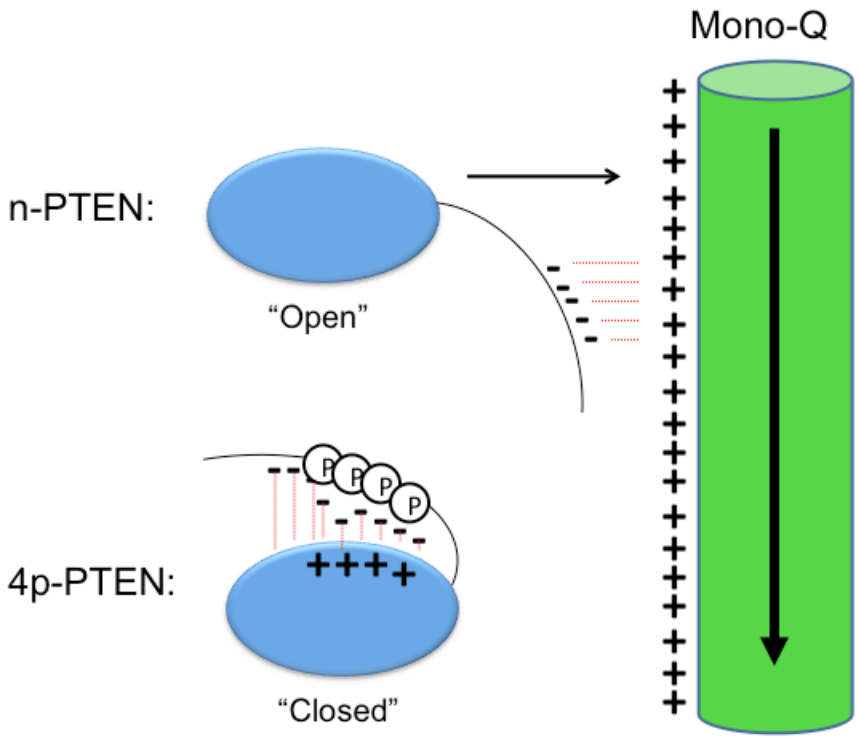

Figure 40: Model for the paradoxical elution pattern 4p-PTEN. 4p-PTEN may elute from the anion exchange column prior to n-PTEN even though it possesses an additional eight negative charges because phosphorylation of the C-terminal tail has caused a conformational change in which the negatively charged tail of PTEN is concealed in an intramolecular binding interaction with the main body of PTEN, preventing it from interacting with the positively charged anion exchange resin.

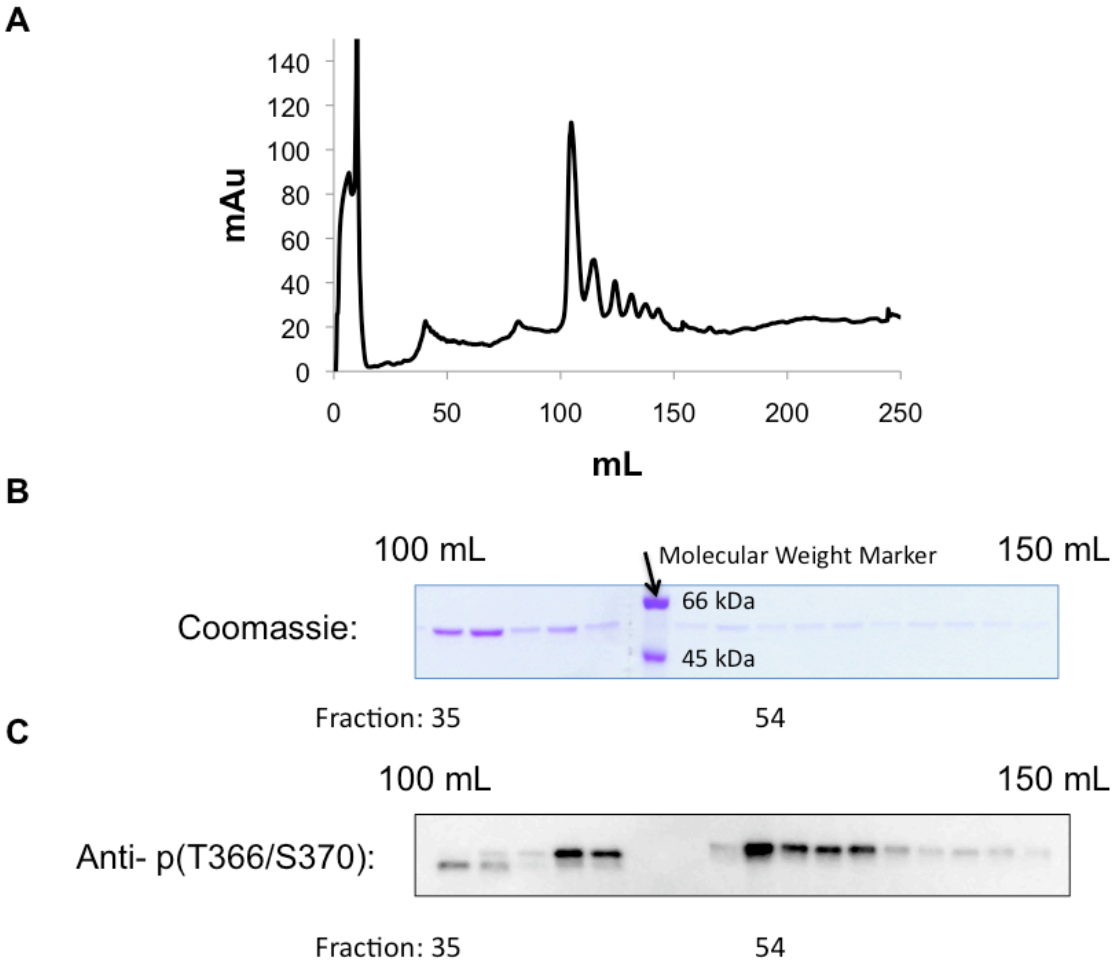

Figure 41: Purification of n-PTEN by anion exchange chromatography. (A) With a gradient of 0-50% Buffer B over 250 mL, n-PTEN elutes from the column initially at ~100 mL in a series of peaks. Buffer A: 50 mM Tris pH 8.0, 5 mM NaCl, 5 mM DTT. Buffer B: 50 mM Tris pH 8.0, 1 M NaCl, 5 mM DTT. (B) Coomassie stained gel of fractions from the chromatogram of n-PTEN above. (C) Western blot of the elution fractions from the chromatogram above with an antibody to phosphorylated T366 and S370. Primary dilution: 1:1000 in 1% BSA in TBS/T. Secondary dilution: 1:10,000 in 1% BSA in TBS/T.

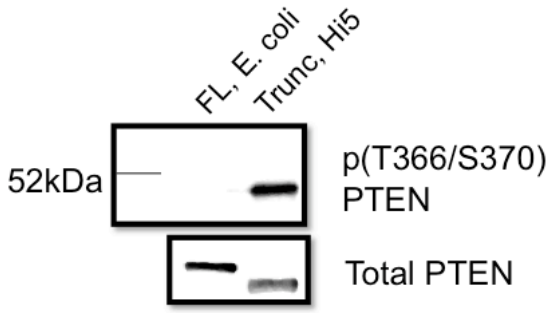

Figure 42: PTEN produced in High Five insect cells is phosphorylated at T366 and/or S370. An antibody recognizing phosphorylated T366 and S370 reveals that PTEN produced in insect cells is phosphorylated at these sites but PTEN produced in *E. coli* is not. Full length PTEN: aa 1-403. Truncated PTEN: aa 1-378.

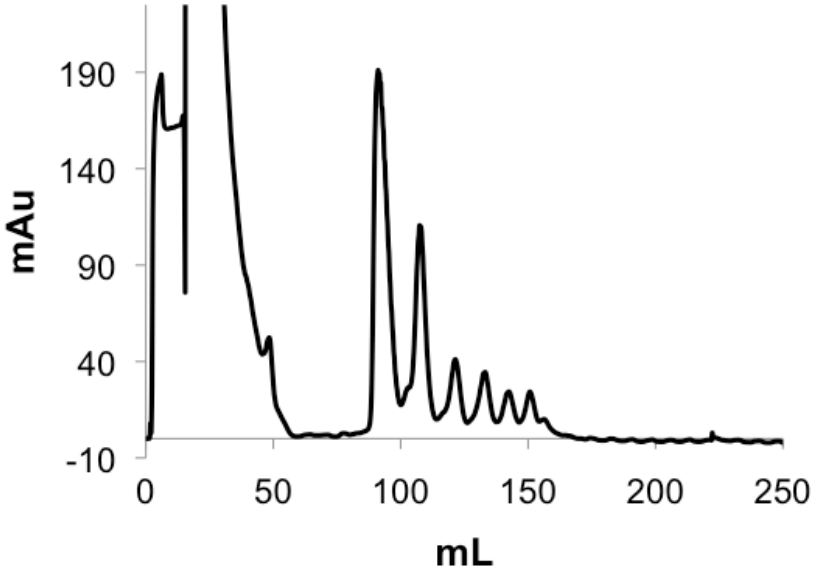

Figure 43: Purification of t-PTEN by anion exchange chromatography. With a gradient of 0-50% Buffer B over 250 mL, t-PTEN elutes from the column initailly at ~90 mL in a series of peaks. Buffer A: 50 mM Tris pH 8.0, 5 mM NaCl, 5 mM DTT. Buffer B: 50 mM Tris pH 8.0, 1 M NaCl, 5 mM DTT.

earlier fractions (Figure 41C). There may be other posttranslational modifications as the presence of phosphorylation at Thr366 and/or Ser370 can account for up to four peaks. There are several other Ser and Thr residues on the tail of PTEN that could be phosphorylated within the insect cells as well. Ser363 has been reported to be phosphorylated by CK2 *in vitro*[108]. 4p-PTEN elutes as a single peak, suggesting that the endogenous phosphorylation sites are concealed during the conformational change. Similar to n-PTEN, t-PTEN elutes as a series of several peaks (Figure 43).

Partial trypsin digestion is a well established method used to study protein conformational changes at a macroscopic level[216–218]. The partial digestion of n-PTEN and 4p-PTEN reveal that 4p-PTEN is more stable to proteolysis than is n-PTEN (Figure 44A). There are several bands visible by colloidal blue staining that are readily observed in the n-PTEN digestion but not in the 4p-PTEN digestion. These bands are highlighted by asterisks in Figure 44. One possible explanation for the detection of these fragments with n-PTEN but not 4p-PTEN is that these Lys or Arg residues are involved in binding the phosphorylated tail directly and therefore cannot be accessed by trypsin during the digestion reaction. These three bands were sequenced using N-terminal Edman degradation. The identity of the cleavage sites were determined to be R15, R84 and R161.

In order to gain more information as to what portions of the PTEN molecule are protected to trypsin proteolysis by tail phosphorylation, the

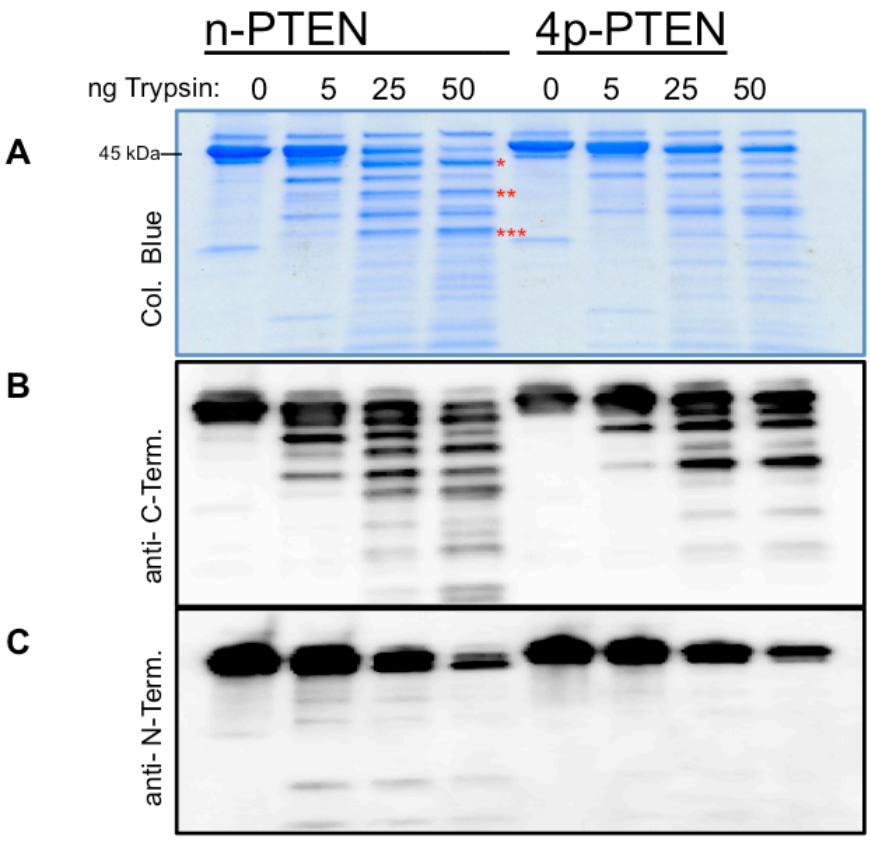

Figure 44: Limited proteolysis of semisynthetic PTEN with trypsin. 2 µg of n-PTEN and 4p-PTEN were digested with varying amounts of trypsin then visualized by (A) colloidal blue staining or by western blot with an antibody to the (B) C-terminus (anti-phospho T366/S370, Novus Biological) or (C) N-terminus (N-19, Santa Cruz Biotechnology) of PTEN. Primary Ab dilution: 1:1000 in 1% BSA in TBS/T. Secondary Ab dilution: 1:10,000 in 1% BSA in TBS/T. Asterisks denote bands that are in higher abundance in the digestion of n-PTEN compared to 4p-PTEN. N-terminal sequencing of these bands identifies the cleavage sites as (*) R15, (**) R84 and (***) R161.

digestion products were subjected to western blot using antibodies to the N- and C-terminus of the protein. The N-terminal antibody which recognizes only the first 19 amino acids of PTEN reveals only the highest molecular weight fragments still contain this epitope (Figure 44C). Conversely an antibody to the C-terminal tail reveals that nearly every fragment still contains the tail of PTEN (Figure 44B). Taken together this suggests that the phosphatase domain rather than the C2 domain is resistant to trypsin proteolysis upon C-terminal tail phosphorylation in 4p-PTEN.

There are several examples of phosphorylation of proteins causing conformational changes such as with Src[204–206], CrkL[207] and SHP-1/2[208,209]. The conformational switching induced by phosphorylation can be measured as a function of the protein's sensitivity to alkaline phosphatase removal of these conformational change inducing phosphorylations[206]. In theory, when PTEN is in the "closed" conformation, then the tail phosphates should be less sensitive to alkaline phosphatase removal than when PTEN is in the "open" conformation due to phosphate concealment in a binding interaction (Figure 45). The removal of tail phosphates can be monitored over time with an antibody to the tail phospho-cluster. We attempted to use this assay to measure the equilibrium between the "open" and "closed" forms of PTEN. 4p-PTEN would serve as "closed" PTEN but a good control for "open" PTEN was not readily available. We attempted to blot the 25mer phospho PTEN tail directly by binding it to commonly used western

blotting membranes. However due to its small molecular weight and highly charged state it could not be bound to any membrane tested. In a related approach, the phospho-tail peptide was ligated to CTPS1 (CTP Synthetase 1) by expressed protein ligation then bound to a membrane and blotted. This resulted in the phospho cluster having reduced sensitivity to alkaline phosphatase under high salt conditions (10 mM $MgCl_2$), not increased as expected. Serendipidously we found that repeated freeze thaw cycles 4p-PTEN led to denaturation of the protein and greatly increased sensitivity to alkaline phosphatase. Treating natively folded 4p-PTEN with 1 μM alkaline phosphatase resulted in about a 50% decrease in tail phosphorylation over 60 min (Figure 46A, C). Treating denatured 4p-PTEN with the same amount of alkaline phosphatase resulted in near complete removal of the phospho cluster in about 15 min. When the amount of alkaline phosphatase was reduced to 0.5 μM, the denatured form of the enzyme had about 50% its tail phosphates removed in 5 min (Figure 46 B, C). Assuming the rate of removal of tail phosphates follows a pseudo-first order mechanism, then the equilibrium between the “open” and “closed” states of PTEN is at least 25:1 favoring the “closed” conformation. Another interesting aspect of this assay is that in the presence of high concentrations of magnesium (10 mM) the rate of phosphate removal for both native and denatured 4p-PTEN is equal. One explanation for this is that Mg^{2+} binds to the negatively charged tail and disrupts its interaction with the body of PTEN, allowing it to be more readily dephosphorylated by alkaline phosphatase.

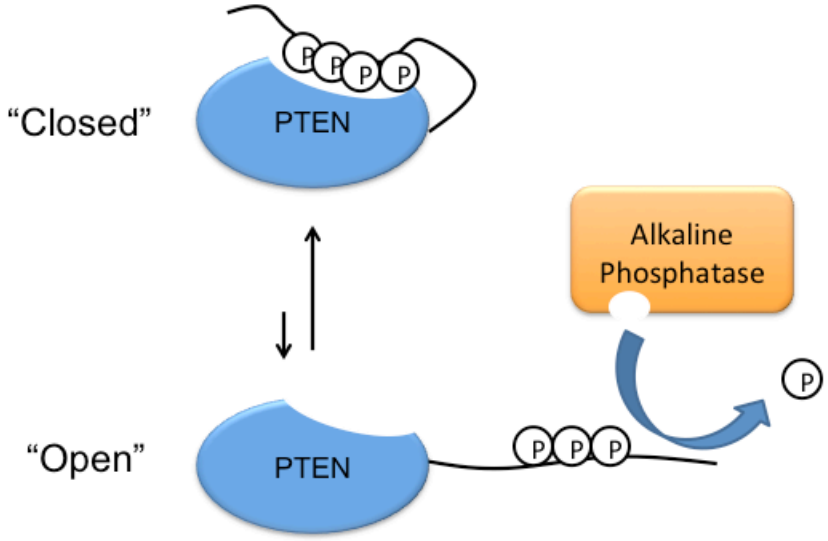

Figure 45: Alkaline phosphatase sensitivity assay. 4p-PTEN exists in two simplified conformational states. In the "closed" conformation the C-terminal tail of 4p-PTEN will be unable to be dephosphorylated by alkaline phosphatase, while in the "open" conformation it can be readily dephosphorylated.

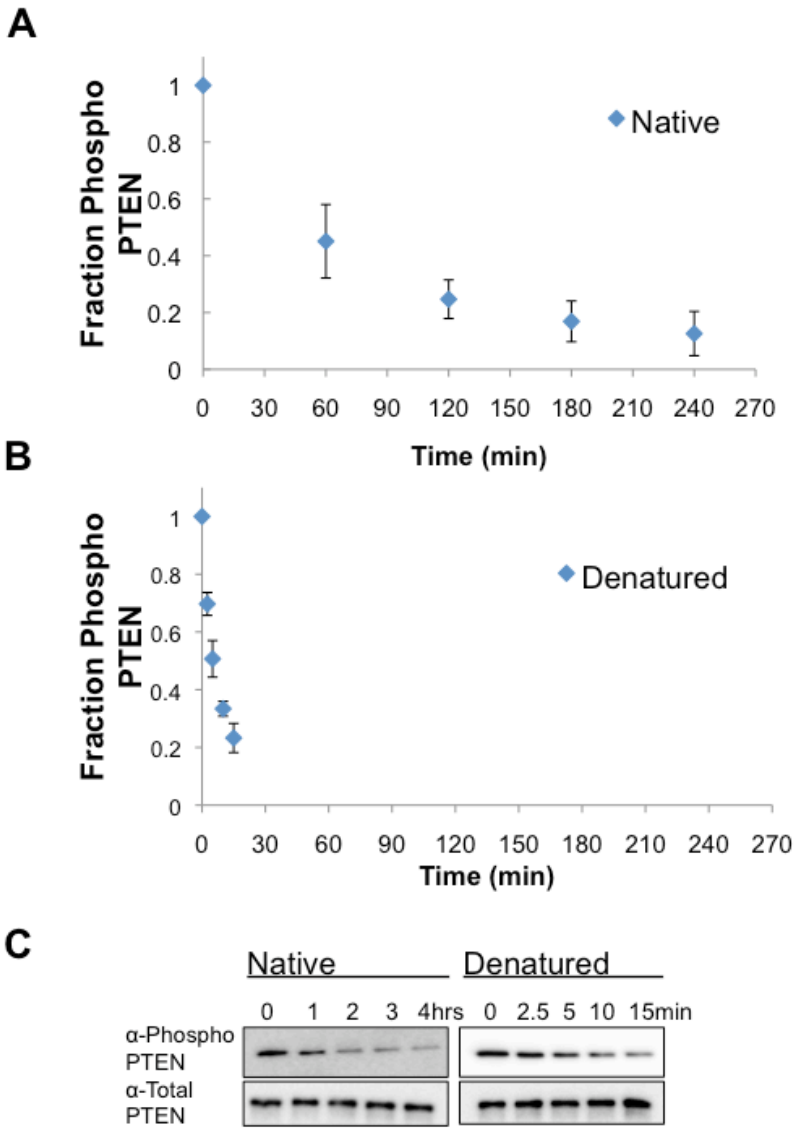

Figure 46: Natively folded versus denatured 4p-PTEN sensitivity to alkaline phosphatase. (A) Natively folded 4p-PTEN show approximately 50% removal of tail phosphorylation with 1 uM alkaline phosphatase in 60 minutes. (B) Denatured 4p-PTEN shows approximately 50% removal of tail phosphorylation with 0.5 uM alkaline phosphatase in 5 minutes. (C) Representative western blots of the alkaline phosphatase hydrolysis of C-terminal tail phosphorylation of PTEN from the graphs shown above. Primary dilution: 1:1000 in 1% BSA in TBS/T. Secondary dilution: 1:10,000 in 1% BSA in TBS/T.

To gain a more detailed view of the conformational changes of PTEN induced by tail phosphorylation, we performed small angle X-ray scattering (SAXS) on the semisynthetic PTEN proteins. The scattering data for t-PTEN, n-PTEN and 4p-PTEN is shown in Figure 47A. An indirect Fourier transform of the radially averaged scattering data yields the pair distribution function (p of r) plot shown in Figure 47B for each protein. The shape of the plot for each protein is similar with a single hump followed by an extended region at higher values of r. The extended region is characteristic of a protein that is elongated in shape. In the case of PTEN the extension may be due the presence of the C-terminal tail. Interestingly the extended region is largest for n-PTEN and is significantly reduced for t-PTEN and 4p-PTEN. This suggests that the tail is no longer in an extended "open" conformation when phosphorylated in 4p-PTEN. Given that half of the C-terminal tail is missing in the t-PTEN, this extension in the p of r plot would be expected to be reduced for this protein. The radius of gyration (R_g) as well as the maximum particle dimension (D_{max}) of each protein can be calculated from the p of r plot. The R_g for 4p-PTEN (27.16 ± 0.02 Å) is reduced compared to n-PTEN (31.91 ± 0.05 Å) and is similar in value to t-PTEN (27.82 ± 0.08 Å). Additionally the D_{max} is largest for n-PTEN (96.5 Å) and smaller for 4p-PTEN (82.5 Å) and t-PTEN (82.5 Å) (Table 3).

Low resolution molecular envelopes were modeled from the SAXS data using the program DAMMIN[167,170]. The outputs from ten DAMMIN runs for each protein were averaged using DAMAVER and are displayed in Figure 48 overlaid

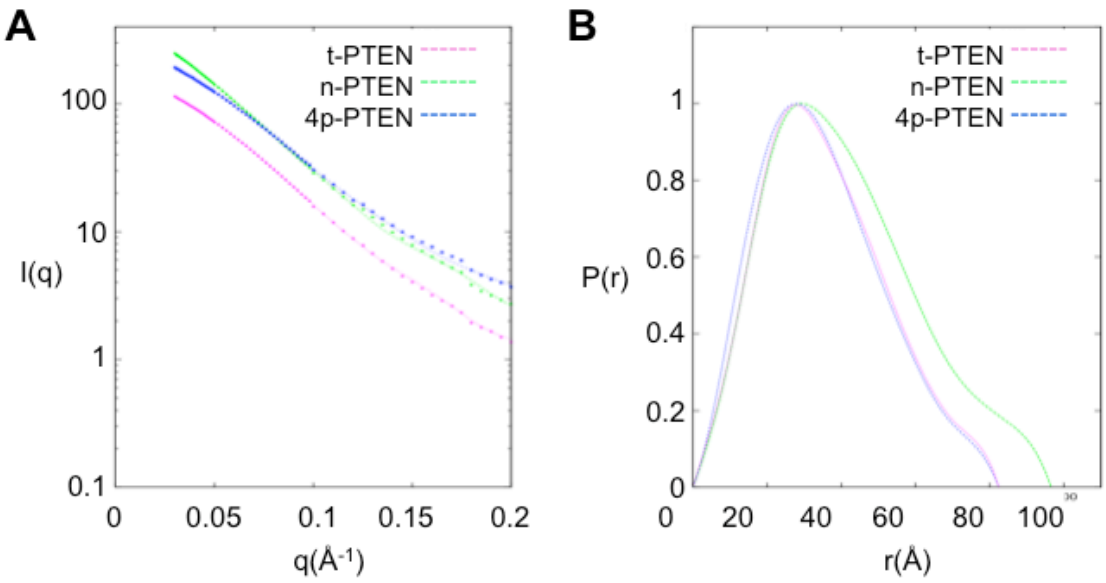

Figure 47: Small angle X-ray scattering of semisynthetic PTENs. The (A) scattering data and (B) pair distance distribution function plot of t-PTEN, n-PTEN and 4p-PTEN.

	R_g (Å)	D_{max} (Å)
t-PTEN	27.82 ± 0.08	82.5
n-PTEN	31.91 ± 0.05	96.5
4p-PTEN	27.16 ± 0.02	82.5

Table 3: Radius of gyration (R_g) and maximum particle dimension (D_{max}) of semisynthetic PTENs. R_g and D_{max} values of t-PTEN, n-PTEN and 4p-PTEN were calculated from the P(r) plot.

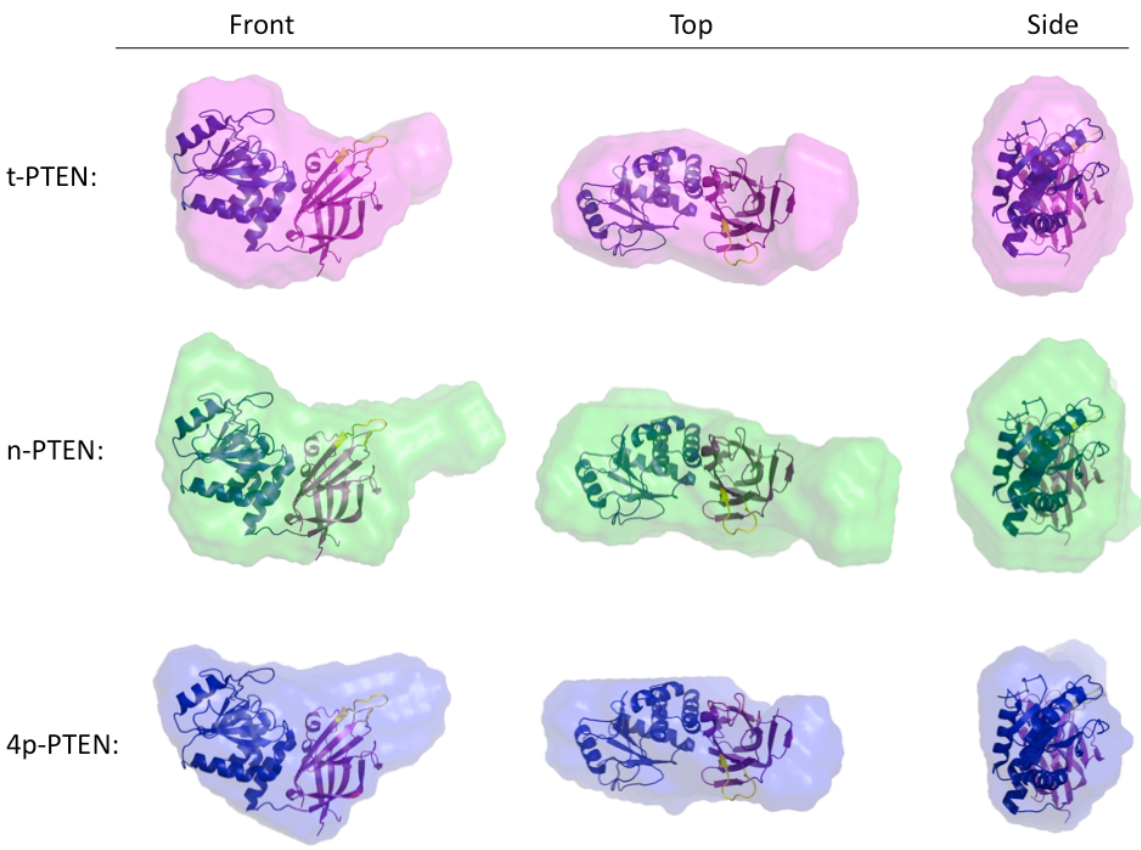

Figure 48: Molecular envelopes of t-PTEN, n-PTEN and 4p-PTEN obtained from SAXS analysis. Molecular envelopes of t-PTEN, n-PTEN and 4p-PTEN were generated from SAXS scattering data using the *ab initio* modeling program DAMMIF. Outputs from ten DAMMIF runs were averaged for each protein using DAMAVER and are shown overlaid with the tailless crystal structure with phosphatase domain shown in blue, the C2 domain shown in magenta and the CBRIII loop shown in yellow. Front, side and top views are shown for each protein.

with the tailless PTEN crystal structure. The tail-less crystal structure fits nicely into the two lobed globular domain of the molecular envelope for protein. In addition to the two lobed globular domain in each envelope there is a protrusion extending from what is likely the C2 domain. This protrusion is likely filled by the C-terminal tail in the full length PTEN molecule. Due to the larger size of the phosphatase domain compared to the C2 domain and the fact that these two domains are tilted off axis to each other, the crystal structure can fit into the molecular envelopes in only one orientation. This places the tail region adjacent to the membrane binding surface of the C2 domain. The tail is longer and narrower in the molecular envelope of n-PTEN compared to 4p-PTEN where the tail appears more compact around the C2 domain. As expected the tail is shorter for t-PTEN compared to n-PTEN. Also of note, the phosphatase domain appears to have a different shape for 4p-PTEN compared to n-PTEN and t-PTEN.

Discussion

The structural changes in PTEN caused by tail phosphorylation observed here provide an understanding into the mechanistic basis for the reduction in membrane binding affinity and decrease in catalytic activity discussed in the previous chapter. The trypsin digestion assays, shift on anion exchange chromatography, alkaline phosphatase sensitivity assay and SAXS molecular envelopes all point to phosphorylation causing a conformational change that leads to a more compact PTEN molecule in which the phospho tail is concealed

by a binding event with the main body of PTEN. The SAXS models would suggest the phospho tail binds to the body of PTEN in the general vicinity of the membrane binding surface of the C2 domain. If the phospho tail competes with membrane binding surfaces on the C2 and/or the phosphatase domain it would cause a reduction in PTEN's ability to bind to membranes and a subsequent reduction in catalytic activity.

Although the SAXS molecular envelopes suggest the phospho tail binds to the C2 domain of PTEN, the trypsin digestion data demonstrate that the phosphatase domain is stabilized to proteolysis when the tail is phosphorylated. This would suggest the tail is inducing a conformational change in the phosphatase domain by either directly binding to it or indirectly through interaction with the C2 domain, which then allosterically influences the conformation of the phosphatase domain. Additionally, the phosphatase domain in SAXS molecular envelopes appears to undergo a change in shape for 4p-PTEN when compared to t-PTEN and n-PTEN, indicating a change in the structural/dynamic state of the domain. As discussed in the introduction of this thesis, the phosphatase and C2 domain are closely interfaced. It therefore wouldn't be surprising if structural changes in one domain would cause perturbations in the other. This observed structural change in the phosphatase domain may account for the elevated K_m of 4p-PTEN for soluble substrates compared to that of n-PTEN which was discussed in the previous chapter.

Phosphorylated PTEN's paradoxical shift on anion exchange chromatography as well as the sensitivity to alkaline phosphatase suggests that the equilibrium between the "open" and "closed" states of PTEN greatly favors the "closed" conformation by at least 25 to 1. It has been reported that PTEN possess "autophosphatase" activity, though we did not detect any as measured by western blot analysis. It may be possible that PTEN does possess weak "autophosphatase" activity with phosphorylated tail peptides. In the case of full length PTEN protein predominantly in the "closed" conformation, the tail phosphates may not be available for dephosphorylation.

n-PTEN eluted from the anion exchange column as a series of multiple peaks, which has been determined to be due to heterogeneous phosphorylation at amino acids Thr366 and Ser370 amongst others, presumably resulting from kinases in insect cells. Though 4p-PTEN was generated from the same truncated PTEN protein from insect cells, it elutes from the anion exchange column as one sharp peak. This suggests that the additional phosphorylation sites at Thr366 and Ser370 are also being concealed by the conformational change induced by phosphorylation at the S380/T382/T383/S385 phospho cluster. It is currently unknown what the major biological ramifications of phosphorylation at T366/S370 are, though phosphorylation at Thr366 has been reported to decrease the stability of the PTEN protein within cells[130]. It is unknown if the phosphorylation events at T366/S370 affects the signaling effects of phosphorylation at the S380/T382/T383/S385 cluster or vise versa. However if the phosphorylations at

Thr366 and Ser370 are concealed by the conformational change induced by phosphorylation at S380/T382/T383/S385, it would suggest that the effects of T366/S370 phosphorylation may be turned off. Further experiments would be necessary to verify this.

Chapter 5: Identification of PTEN Surfaces and Amino Acids Implicated in Phosphorylated Tail Binding

Introduction

The conformational changes observed in the previous chapter suggest that phosphorylation of the C-terminal tail causes structural changes in both the phosphatase and C2 domains of PTEN. The molecular envelopes generated from the small angle X-ray scattering data indicate that the phosphorylated tail binds to the C2 domain along its membrane binding surface. Additionally, the same envelopes show apparent changes in the shape of the phosphatase domain when the tail is phosphorylated. Furthermore, the phosphatase domain is protected from trypsin proteolysis and the protein shows an elevated K_m for soluble substrates conferred by tail phosphorylation, suggesting there are structural changes in this domain. At approximately 175 Å in extended length, the C-terminal tail is long enough to bind surfaces of both the phosphatase and C2 domain concurrently.

Previous evidence for a phosphorylation induced conformational change was established using an *in trans* binding experiment in which the main body of PTEN (aa 1-352) and tail (aa 353-403) were expressed in eukaryotic cells and shown to co-immunoprecipitate[109,137]. While this did not prove the interaction was an *in cis* binding event and wasn't mediated by a secondary protein, this assay was used in attempt to identify point mutations in PTEN that would disrupt the co-

immunoprecipitation. These authors identified mutations on the phosphatase domain (K13A, R14A, R15A) and C2 domain (K260A, K263A, K266A, K267A, K269A) that disrupted the co-immunoprecipitation of the two PTEN fragments[109]. Interestingly, as discussed in the previous chapter, we found that R15 was protected from trypsin proteolysis suggesting it could be involved in phospho tail binding.

In the present chapter we have generated a series of semisynthetic PTEN mutants to screen for amino acids on the main body of PTEN that are important for phospho tail binding. Point mutants localized to both the phosphatase domain and C2 domain were examined. One set of mutations on the CBRIII loop of the C2 domain was found to significantly disrupt the binding interaction between the phosphorylated C-terminal tail and the body of PTEN.

Methods

Anion Exchange Chromatography:

The semisynthetic PTEN protein was further purified for SAXS and other biochemical experiments by anion exchange chromatography (monoQ) using an AKTA FPLC from GE Healthcare. Proteins were purified with a gradient of 0-50% Buffer B over 250 mL at a flow rate of 1.0 mL/min. (Buffer A: 50 mM Tris pH 8.0, 10 mM DTT; Buffer B: 50 mM Tris pH 8.0, 1.0 M NaCl, 10 mM DTT).

Phosphatase Sensitivity Assay:

50 ng of semisynthetic phosphorylated PTEN and its mutants were dephosphorylated in the presence of 1 μM alkaline phosphatase from NEB (CIP) for varying periods of time in phosphatase assay buffer (50 mM Tris pH 8.0, 20 mM NaCl, 25 μM $MgCl_2$ and 10 mM DTT) at room temperature in 20 μL reactions. Reactions were quenched with SDS loading dye and run on 10% SDS-PAGE gel. Dephosphorylation of PTEN was monitored by western blot with an antibody to the phospho-tail cluster (NBP1-4136). Primary dilution: 1:1000 in 1% BSA in TBS/T. Secondary dilution: 1:10,000 in 1% BSA in TBS/T. The fraction of phospho-PTEN remaining was determined using Carestream Media image quantification software.

Soluble Substrate Activity Assay:

PTEN activity to a water soluble substrate (diC6-PIP_3) was determined by measuring the release of inorganic phosphate with a malachite green detection kit from R and D Biosystems[187,188]. 25 μL reactions were allowed to proceed for 5-10 minutes at 30ºC in assay buffer (50 mM Tris pH 8.0, 10 mM BME) before being quenched by malachite green reagent according to the manufacturer's protocol. Amounts of PTEN used per data point ranged from 0.5 to 20 μg. Reactions were shown to be linear with respect to time and enzyme

concentration in the ranges used. Careful consideration of background signal was needed here. The addition of enzyme, substrate and buffer components led to increases background signal that needed to be accounted for (by subtraction) in the final calculation of the amount of phosphate released by PTEN.

Results

With overwhelming evidence that PTEN undergoes a conformational change when phosphorylated at the S380/T382/T383/S385 cluster on its C-terminal tail, we set out to determine what amino acids and regions of the PTEN protein are more or less important for binding the phosphorylated tail.

It has been proposed that the active site of PTEN may directly interact with the tail of PTEN when it is phosphorylated given that mutation of catalytic Cys124 prevents intermolecular binding interactions between the tail and the body of PTEN. To gain insight into potential interactions between the phosphorylated tail and the catalytic pocket, we digested n-PTEN and 4p-PTEN with trypsin in the presence of different compounds that bind the active site. Unexpectedly, all molecules tested that bind to the catalytic pocket enhanced PTEN sensitivity to trypsin proteolysis rather than stabilizing the protein (Figure 49). Digesting PTEN in the presence of vanadate, VO-OHpic and soluble PIP_2 all have the effect of destabilizing PTEN even when the tail is phosphorylated (Figure 49). However, there is still a different banding pattern for 4p-PTEN

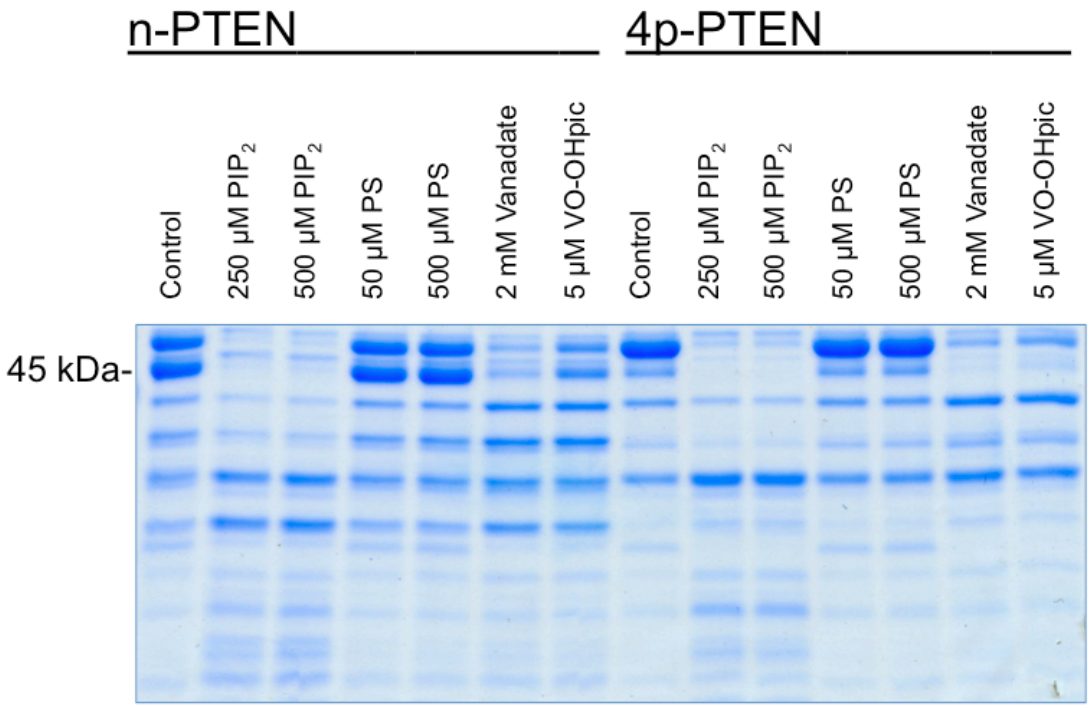

Figure 49: Trypsin digestion of n-PTEN and 4p-PTEN in presence of active site binding small molecules. 2 µg of n-PTEN or 4p-PTEN were digested with 25 ng of trypsin in the presence or absence of indicated amounts of diC6 PIP_2 or diC4 phosphatidylserine (PS), vanadate or VO-OHpic. Digestion fragments were visualized by colloidal blue staining.

compared to n-PTEN. This would suggest that even though the active site is occupied, the phosphorylated tail is still binding the body of PTEN. The addition of soluble phosphatidylserine (PS) had no affect on PTEN's stability to trypsin proteolysis regardless of tail phosphorylation state (Figure 49). PS embedded in membranes has been suggested to bind the C2 domain of PTEN though it is unknown if soluble PS can bind PTEN.

The internal flexible loop (aa 286-309) of the C2 domain, referred to as the "D-loop", has unknown function. It was deleted from the truncated PTEN protein that was ultimately crystallized, presumably because the D-loop introduced flexibility into the protein. Flexible loops of proteins often participate in conformational changes and binding events between proteins. The D-loop of PTEN was deleted to determine if it was involved in the interaction between the phosphorylated tail and the main body of PTEN. Partial trypsin digestion of the phosphorylated and unphosphorylated D-loop deleted semisynthetic proteins revealed that phosphorylation still conferred protection to proteolysis suggesting that the phospho tail was still causing a conformational change (Figure 50). Furthermore, the D-loop deleted protein showed phosphorylation dependent reduction in membrane binding ablitiy (Figure 51). Taken together this would indicate that the D-loop does not stabilize or mediate the binding event between the phosphorylated tail and the body of PTEN.

To try to better understand the phospho-tail binding interaction, we made a number of semisynthetic PTEN mutants with point mutations targeted to the

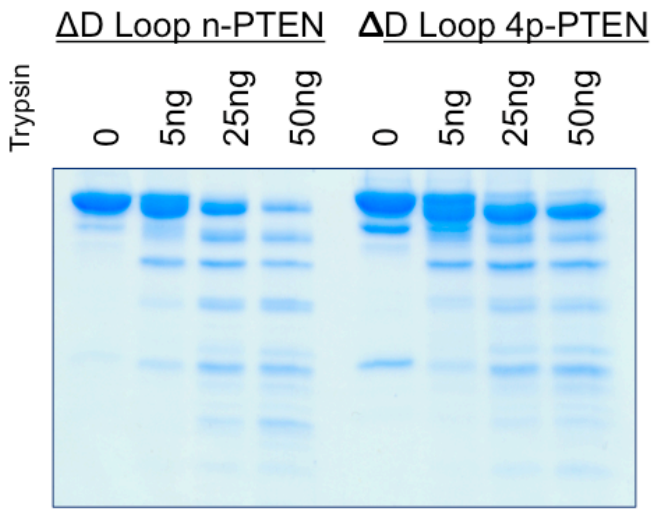

Figure 50: Partial trypsin digestion of n-PTEN and 4p-PTEN containing D-loop (aa 286-309) deletions. 2 µg of the semisynthetic proteins were digested with the indicated amounts of trypsin. Digestion fragments were visualized by colloidal blue staining.

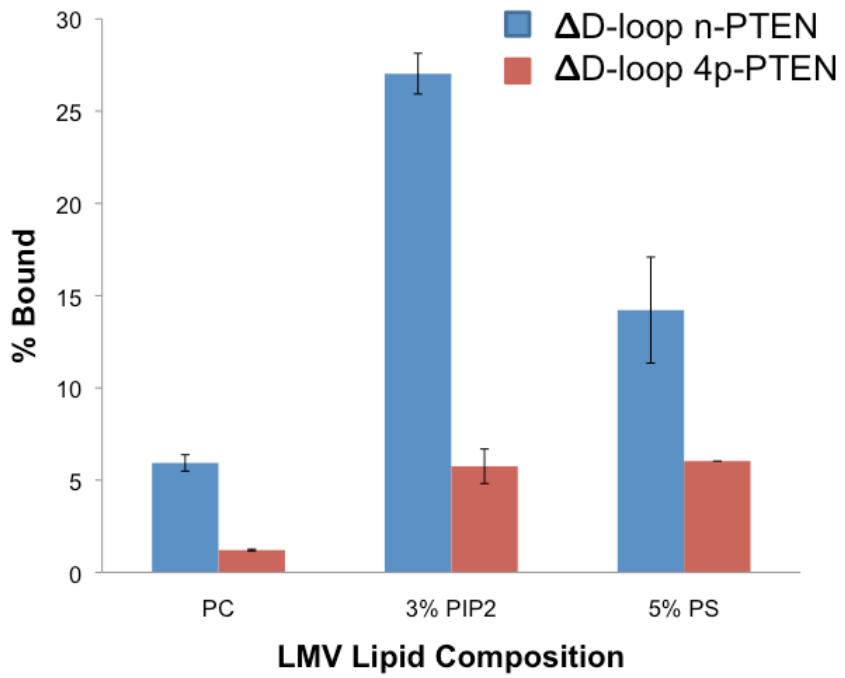

Figure 51: D-loop deleted n-PTEN and 4p-PTEN binding to large multilamellar vesicles (LMVs). That amount of semisynthetic PTEN protein that pelleted with 1 mM LMVs containing various concentrations of phosphatidylcholine, phosphatidylserine and/or PIP_2 was determined by western blot. Data are represented as the mean +/- the S.D. of two experiments performed in duplicate.

phosphatase domain as well as the C2 domain. The mutants were chosen based on previous models, trypsin digestion experiments, and educated guesses. Presumably, regions on the body of PTEN that bind to the phosphorylated tail are positively charged given that the tail is multiply phosphorylated and has numerous acid aspartate and glutamate residues. Therefore, all of the point mutants that were generated where either lysine or arginine amino acids. Several of the mutants are outlined in Figure 52. The N-mutant contained amino acids K13, R14, R15 and R161 mutated to alanines (Figure 53). This mutant was chosen based partially on the trypsin digestion data which revealed R15 and R161 were protected from proteolysis when the tail was phosphorylated and partially because mutations of these amino acids were previously reported to disrupt the *in trans* binding interaction between the phospho-tail and body of PTEN[109]. These four amino acids are co-localized in the crystal structure of PTEN and are important for targeting PTEN to the plasma membrane[51,95,96]. Another mutant targeted five lysine residues (aa 260, 263, 266, 267 and 269) on the CBRIII loop of the C2 domain. These lysine residues have been shown to be important for lipid binding and have previously been proposed to disrupt an *in trans* biding event between the phospho-tail and the body of PTEN[51,99,109]. The five lysines were mutated to alanines to neutralize the positive charge in one mutant (A5-mutant) and to aspartates as a charge reversal mutant (D5-mutant) (Figure 54). The final mutant was chosen to mimic the crystallized form of PTEN. This mutant (X-mutant) contained deletions at the N-terminus (aa 1-6), D-loop (aa 286-309) and C-terminus (aa 396-403). Additionally this mutant contained the

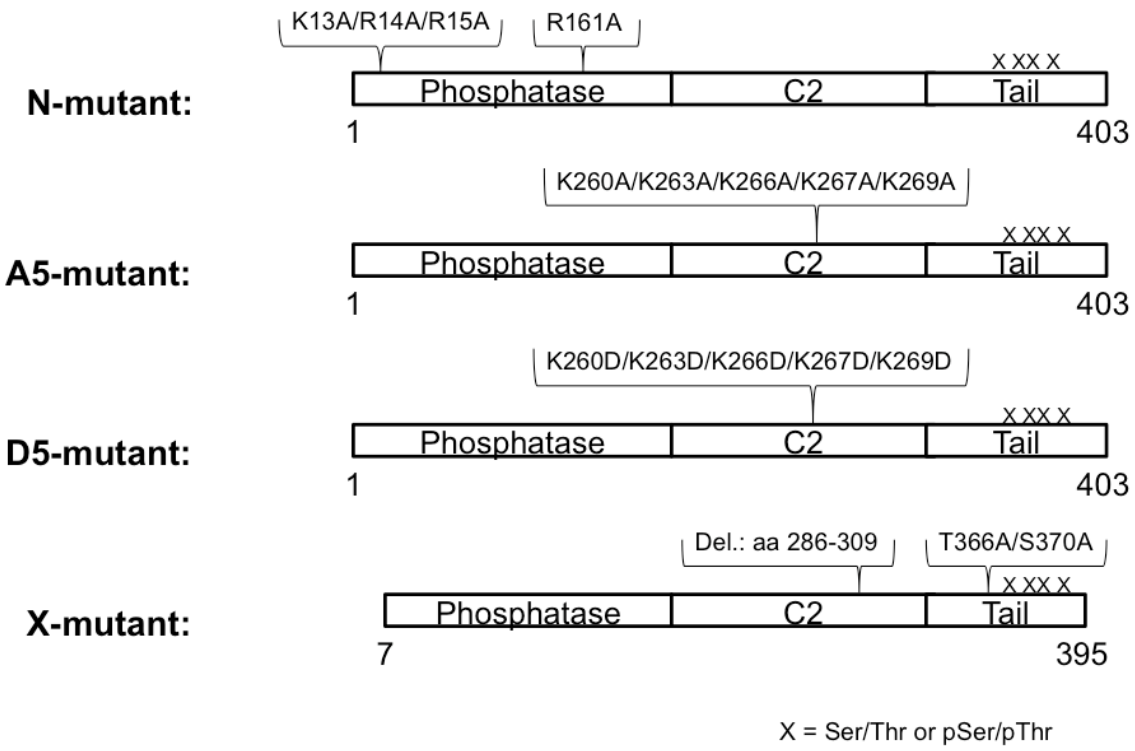

Figure 52: Schematic view of semisynthetic PTEN mutants. PTEN mutants were generated analogously to n-PTEN and 4p-PTEN semisynthetic proteins as outlined in the methods section.

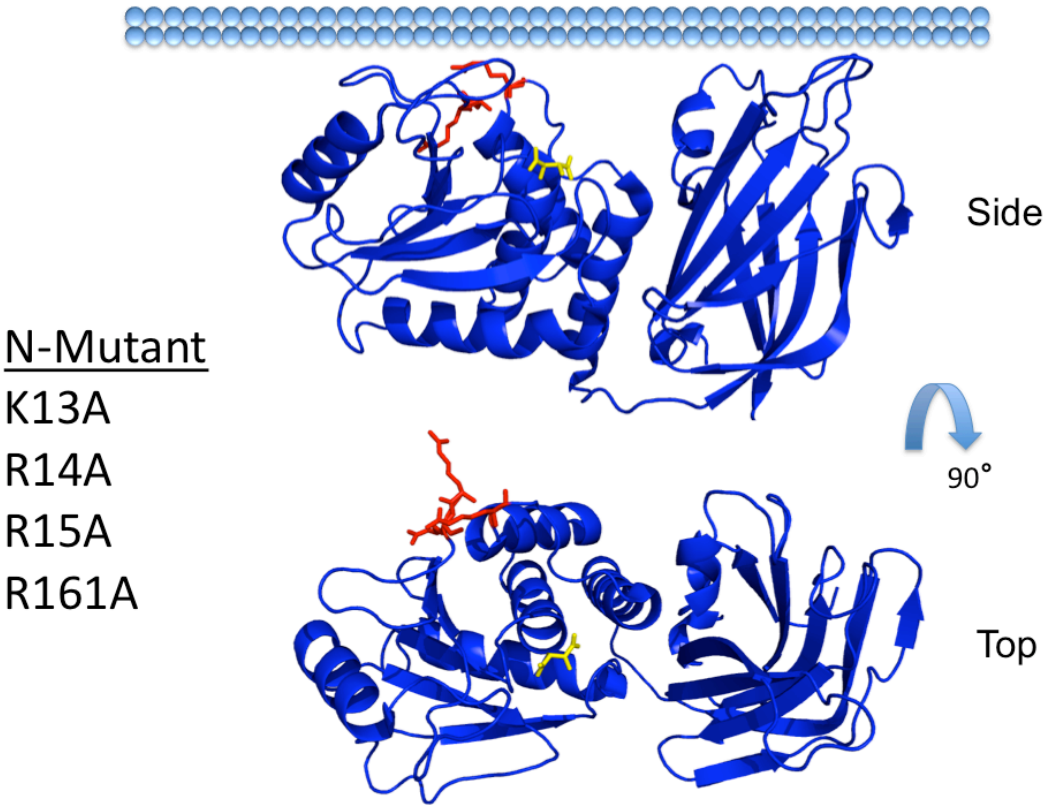

Figure 53: Crystal structure of PTEN highlighting point mutations of the N-mutant. R14, R15 and R161, shown in red, were mutated to either alanines in the N-mutant. The N-mutant also contains K13 mutated to alanine though it is not shown in the crystal structure. Top and side views of the PTEN protein are shown with the membrane binding surface oriented towards the plasma membrane. Tartrate, in yellow, binds to the active site of PTEN.

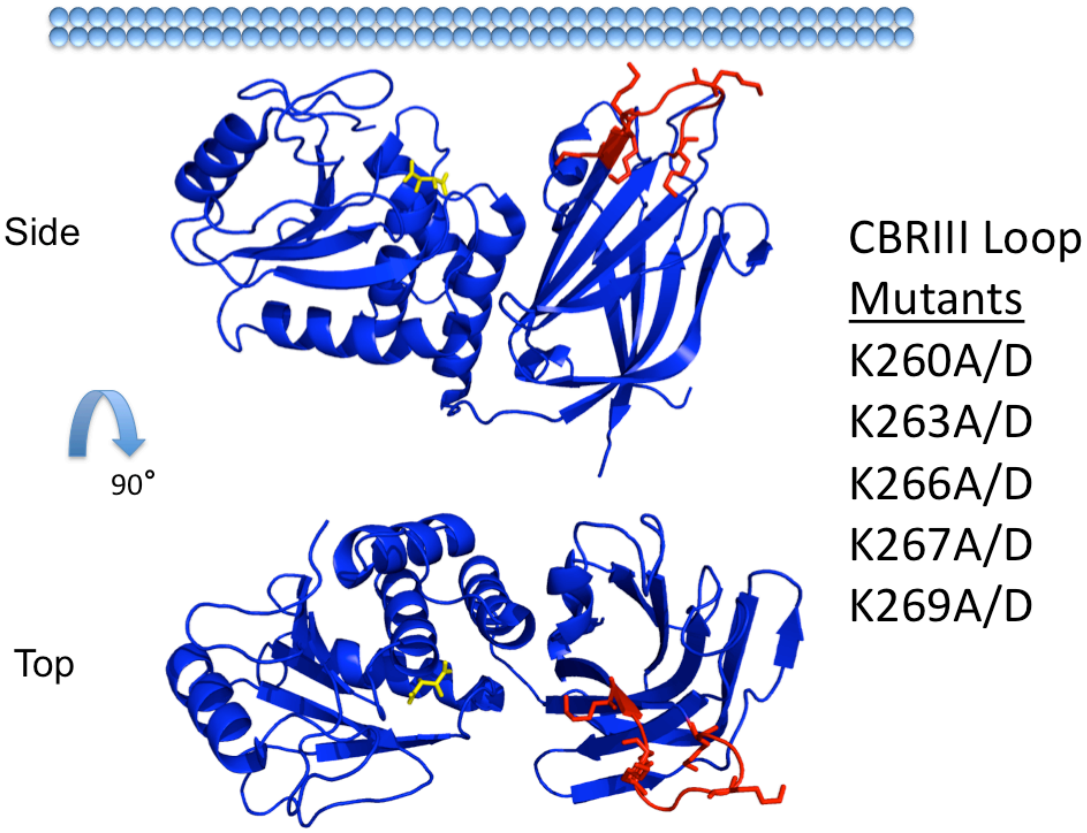

Figure 54: Crystal structure of PTEN highlighting point mutations of the D5- and A5-mutant. Lysines 260, 263, 266, 267 and 269 of the CBRIII loop, shown in red, were mutated to either alanines in the A5-mutant or aspartates in the D5-mutant. Top and side views of the PTEN protein are shown with the membrane binding surface oriented towards the plasma membrane. Tartrate, in yellow, binds to the active site of PTEN.

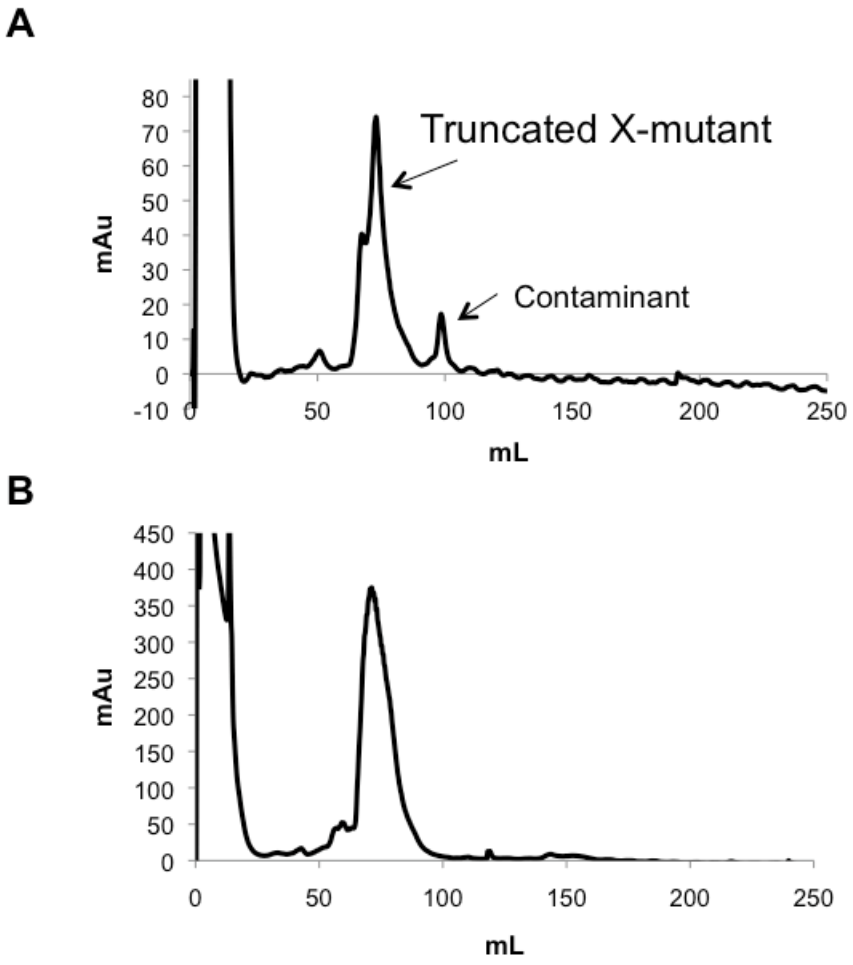

Figure 55: Characterization of the X-mutant by anion exchange chromatography. (A) The unligated X-mutant elutes from the anion exchange column as one peak, indicating the heterogenous phosphorylation occurring from insect cell expression has been eliminated. (B) The full length 4p-PTEN X-mutant elutes from the anion exchange column just before the unligated X-mutant, indicative of the phosphorylation induced conformational change.

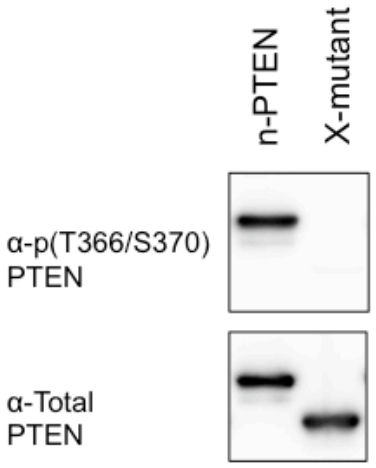

Figure 56: The X-mutant is not phosphorylated at T366 or S370. Using an antibody to phospho T366/S370, it can be seen that n-PTEN which is wt at these two amino acids is phosphorylated while the X-mutant which contains T366A/S370A mutations is not. Primary dilution: 1:1000 in 1% BSA in TBS/T. Secondary dilution: 1:10,000 in 1% BSA in TBS/T.

mutation of T366 and S370 to alanine to remove phosphorylation modifications on the tail of PTEN that were a result of insect cell expression (Figure 56). The unligated X-mutant eluted as a single peak on anion exchange chromatography (Figure 55A), suggesting the mutation of these two residues eliminated phosphorylation events not only at these two sites but also perhaps at nearby serine and threonine residues.

Any mutants that prevent the phosphorylated tail from binding the body of PTEN would be expected to have at least three distinct biochemical characteristics compared to the wild type protein. The mutant protein should no longer exhibit the paradoxical elution patterns observed on anion exchange chromatography. That is, the phosphorylated mutant should elute after, rather than before, the unphosphorylated mutant (Figure 57). Additionally, the phosphorylated mutant should be more sensitive to alkaline phosphatase removal of the phospho-tail cluster compared to wild type PTEN if the equilibrium between the “open” and “closed” forms of PTEN were shifted to favor the “open” conformation (Figure 58). Finally the phosphorylated mutant PTEN should exhibit increased catalytic activity with a decreased K_m with soluble PIP_3 substrates given that the unphosphorylated form of PTEN shows increased activity and a reduced K_m relative to phosphorylated PTEN.

The A5-mutant, N-mutant and X-mutant all exhibited the same paradoxical elution patterns on anion exchange chromatography (Figures 55, 59) where the

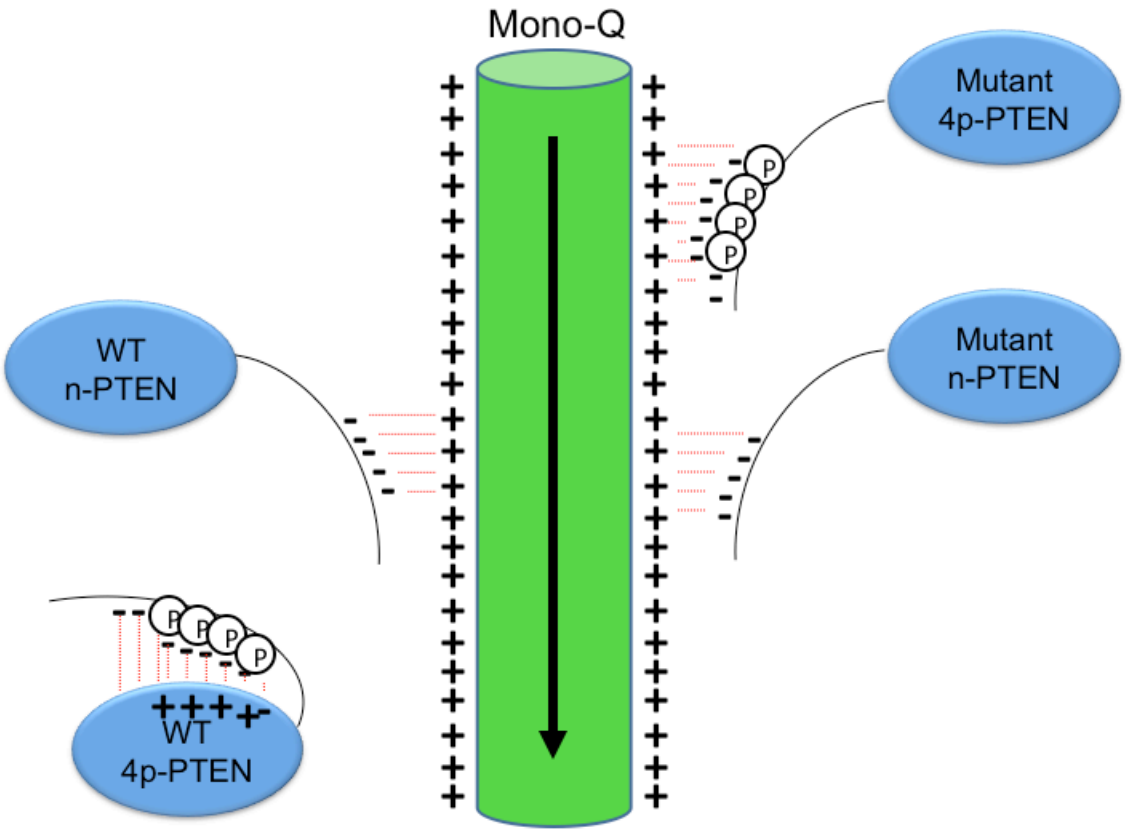

Figure 57: Screening for PTEN mutants that disrupt the phosphorylation induced conformational change by anion exchange chromatography. While WT n-PTEN and 4p-PTEN exhibit the paradoxical elution patter where 4p-PTEN elutes prior to n-PTEN, mutant 4p-PTEN should elute after mutant n-PTEN if the binding interaction between the phospho-tail and the main body of PTEN has been disrupted.

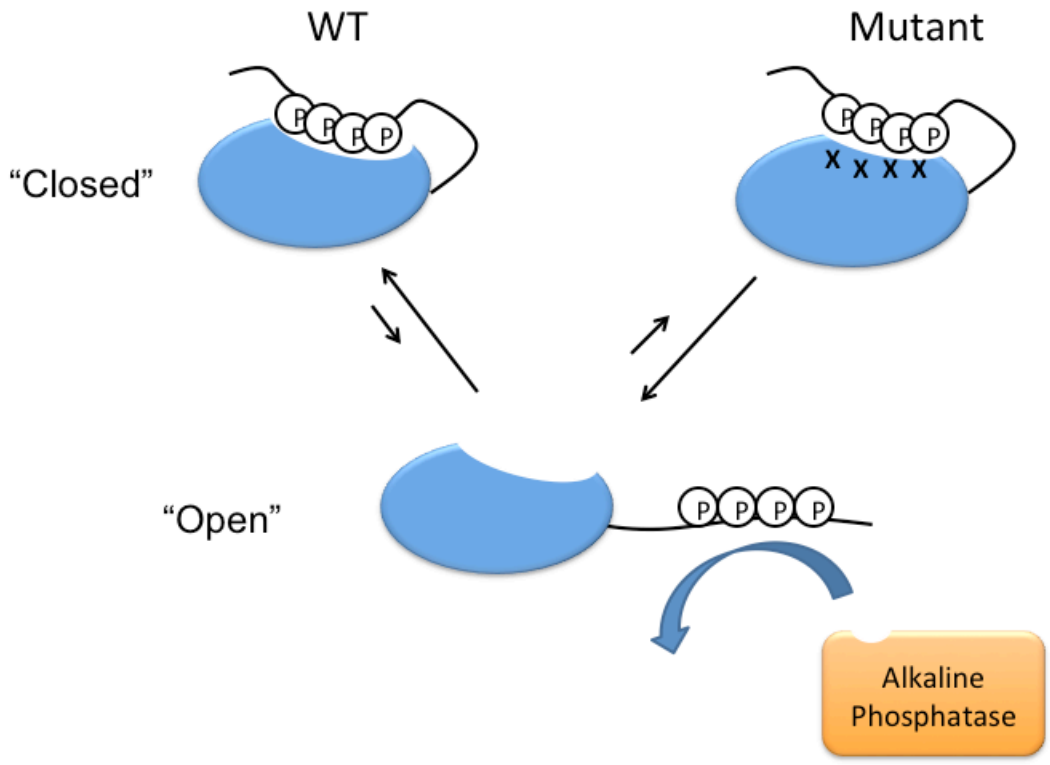

Figure 58: Screening for PTEN mutants that disrupt the phosphorylation induced conformational change by sensitivity to alkaline phosphatase removal of tail phosphates. When phosphorylated the equilibrium between the "open" and "closed" forms of PTEN favors the "closed" conformation. Mutations that disrupt the binding interaction should shift the equilibrium to the "open" conformation, leading to increased sensitivity to alkaline phosphatase.

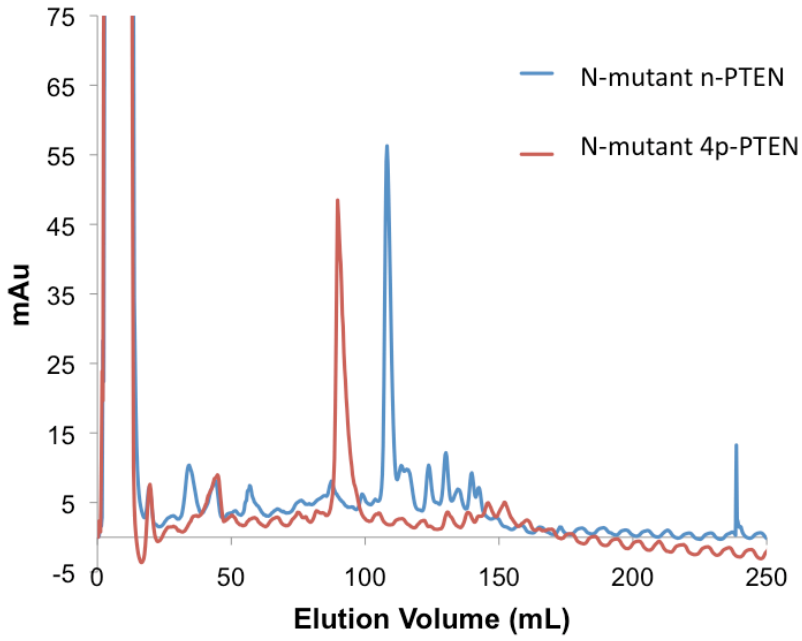

Figure 59: Characterization of the N-mutant by anion exchange chromatography. The N-mutant exhibits the same paradoxical elution pattern as WT phosphorylated and unphosphorylated PTEN, indicating the mutations contained in the N-mutant do not disrupt the tail binding interaction. The elution of 1 mg of each protein was monitored at 280 nm (milli-absorbance units). Gradient: 0-50% Buffer B over 250 mL. Buffer A: 50 mM Tris pH 8.0, 5 mM NaCl, 5 mM DTT. Buffer B: 50 mM Tris pH 8.0, 1 M NaCl, 5 mM DTT.

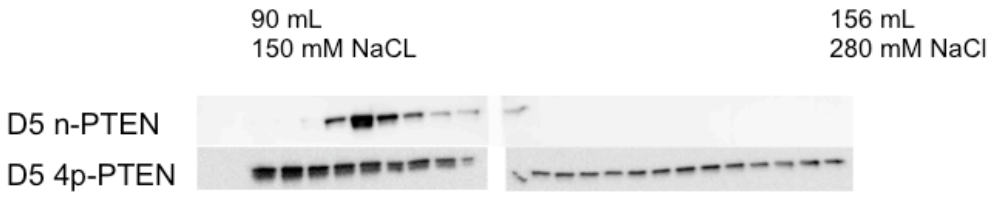

Figure 60: Characterization of the 5D-mutant by anion exchange chromatography. The phosphorylated 5D-mutant initially elutes as a broad peak from the anion exchange column just prior to the unphosphorylated 5D-mutant. However much of the phosphorylated 5D-mutant elutes long after the unphosphorylated mutant. Gradient: 0-50% Buffer B over 250 mL. Buffer A: 50 mM Tris pH 8.0, 5 mM NaCl, 5 mM DTT. Buffer B: 50 mM Tris pH 8.0, 1 M NaCl, 5 mM DTT.

phosphorylated form eluted before the unphosphorylated form of the PTEN mutant. However the phosphorylated D5-mutant eluted as a very broad peak with a portion of the peak eluting both before and after the unphosphorylated D5-mutant (Figure 60). The phosphorylated D5-mutant was also significantly more sensitive to alkaline phosphatase removal of its tail phosphates compared to the A5-mutant, N-mutant and X-mutant phosphorylated PTEN proteins which displayed similar sensitivity to alkaline phosphatase compared to WT 4p-PTEN (Figures 61, 62). The D5-mutant however was not as sensitive to alkaline phosphatase removal of tail phosphates as a denatured WT form of the PTEN. The D5-mutant displayed dephosphorylation kinetics about 7 fold faster than WT but about 3 fold slower than the denatured form (Figures 61, 62). Taken together these data suggest that the phosphorylated D5-mutant is in a partially “open” conformation that is significantly more “open” than WT.

We considered the possibility that mutating the five lysine residues to five aspartates was denaturing in the D5-mutant. However the D5-mutant was found to not only be active, but to have higher specific activity with soluble diC6-PIP_3 than the WT 4p-PTEN and the phosphorylated A5-mutant (Figure 63). More detailed characterization of the enzymatic activity of the phosphorylated D5-mutant shows a reduced K_m for diC6-PIP_3 compared to WT 4p-PTEN (Figure 64). Given that n-PTEN was found to have higher activity and a reduced K_m to soluble substrates than 4p-PTEN, this is further evidence that the phosphorylated 5D-

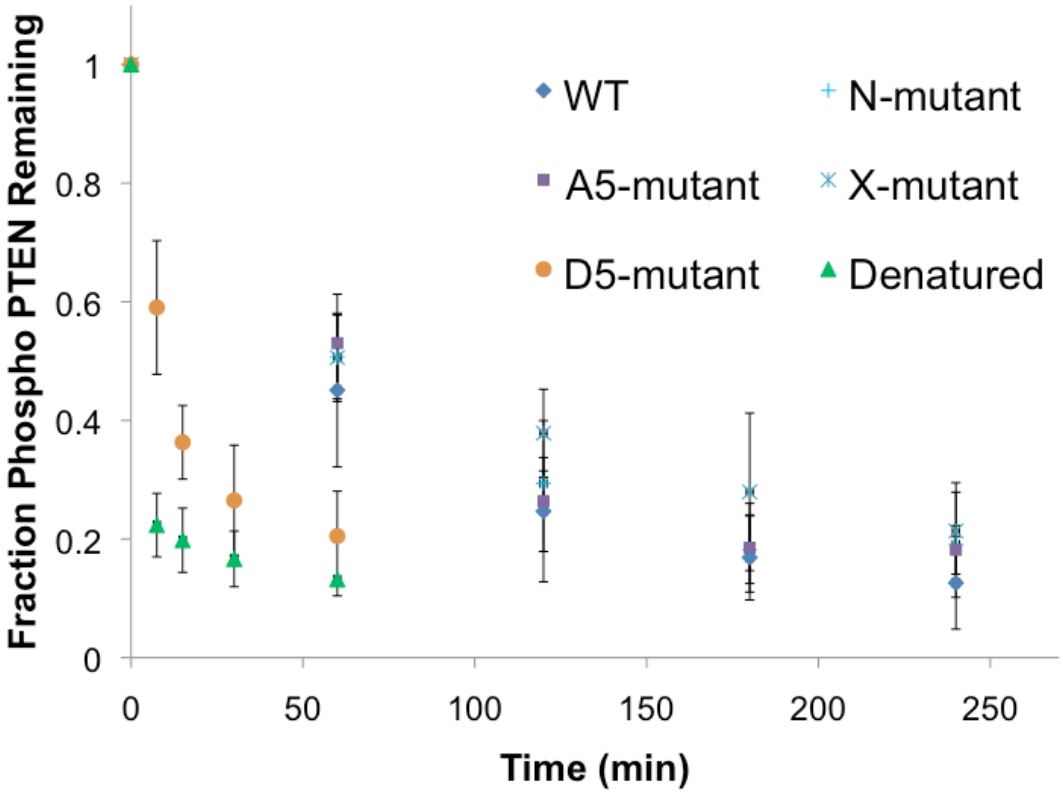

Figure 61: Alkaline phosphatase sensitivity of 4p-PTEN and its mutants. The rate of dephosphorylation of 4p-PTEN and its mutants was measured by quantification of bands from western blot analysis after treatment of the PTEN protein with 1 μM alkaline phosphatase. Data points are shown as the mean +/- the SEM of three experiments.

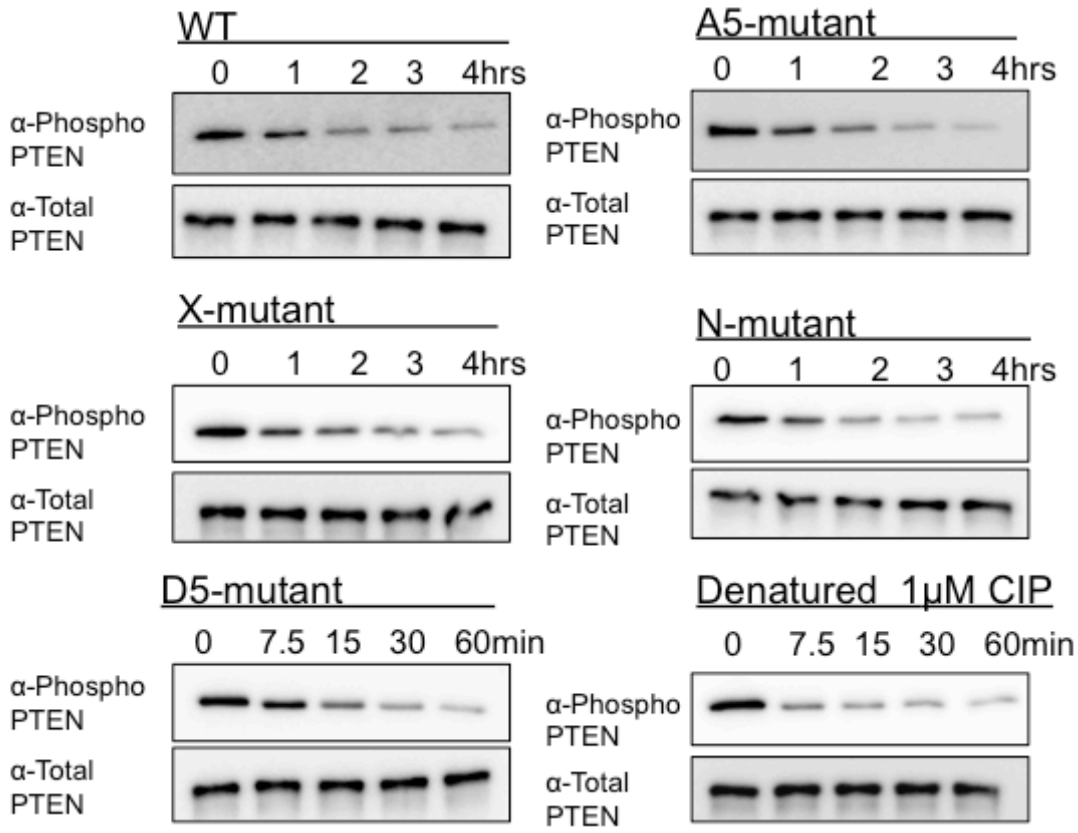

Figure 62: Western blots of the alkaline phosphatase sensitivity of 4p-PTEN and mutant forms. 4p-PTEN and its mutants were treated with 1 μM alkaline phosphatase. Dephosphorylation of the phospho-tail cluster was monitored by western blot with an antibody to the phospho-tail. Primary Ab dilution: 1:1000 in 1% BSA in TBS/T. Secondary Ab dilution: 1:10,000 in 1% BSA in TBS/T.

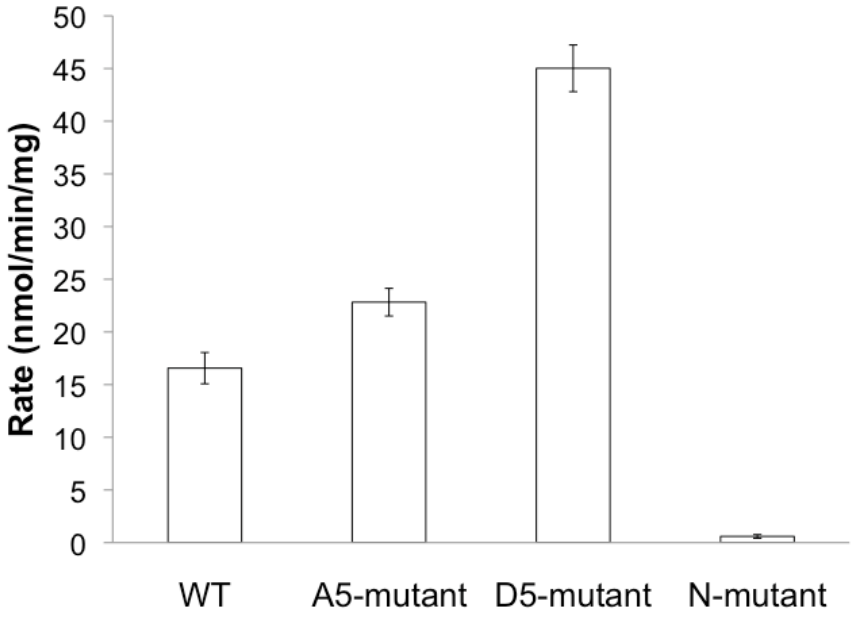

Figure 63: Phosphatase activity of 4p-PTEN and its mutants with diC6-PIP_3 substrate. PTEN activity was measured against 160 μM diC6-PIP_3 substrate. Data points are shown as the mean +/- the SEM of three experiments performed in duplicate.

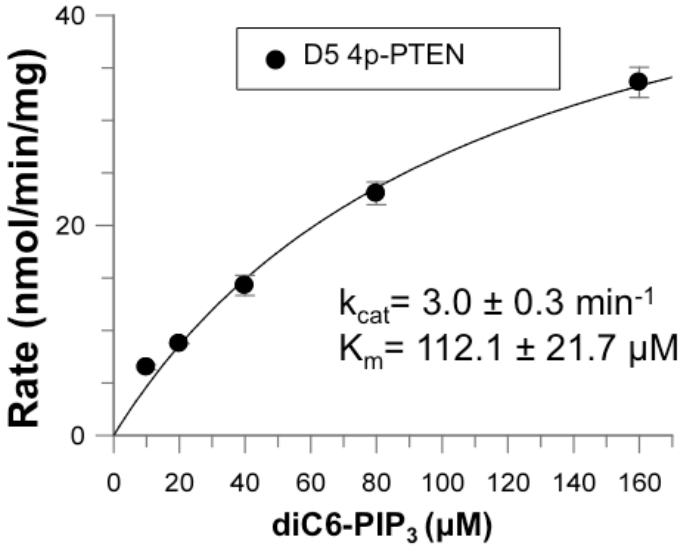

Figure 64: Phosphatase activity of the 5D 4p-PTEN mutant with soluble diC6-PIP_3 substrate. (A) Km curve of 5D 4p-PTEN compared to n-PTEN and WT 4p-PTEN. (B) K_m curve of 5D 4p-PTEN with k_{cat} and K_m values determined from nonlinear regression analysis. Data are represented as the mean +/- the S.D. of three experiments performed in duplicate.

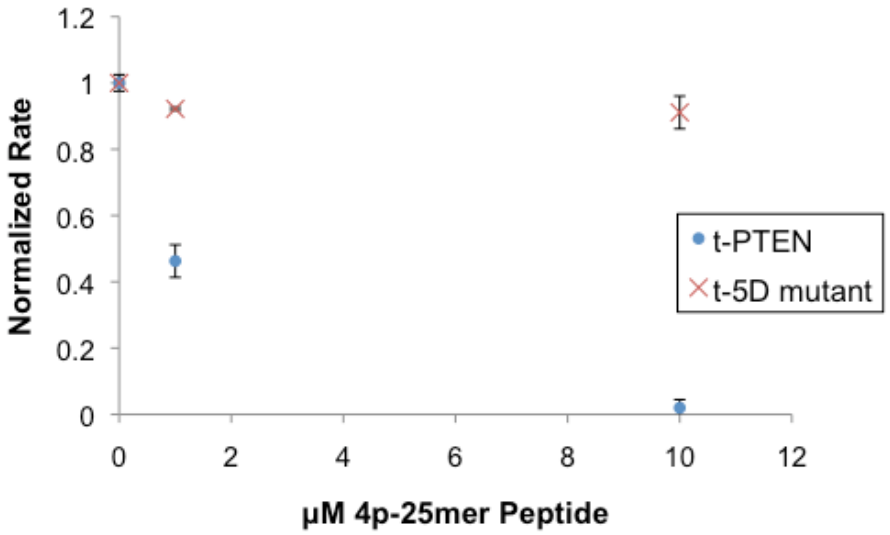

Figure 65: *In trans* inhibition of 5D t-PTEN phosphatase activity with phosphorylated tail peptide compared to WT t-PTEN. Activity was measured with 160 µM diC6-PIP_3 substrate. Data are represented as the mean +/- the S.D. of three experiments performed in duplicate.

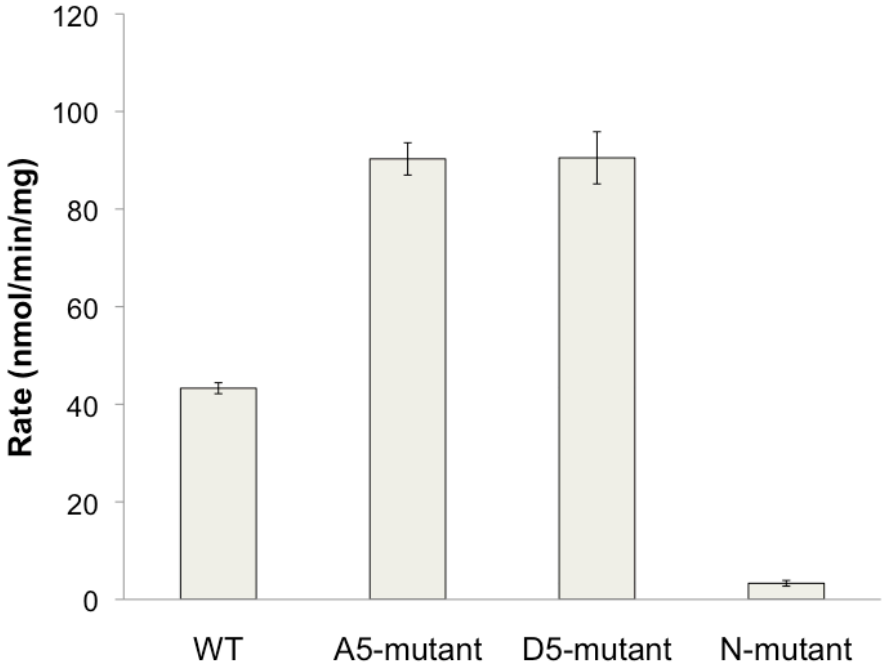

Figure 66: WT and mutant n-PTEN phosphatase activity with diC6-PIP_3 substrate. n-PTEN and its mutants activity was measured with 160 µM soluble diC6-PIP_3. Phosphate release was monitored by Malachite green detection. Data are represented as the mean +/- the SEM of three experiments preformed in duplicate.

mutant exists in a more “open” conformation than the WT 4p-PTEN protein. Furthermore, we found that unlike WT t-PTEN, 5D t-PTEN was nearly completely resistant to *in trans* inhibition of catalytic activity by the 25mer phosphopeptide (Figure 65) suggesting the phospho-tail can no longer bind to the body of PTEN when the five lysines in the CBRIII loop have been mutated to aspartates.

As previously reported, we found that the N-mutant of PTEN showed significantly reduced activity compared to WT (Figures 63, 66). The mechanistic basis for this reduction in activity is unknown, though the amino acids mutated in the N-mutant are known to be important for PIP_2 binding and allosteric activation of the enzyme.

Discussion

Identification of the D5-mutant as a mutant form of the phosphorylated PTEN that is in a more “open” state compared to WT suggests that the membrane binding surface of the C2 domain is implicated in phospho-tail binding. This gives credence to the molecular envelope models generated from the small angle X-ray scattering data discussed in the previous chapter where it appeared as the though the phospho-tail was binding to the body of PTEN in the vicinity of the membrane binding surface of the C2 domain (Figure 67). This provides a simple mechanism by which the phosphorylated C-terminal tail

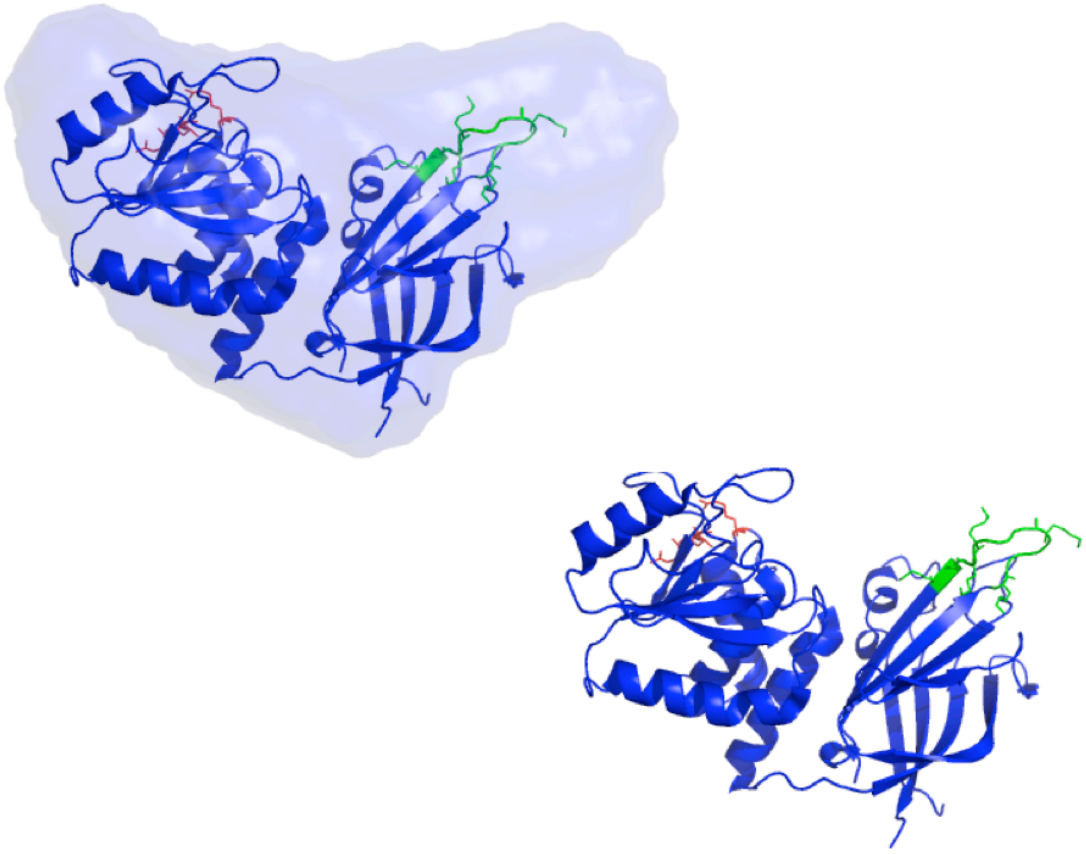

Figure 67: N-terminal and CBRIII mutant crystal structures overlaid with the SAXS generated molecular envelope from 4p-PTEN.

decreases PTEN's ability to bind to phospholipid membranes by competing for membrane binding surfaces on the C2 domain.

It is unknown why mutating the five lysines on the CBRIII loop of the C2 domain to aspartates has the effect of "opening" the PTEN molecule while mutating the same five lysines to alanine has no effect on the "open" and "closed" equilibrium. Although direct contact of the phospho-tail with the CBRIII loop cannot be ruled out, those results likely suggest that the phosphorylated tail does not bind directly to the lysine residues. The most likely scenario is one in which the phospho-tail binds to the C2 domain in the general vicinity of the CBRIII loop and that the negatively charged aspartates repel the negatively charged tail, inducing the more "open" conformation of PTEN.

Contrary to our findings, the N-mutant and 5A-mutant have previously been shown to disrupt the phospho-tail binding event with an *in trans* binding assay[109]. In this assay, the body of PTEN (aa 1-352) and the tail (aa 353-403) were expressed as tagged proteins and shown to co-immunoprecipitate with each other. The N-terminal and CBRIII loop alanine mutations abrogated this co-immunoprecipitation. The differences between the methodologies used likely are the reason for these inconsistent findings. It may be that the phosphorylated tail interacts with the body of PTEN in a different way when the tail and body are detached from each other versus when they are part of the same molecule.

The mutations of the N-mutant were originally chosen partially based upon the previous model discussed above and partially because two of the amino acids (R15 and R161) were found to be protected during proteolysis with trypsin when the PTEN tail was phosphorylated. One explanation for the protection of these amino acids from proteolysis is that the tail directly binds to them and therefore prevents trypsinization at these sites. Given that the N-mutant did not display any characteristics of the "open" form of PTEN, it is unlikely that these residues were directly protected from proteolysis but rather indirectly so by the stabilization of the entire phosphatase domain when the PTEN tail is phosphorylated.

The exact amino acids on the C2 domain of PTEN that are responsible for binding to the S380/T382/T383/S385 phospho cluster remain to be determined. Further mutagenesis of the C2 domain my help to determine which key amino acids may be involved. Given that phosphorylation is the major switch from the "open" to "closed" conformation, it should be possible to completely disrupt the tail binding interaction by mutating the key amino acids that bind to the tail phosphates. In this thesis, only positively charged lysine and arginine residues were mutated. Given that the phospho tail is highly negatively charged, it would be expected that positively charged amino acids play some role in stabilizing the binding interaction. That being said, the amino acids that have been found to most frequently bind to phosphates are actually glycine>threonine>arginine>serine>lysine in decreasing order[12]. Interestingly,

there is a loop on the C2 domain that has a stretch of glycine, serine and threonine residues. While mutational analysis could be informative, the only way to definitively identify the key amino acids involved in phosphate cluster binding would be to obtain a high resolution structure of 4p-PTEN by X-ray crystallography or NMR.

Conclusion

The uncompromised normal function of PTEN is essential for negatively regulating the PI3K/PTEN/AKT signaling pathway, thereby preventing carcinogenesis[3,18,37]. PTEN's importance as a tumor suppressor is demonstrated by its high frequency of mutation in many cancer types and cancer predisposition syndromes[35,53–55,57]. PTEN can be regulated by a variety of mechanisms within cells. One of these modes of regulation is through the phosphorylation of a cluster of serine and threonine residues on PTEN's C-terminal tail[109,110,129,131]. While the regulation of PTEN functions by phosphorylation has been the subject of several studies[109,110,129,131], the detailed mechanism by which phosphorylation regulates PTEN's activities has remained largely unknown. In this thesis work, we have employed expressed protein ligation to generate PTEN in its phosphorylated and unphosphorylated forms in order to get a better understanding of how phosphorylation regulates PTEN.

We find that PTEN's catalytic efficiency with respect to a soluble PIP_3 substrate is reduced about 7-fold for phosphorylated 4p-PTEN compared to unphosphorylated n-PTEN. The reduction in catalytic efficiency is due at least in part to an elevated K_m for 4p-PTEN compared to n-PTEN. Additionally the phosphorylated tail peptide is a potent (IC_{50} ~1 μM) inhibitor of C-terminally truncated t-PTEN *in trans* while the unphosphorylated tail peptide shows little to no inhibition at 10 μM. Taken together this suggests the phosphorylated tail is auto-inhibitory. An interfacial kinetic analysis of t-PTEN, n-PTEN and 4p-PTEN

reveals that all three enzyme forms have the same interfacial K_m (iK_m) while 4p-PTEN has a larger vesicle binding constant (K_s) than t-PTEN and n-PTEN, suggesting reduced binding affinity for phospholipid membranes. The differences in vesicle binding affinity calculated in the values of K_s were verified with the use of a vesicle sedimentation assay. Under all conditions tested 4p-PTEN demonstrated reduced binding affinity for phospholipid vesicles compared to n-PTEN. Additionally the phosphorylated tail peptide reduced the amount of t-PTEN that sedimented with phospholipid vesicles. Also of note, at low surface concentrations (<0.125%) of PIP_3 substrate within vesicle membranes, 4p-PTEN has reduced catalytic activity compared to n-PTEN. This is important because physiological levels of PIP_3 are thought to be less than 0.001%; therefore phosphorylated PTEN should have lower activity *in vivo* than its unphosphorylated form.

We have identified several lines of evidence to suggest that PTEN undergoes a conformational change when it is phosphorylated at its C-terminal tail. Serendipitously, we found that upon purification of n-PTEN and 4p-PTEN by anion exchange chromatography, 4p-PTEN elutes at an earlier elution volume compared to n-PTEN even though it possesses eight additional negative charges. This suggests that the phosphorylated tail is being concealed in an intramolecular binding event thereby preventing it from interacting with the positively charged anion exchange resin. Additional evidence to suggest that phosphorylation of PTEN induces a conformational change includes 4p-PTEN's

reduced susceptibility to trypsin proteolysis compared to n-PTEN and the fact that natively folded 4p-PTEN is more resistant to alkaline phosphatase removal of its tail phosphates than a denatured form of the protein.

Small angle X-ray scattering (SAXS) of t-PTEN, n-PTEN and 4p-PTEN revealed that 4p-PTEN is smaller and more compact compared to n-PTEN with reductions in both its radius of gyration (R_g) and maximum particle dimension (D_{max}). The molecular envelopes generated from the SAXS data suggests that the phosphorylated tail binds to the body of PTEN in the general vicinity of the membrane binding surface of the C2 domain. Mutation of five lysines of the membrane binding CBRIII loop of the C2 domain to aspartates at least partially prevents the phosphorylated tail from binding the main body of PTEN. This D5-mutant 4p-PTEN protein demonstrated more normal elution patterns on anion exchange chromatography where much of the phosphorylated D5-mutant elutes after the unphosphorylated D5-mutant. The D5 4p-PTEN mutant also shows increased sensitivity to alkaline phosphatase removal of its tail phosphates compared to wild type. Additionally, the D5-mutant possesses catalytic activity with soluble PIP_3 substrate comparable to n-PTEN with a significantly reduced K_m compared to wild type 4p-PTEN. Furthermore the C-terminally truncated D5-mutant is nearly completely resistant to 4p-25mer phosphopeptide inhibition of its catalytic activity.

Analysis of the D5-mutant along with the SAXS, vesicle binding and interfacial kinetic data of wild type 4p-PTEN suggests that the phosphorylated tail

exerts its auto-inhibitory effects by directly interacting with the membrane binding surfaces on the C2 domain of PTEN. This interaction prevents the C2 domain of 4p-PTEN from binding to membranes and accessing its substrate. The fact that n-PTEN and 4p-PTEN have similar iK_m for vesicle embedded PIP_3 substrate but different K_m values for soluble PIP_3 substrate suggests the two enzyme forms have similar conformations when bound to phospholipid membranes but different conformations in solution when acting on a soluble substrate. The solution conformations of the two enzymes are visualized in the SAXS generated molecular envelopes. This model of PTEN regulation by phosphorylation is shown in Figure 68. Here, when PTEN is not phosphorylated, it exists in a more "open" state where it can easily bind to the plasma membrane and act on its substrate. When PTEN is phosphorylated on its C-terminal tail at the S380/T382/T383/S385 phosphocluster it adopts a more compact "closed" conformation. In this compact conformation, the phosphorylated tail prevents PTEN from interacting with the plasma membrane by binding to the C2 domain in the general vicinity of the phospholipid binding CBRIII loop.

In conclusion, expressed protein ligation has allowed us to examine how PTEN is regulated by phosphorylation in a detailed manner that has not previously been possible. Using these newly developed tools for studying PTEN phosphorylation, we demonstrate unequivocally that phosphorylation leads to a conformational change and that this causes a reduction in PTEN's phospholipid membrane binding ability and catalytic activity. The utility of semisynthetic n-

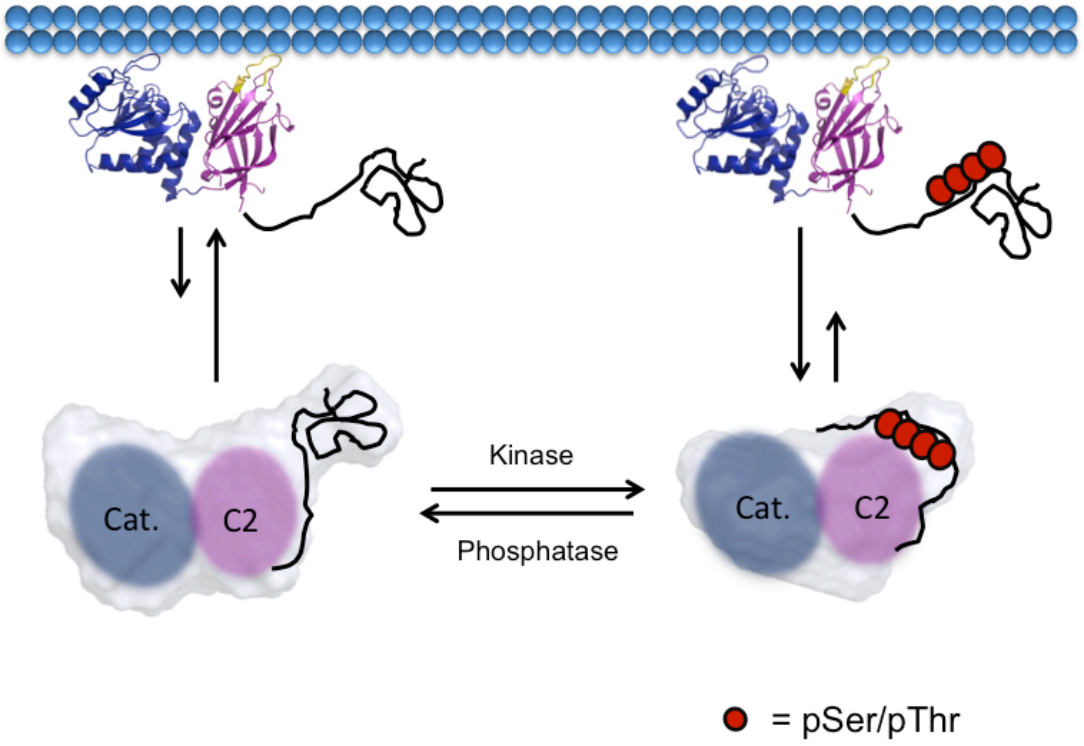

Figure 68: Model of PTEN regulation by phosphorylation. Upon phosphorylation, PTEN adopts a more compact conformation with the phosphorylated tail condensing around the CBRIII loop and membrane binding surface of the C2 domain, preventing it from binding to the plasma membrane. When dephosphorylated, the tail of PTEN is no longer bound tightly to the C2 domain, allowing for the open PTEN protein to bind efficiently to the plasma membrane. Both forms of PTEN are in the same open conformation when bound to the plasma membrane.

PTEN and 4p-PTEN to study PTEN phosphorylation is not limited to the examination of protein conformational changes, membrane binding and catalytic parameters. These tools can be used to examine other potential PTEN phosphorylation-dependent functions such as protein-protein interactions, ubiquitination, cellular localization and protein stability.

Bibliography

1. Alberts, B. *Molecular Biology of the Cell*. (Garland Science, 2002).
2. Berg, J. M. *Biochemistry*. (W.H. Freeman, 2002).
3. Fresno Vara, J. A. *et al.* PI3K/Akt signalling pathway and cancer. *Cancer Treat. Rev.* **30,** 193–204 (2004).
4. Weigel. Kinases and protein phosphorylation as regulators of steroid hormone action. *Nucl. Recept. Signal.* **4,** (2007).
5. *Protein phosphorylation*. (Academic Press, 1998).
6. Hardie, D. G. *Protein phosphorylation: a practical approach*. (Oxford University Press, 1999).
7. Blero, D., Payrastre, B., Schurmans, S. & Erneux, C. Phosphoinositide phosphatases in a network of signalling reactions. *Pflügers Arch. Eur. J. Physiol.* **455,** 31–44 (2007).
8. Alonso, A. *et al.* Protein tyrosine phosphatases in the human genome. *Cell* **117,** 699–711 (2004).
9. Brautigan, D. L. Protein Ser/Thr phosphatases--the ugly ducklings of cell signalling. *FEBS J.* **280,** 324–345 (2013).
10. Patterson, K. I., Brummer, T., O'Brien, P. M. & Daly, R. J. Dual-specificity phosphatases: critical regulators with diverse cellular targets. *Biochem. J.* **418,** 475–489 (2009).
11. Newman, R. H. *et al.* Construction of human activity-based phosphorylation networks. *Mol. Syst. Biol.* **9,** 655 (2013).
12. Hirsch, A. K. H., Fischer, F. R. & Diederich, F. Phosphate recognition in structural biology. *Angew. Chem. Int. Ed Engl.* **46,** 338–352 (2007).
13. Yaffe, M. B. & Smerdon, S. J. PhosphoSerine/threonine binding domains: you can't pSERious? *Struct. Lond. Engl. 1993* **9,** R33–38 (2001).
14. Yaffe, M. B. Phosphotyrosine-binding domains in signal transduction. *Nat. Rev. Mol. Cell Biol.* **3,** 177–186 (2002).
15. Yan, K. S., Kuti, M. & Zhou, M. M. PTB or not PTB -- that is the question. *FEBS Lett.* **513,** 67–70 (2002).
16. Sasaki, T. *et al.* Mammalian phosphoinositide kinases and phosphatases. *Prog. Lipid Res.* **48,** 307–343 (2009).
17. Martin-Belmonte, F. *et al.* PTEN-mediated apical segregation of phosphoinositides controls epithelial morphogenesis through Cdc42. *Cell* **128,** 383–397 (2007).

18. Carnero, A., Blanco-Aparicio, C., Renner, O., Link, W. & Leal, J. F. M. The PTEN/PI3K/AKT signalling pathway in cancer, therapeutic implications. *Curr. Cancer Drug Targets* **8,** 187–198 (2008).
19. Falasca, M. PI3K/Akt signalling pathway specific inhibitors: a novel strategy to sensitize cancer cells to anti-cancer drugs. *Curr. Pharm. Des.* **16,** 1410–1416 (2010).
20. LoPiccolo, J., Blumenthal, G. M., Bernstein, W. B. & Dennis, P. A. Targeting the PI3K/Akt/mTOR pathway: effective combinations and clinical considerations. *Drug Resist. Updat. Rev. Comment. Antimicrob. Anticancer Chemother.* **11,** 32–50 (2008).
21. Stambolic, V. *et al.* Negative regulation of PKB/Akt-dependent cell survival by the tumor suppressor PTEN. *Cell* **95,** 29–39 (1998).
22. Laplante, M. & Sabatini, D. M. mTOR Signaling. *Cold Spring Harb. Perspect. Biol.* **4,** (2012).
23. Zoncu, R., Efeyan, A. & Sabatini, D. M. mTOR: from growth signal integration to cancer, diabetes and ageing. *Nat. Rev. Mol. Cell Biol.* **12,** 21–35 (2011).
24. Zoncu, R., Efeyan, A. & Sabatini, D. M. mTOR: from growth signal integration to cancer, diabetes and ageing. *Nat. Rev. Mol. Cell Biol.* **12,** 21–35 (2011).
25. Wade, M., Li, Y.-C. & Wahl, G. M. MDM2, MDMX and p53 in oncogenesis and cancer therapy. *Nat. Rev. Cancer* **13,** 83–96 (2013).
26. Zhou, B. P. *et al.* HER-2/neu induces p53 ubiquitination via Akt-mediated MDM2 phosphorylation. *Nat. Cell Biol.* **3,** 973–982 (2001).
27. Liang, J. *et al.* PKB/Akt phosphorylates p27, impairs nuclear import of p27 and opposes p27-mediated G1 arrest. *Nat. Med.* **8,** 1153–1160 (2002).
28. Shin, I. *et al.* PKB/Akt mediates cell-cycle progression by phosphorylation of p27(Kip1) at threonine 157 and modulation of its cellular localization. *Nat. Med.* **8,** 1145–1152 (2002).
29. Rössig, L. *et al.* Akt-dependent phosphorylation of p21(Cip1) regulates PCNA binding and proliferation of endothelial cells. *Mol. Cell. Biol.* **21,** 5644–5657 (2001).
30. Harms, C. *et al.* Phosphatidylinositol 3-Akt-kinase-dependent phosphorylation of p21(Waf1/Cip1) as a novel mechanism of neuroprotection by glucocorticoids. *J. Neurosci.* **27,** 4562–4571 (2007).
31. Bouchard, C., Marquardt, J., Brás, A., Medema, R. H. & Eilers, M. Myc-induced proliferation and transformation require Akt-mediated phosphorylation of FoxO proteins. *EMBO J.* **23,** 2830–2840 (2004).
32. Zhang, X., Tang, N., Hadden, T. J. & Rishi, A. K. Akt, FoxO and regulation of apoptosis. *Biochim. Biophys. Acta* **1813,** 1978–1986 (2011).

33. Maehama, T. The Tumor Suppressor, PTEN/MMAC1, Dephosphorylates the Lipid Second Messenger, Phosphatidylinositol 3,4,5-Trisphosphate. *J. Biol. Chem.* **273,** 13375–13378 (1998).
34. Myers, M. P. *et al.* The lipid phosphatase activity of PTEN is critical for its tumor supressor function. *Proc. Natl. Acad. Sci.* **95,** 13513–13518 (1998).
35. Hollander, M. C., Blumenthal, G. M. & Dennis, P. A. PTEN loss in the continuum of common cancers, rare syndromes and mouse models. *Nat. Rev. Cancer* **11,** 289–301 (2011).
36. Steck, P. A. *et al.* Identification of a candidate tumour suppressor gene, MMAC1, at chromosome 10q23.3 that is mutated in multiple advanced cancers. *Nat. Genet.* **15,** 356–362 (1997).
37. Courtney, K. D., Corcoran, R. B. & Engelman, J. A. The PI3K pathway as drug target in human cancer. *J. Clin. Oncol. Off. J. Am. Soc. Clin. Oncol.* **28,** 1075–1083 (2010).
38. Jones, K. L. & Buzdar, A. U. Evolving novel anti-HER2 strategies. *Lancet Oncol.* **10,** 1179–1187 (2009).
39. Nahta, R. & O'Regan, R. M. Evolving strategies for overcoming resistance to HER2-directed therapy: targeting the PI3K/Akt/mTOR pathway. *Clin. Breast Cancer* **10 Suppl 3,** S72–78 (2010).
40. Koul, D. *et al.* Cellular and in vivo activity of a novel PI3K inhibitor, PX-866, against human glioblastoma. *Neuro-Oncol.* **12,** 559–569 (2010).
41. Le Cras, T. D. *et al.* Inhibition of PI3K by PX-866 prevents transforming growth factor-alpha-induced pulmonary fibrosis. *Am. J. Pathol.* **176,** 679–686 (2010).
42. Meadows, S. A. *et al.* PI3Kδ inhibitor, GS-1101 (CAL-101), attenuates pathway signaling, induces apoptosis, and overcomes signals from the microenvironment in cellular models of Hodgkin lymphoma. *Blood* **119,** 1897–1900 (2012).
43. Kuger, S. *et al.* Radiosensitization of Glioblastoma Cell Lines by the Dual PI3K and mTOR Inhibitor NVP-BEZ235 Depends on Drug-Irradiation Schedule. *Transl. Oncol.* **6,** 169–179 (2013).
44. Yang, F. *et al.* Dual phosphoinositide 3-kinase/mammalian target of rapamycin inhibitor NVP-BEZ235 has a therapeutic potential and sensitizes cisplatin in nasopharyngeal carcinoma. *PloS One* **8,** e59879 (2013).
45. Wallin, J. J. *et al.* GDC-0980 is a novel class I PI3K/mTOR kinase inhibitor with robust activity in cancer models driven by the PI3K pathway. *Mol. Cancer Ther.* **10,** 2426–2436 (2011).

46. Mallon, R. *et al.* Antitumor efficacy profile of PKI-402, a dual phosphatidylinositol 3-kinase/mammalian target of rapamycin inhibitor. *Mol. Cancer Ther.* **9,** 976–984 (2010).
47. Garlich, J. R. *et al.* A vascular targeted pan phosphoinositide 3-kinase inhibitor prodrug, SF1126, with antitumor and antiangiogenic activity. *Cancer Res.* **68,** 206–215 (2008).
48. Burke, T. R., Jr & Zhang, Z. Y. Protein-tyrosine phosphatases: structure, mechanism, and inhibitor discovery. *Biopolymers* **47,** 225–241 (1998).
49. Jemc, J. & Rebay, I. The eyes absent family of phosphotyrosine phosphatases: properties and roles in developmental regulation of transcription. *Annu. Rev. Biochem.* **76,** 513–538 (2007).
50. Whisstock, J. C., Wiradjaja, F., Waters, J. E. & Gurung, R. The structure and function of catalytic domains within inositol polyphosphate 5-phosphatases. *IUBMB Life* **53,** 15–23 (2002).
51. Lee, J.-O. *et al.* Crystal Structure of the PTEN Tumor Suppressor. *Cell* **99,** 323–334 (1999).
52. Li, J. PTEN, a Putative Protein Tyrosine Phosphatase Gene Mutated in Human Brain, Breast, and Prostate Cancer. *Science* **275,** 1943–1947 (1997).
53. Nelen, M. Germline mutations in the PTEN/MMAC1 gene in patients with Cowden disease. *Hum. Mol. Genet.* **6,** 1383–1387 (1997).
54. Zhou, X.-P. *et al.* Germline PTEN promoter mutations and deletions in Cowden/Bannayan-Riley-Ruvalcaba syndrome result in aberrant PTEN protein and dysregulation of the phosphoinositol-3-kinase/Akt pathway. *Am. J. Hum. Genet.* **73,** 404–411 (2003).
55. Suzuki, A. *et al.* High cancer susceptibility and embryonic lethality associated with mutation of the PTEN tumor suppressor gene in mice. *Curr. Biol.* **8,** 1169–1178 (1998).
56. Shen-Li, H., Koujak, S., Szablocs, M. & Parsons, R. Reduction of Pten dose leads to neoplastic development in multiple organs of Pten (shRNA) mice. *Cancer Biol. Ther.* **10,** 1194–1200 (2010).
57. Alimonti, A. *et al.* Subtle variations in Pten dose determine cancer susceptibility. *Nat. Genet.* **42,** 454–458 (2010).
58. Berger, A. H., Knudson, A. G. & Pandolfi, P. P. A continuum model for tumour suppression. *Nature* **476,** 163–169 (2011).
59. Fine, B. *et al.* Activation of the PI3K pathway in cancer through inhibition of PTEN by exchange factor P-REX2a. *Science* **325,** 1261–1265 (2009).
60. Shen, W. H. *et al.* Essential role for nuclear PTEN in maintaining chromosomal integrity. *Cell* **128,** 157–170 (2007).

61. Song, M. S. *et al.* Nuclear PTEN regulates the APC-CDH1 tumor-suppressive complex in a phosphatase-independent manner. *Cell* **144,** 187–199 (2011).
62. Trotman, L. C. *et al.* Ubiquitination regulates PTEN nuclear import and tumor suppression. *Cell* **128,** 141–156 (2007).
63. Salvesen, H. B. *et al.* PTEN methylation is associated with advanced stage and microsatellite instability in endometrial carcinoma. *Int. J. Cancer* **91,** 22–26 (2001).
64. Meng, F. *et al.* MicroRNA-21 Regulates Expression of the PTEN Tumor Suppressor Gene in Human Hepatocellular Cancer. *Gastroenterology* **133,** 647–658 (2007).
65. Escrivà, M. *et al.* Repression of PTEN phosphatase by Snail1 transcriptional factor during gamma radiation-induced apoptosis. *Mol. Cell. Biol.* **28,** 1528–1540 (2008).
66. Stambolic, V. *et al.* Regulation of PTEN transcription by p53. *Mol. Cell* **8,** 317–325 (2001).
67. Whelan, J. T., Forbes, S. L. & Bertrand, F. E. CBF-1 (RBP-J kappa) binds to the PTEN promoter and regulates PTEN gene expression. *Cell Cycle Georget. Tex* **6,** 80–84 (2007).
68. Stambolic, V. *et al.* High incidence of breast and endometrial neoplasia resembling human Cowden syndrome in pten+/- mice. *Cancer Res.* **60,** 3605–3611 (2000).
69. Singh, B., Ittmann, M. M. & Krolewski, J. J. Sporadic breast cancers exhibit loss of heterozygosity on chromosome segment 10q23 close to the Cowden disease locus. *Genes. Chromosomes Cancer* **21,** 166–171 (1998).
70. Saal, L. H. *et al.* Recurrent gross mutations of the PTEN tumor suppressor gene in breast cancers with deficient DSB repair. *Nat. Genet.* **40,** 102–107 (2008).
71. Pérez-Tenorio, G. *et al.* PIK3CA mutations and PTEN loss correlate with similar prognostic factors and are not mutually exclusive in breast cancer. *Clin. Cancer Res. Off. J. Am. Assoc. Cancer Res.* **13,** 3577–3584 (2007).
72. Maxwell, G. L. *et al.* Mutation of the PTEN tumor suppressor gene in endometrial hyperplasias. *Cancer Res.* **58,** 2500–2503 (1998).
73. Risinger, J. I., Hayes, A. K., Berchuck, A. & Barrett, J. C. PTEN/MMAC1 mutations in endometrial cancers. *Cancer Res.* **57,** 4736–4738 (1997).
74. Daikoku, T. *et al.* Conditional loss of uterine Pten unfailingly and rapidly induces endometrial cancer in mice. *Cancer Res.* **68,** 5619–5627 (2008).
75. Perren, A. *et al.* Mutation and expression analyses reveal differential subcellular compartmentalization of PTEN in endocrine pancreatic tumors compared to normal islet cells. *Am. J. Pathol.* **157,** 1097–1103 (2000).

76. Frisk, T. *et al.* Silencing of the PTEN tumor-suppressor gene in anaplastic thyroid cancer. *Genes. Chromosomes Cancer* **35,** 74–80 (2002).
77. Halachmi, N. *et al.* Somatic mutations of the PTEN tumor suppressor gene in sporadic follicular thyroid tumors. *Genes. Chromosomes Cancer* **23,** 239–243 (1998).
78. Puxeddu, E. *et al.* Characterization of novel non-clonal intrachromosomal rearrangements between the H4 and PTEN genes (H4/PTEN) in human thyroid cell lines and papillary thyroid cancer specimens. *Mutat. Res.* **570,** 17–32 (2005).
79. Abate-Shen, C. *et al.* Nkx3.1; Pten mutant mice develop invasive prostate adenocarcinoma and lymph node metastases. *Cancer Res.* **63,** 3886–3890 (2003).
80. Carver, B. S. *et al.* Aberrant ERG expression cooperates with loss of PTEN to promote cancer progression in the prostate. *Nat. Genet.* **41,** 619–624 (2009).
81. Kwabi-Addo, B. *et al.* Haploinsufficiency of the Pten tumor suppressor gene promotes prostate cancer progression. *Proc. Natl. Acad. Sci. U. S. A.* **98,** 11563–11568 (2001).
82. Wang, S. *et al.* Prostate-specific deletion of the murine Pten tumor suppressor gene leads to metastatic prostate cancer. *Cancer Cell* **4,** 209–221 (2003).
83. Bigner, S. H., Mark, J., Mahaley, M. S. & Bigner, D. D. Patterns of the early, gross chromosomal changes in malignant human gliomas. *Hereditas* **101,** 103–113 (1984).
84. Wei, Q. *et al.* High-grade glioma formation results from postnatal pten loss or mutant epidermal growth factor receptor expression in a transgenic mouse glioma model. *Cancer Res.* **66,** 7429–7437 (2006).
85. Lahtz, C., Stranzenbach, R., Fiedler, E., Helmbold, P. & Dammann, R. H. Methylation of PTEN as a prognostic factor in malignant melanoma of the skin. *J. Invest. Dermatol.* **130,** 620–622 (2010).
86. Mikhail, M. *et al.* PTEN expression in melanoma: relationship with patient survival, Bcl-2 expression, and proliferation. *Clin. Cancer Res.* **11,** 5153–5157 (2005).
87. Yanagi, S. *et al.* Pten controls lung morphogenesis, bronchioalveolar stem cells, and onset of lung adenocarcinomas in mice. *J. Clin. Invest.* **117,** 2929–2940 (2007).
88. Yokomizo, A. *et al.* PTEN/MMAC1 mutations identified in small cell, but not in non-small cell lung cancers. *Oncogene* **17,** 475–479 (1998).

89. Stiles, B. *et al.* Liver-specific deletion of negative regulator Pten results in fatty liver and insulin hypersensitivity [corrected]. *Proc. Natl. Acad. Sci. U. S. A.* **101,** 2082–2087 (2004).
90. Yao, Y. J. *et al.* PTEN/MMAC1 mutations in hepatocellular carcinomas. *Oncogene* **18,** 3181–3185 (1999).
91. Cairns, P. *et al.* Point mutation and homozygous deletion of PTEN/MMAC1 in primary bladder cancers. *Oncogene* **16,** 3215–3218 (1998).
92. Puzio-Kuter, A. M. *et al.* Inactivation of p53 and Pten promotes invasive bladder cancer. *Genes Dev.* **23,** 675–680 (2009).
93. Stiles, B. L. *et al.* Selective deletion of Pten in pancreatic beta cells leads to increased islet mass and resistance to STZ-induced diabetes. *Mol. Cell. Biol.* **26,** 2772–2781 (2006).
94. Myers, M. P. *et al.* P-TEN, the tumor suppressor from human chromosome 10q23, is a dual-specificity phosphatase. *Proc. Natl. Acad. Sci. U. S. A.* **94,** 9052–9057 (1997).
95. Iijima, M. & Devreotes, P. Tumor Suppressor PTEN Mediates Sensing of Chemoattractant Gradients. *Cell* **109,** 599–610 (2002).
96. Iijima, M. Novel Mechanism of PTEN Regulation by Its Phosphatidylinositol 4,5-Bisphosphate Binding Motif Is Critical for Chemotaxis. *J. Biol. Chem.* **279,** 16606–16613 (2004).
97. Campbell, R. B. Allosteric Activation of PTEN Phosphatase by Phosphatidylinositol 4,5-Bisphosphate. *J. Biol. Chem.* **278,** 33617–33620 (2003).
98. Denning, G., Jean-Joseph, B., Prince, C., Durden, D. L. & Vogt, P. K. A short N-terminal sequence of PTEN controls cytoplasmic localization and is required for suppression of cell growth. *Oncogene* **26,** 3930–3940 (2007).
99. Shenoy, S. *et al.* Membrane Association of the PTEN Tumor Suppressor: Molecular Details of the Protein-Membrane Complex from SPR Binding Studies and Neutron Reflection. *PLoS ONE* **7,** e32591 (2012).
100. Al-Khouri, A. M. Cooperative Phosphorylation of the Tumor Suppressor Phosphatase and Tensin Homologue (PTEN) by Casein Kinases and Glycogen Synthase Kinase 3. *J. Biol. Chem.* **280,** 35195–35202 (2005).
101. Miller, S. J., Lou, D. Y., Seldin, D. C., Lane, W. S. & Neel, B. G. Direct identification of PTEN phosphorylation sites. *FEBS Lett.* **528,** 145–153 (2002).
102. García, J. M. *et al.* Promoter methylation of the PTEN gene is a common molecular change in breast cancer. *Genes. Chromosomes Cancer* **41,** 117–124 (2004).

103. Goel, A. *et al.* Frequent inactivation of PTEN by promoter hypermethylation in microsatellite instability-high sporadic colorectal cancers. *Cancer Res.* **64,** 3014–3021 (2004).
104. Khan, S. *et al.* PTEN promoter is methylated in a proportion of invasive breast cancers. *Int. J. Cancer J. Int. Cancer* **112,** 407–410 (2004).
105. Lu, J. *et al.* Stem cell factor SALL4 represses the transcriptions of PTEN and SALL1 through an epigenetic repressor complex. *PloS One* **4,** e5577 (2009).
106. Hettinger, K. *et al.* c-Jun promotes cellular survival by suppression of PTEN. *Cell Death Differ.* **14,** 218–229 (2007).
107. Wang, Q., Zhou, Y., Wang, X., Chung, D. H. & Evers, B. M. Regulation of PTEN expression in intestinal epithelial cells by c-Jun NH2-terminal kinase activation and nuclear factor-kappaB inhibition. *Cancer Res.* **67,** 7773–7781 (2007).
108. Cordier, F. *et al.* Ordered Phosphorylation Events in Two Independent Cascades of the PTEN C-tail Revealed by NMR. *J. Am. Chem. Soc.* **134,** 20533–20543 (2012).
109. Rahdar, M. *et al.* A phosphorylation-dependent intramolecular interaction regulates the membrane association and activity of the tumor suppressor PTEN. *Proc. Natl. Acad. Sci.* **106,** 480–485 (2008).
110. Vazquez, F. Phosphorylation of the PTEN Tail Acts as an Inhibitory Switch by Preventing Its Recruitment into a Protein Complex. *J. Biol. Chem.* **276,** 48627–48630 (2001).
111. Okumura, K. PCAF Modulates PTEN Activity. *J. Biol. Chem.* **281,** 26562–26568 (2006).
112. Huang, J. *et al.* SUMO1 modification of PTEN regulates tumorigenesis by controlling its association with the plasma membrane. *Nat. Commun.* **3,** 911 (2012).
113. Wang, X. *et al.* NEDD4-1 Is a Proto-Oncogenic Ubiquitin Ligase for PTEN. *Cell* **128,** 129–139 (2007).
114. Drinjakovic, J. *et al.* E3 ligase Nedd4 promotes axon branching by downregulating PTEN. *Neuron* **65,** 341–357 (2010).
115. Fouladkou, F. *et al.* The ubiquitin ligase Nedd4-1 is dispensable for the regulation of PTEN stability and localization. *Proc. Natl. Acad. Sci. U. S. A.* **105,** 8585–8590 (2008).
116. Maddika, S. *et al.* WWP2 is an E3 ubiquitin ligase for PTEN. *Nat. Cell Biol.* **13,** 728–733 (2011).

117. Van Themsche, C., Leblanc, V., Parent, S. & Asselin, E. X-linked inhibitor of apoptosis protein (XIAP) regulates PTEN ubiquitination, content, and compartmentalization. *J. Biol. Chem.* **284,** 20462–20466 (2009).
118. Lee, S.-R. *et al.* Reversible inactivation of the tumor suppressor PTEN by H2O2. *J. Biol. Chem.* **277,** 20336–20342 (2002).
119. McConnachie, G., Pass, I., Walker, S. M. & Downes, C. P. Interfacial kinetic analysis of the tumour suppressor phosphatase, PTEN: evidence for activation by anionic phospholipids. *Biochem. J.* **371,** 947–955 (2003).
120. Anderson, D. H. p85 plays a critical role in controlling flux through the PI3K/PTEN signaling axis through dual regulation of both p110 (PI3K) and PTEN. *Cell Cycle* **9,** 2055–2056 (2010).
121. Barber, D. F., Alvarado-Kristensson, M., González-García, A., Pulido, R. & Carrera, A. C. PTEN regulation, a novel function for the p85 subunit of phosphoinositide 3-kinase. *Sci. STKE Signal Transduct. Knowl. Environ.* **2006,** pe49 (2006).
122. Chagpar, R. B. *et al.* Direct positive regulation of PTEN by the p85 subunit of phosphatidylinositol 3-kinase. *Proc. Natl. Acad. Sci.* **107,** 5471–5476 (2010).
123. Sumitomo, M. *et al.* Synergy in tumor suppression by direct interaction of Neutral Endopeptidase with PTEN. *Cancer Cell* **5,** 67–78 (2004).
124. Van Diepen, M. T. *et al.* MyosinV controls PTEN function and neuronal cell size. *Nat. Cell Biol.* **11,** 1191–1196 (2009).
125. Wu, X. *et al.* Evidence for regulation of the PTEN tumor suppressor by a membrane-localized multi-PDZ domain containing scaffold protein MAGI-2. *Proc. Natl. Acad. Sci.* **97,** 4233–4238 (2000).
126. Vemula, S., Shi, J., Hanneman, P., Wei, L. & Kapur, R. ROCK1 functions as a suppressor of inflammatory cell migration by regulating PTEN phosphorylation and stability. *Blood* **115,** 1785–1796 (2010).
127. Li, Z. *et al.* Regulation of PTEN by Rho small GTPases. *Nat. Cell Biol.* **7,** 399–404 (2005).
128. Yim, E.-K. *et al.* Rak functions as a tumor suppressor by regulating PTEN protein stability and function. *Cancer Cell* **15,** 304–314 (2009).
129. Vazquez, F., Ramaswamy, S., Nakamura, N. & Sellers, W. R. Phosphorylation of the PTEN Tail Regulates Protein Stability and Function. *Mol. Cell. Biol.* **20,** 5010–5018 (2000).
130. Maccario, H., Perera, N. M., Davidson, L., Downes, C. P. & Leslie, N. R. PTEN is destabilized by phosphorylation on Thr366. *Biochem. J.* **405,** 439–444 (2007).

131. Torres, J. The Tumor Suppressor PTEN Is Phosphorylated by the Protein Kinase CK2 at Its C Terminus. Implications for PTEN stability to proteasome-mediated degradation. *J. Biol. Chem.* **276,** 993–998 (2000).
132. Moult, P. R. *et al.* Leptin regulates AMPA receptor trafficking via PTEN inhibition. *J. Neurosci.* **30,** 4088–4101 (2010).
133. Ning, K. *et al.* Leptin-dependent phosphorylation of PTEN mediates actin restructuring and activation of ATP-sensitive K+ channels. *J. Biol. Chem.* **284,** 9331–9340 (2009).
134. Ning, K. *et al.* A novel leptin signalling pathway via PTEN inhibition in hypothalamic cell lines and pancreatic beta-cells. *EMBO J.* **25,** 2377–2387 (2006).
135. Zhang, X. C., Piccini, A., Myers, M. P., Van Aelst, L. & Tonks, N. K. Functional analysis of the protein phosphatase activity of PTEN. *Biochem. J.* **444,** 457–464 (2012).
136. Rabinovsky, R. *et al.* p85 Associates with unphosphorylated PTEN and the PTEN-associated complex. *Mol. Cell. Biol.* **29,** 5377–5388 (2009).
137. Odriozola, L., Singh, G., Hoang, T. & Chan, A. M. Regulation of PTEN Activity by Its Carboxyl-terminal Autoinhibitory Domain. *J. Biol. Chem.* **282,** 23306–23315 (2007).
138. Raftopoulou, M., Etienne-Manneville, S., Self, A., Nicholls, S. & Hall, A. Regulation of cell migration by the C2 domain of the tumor suppressor PTEN. *Science* **303,** 1179–1181 (2004).
139. Tamura, M. *et al.* Inhibition of cell migration, spreading, and focal adhesions by tumor suppressor PTEN. *Science* **280,** 1614–1617 (1998).
140. Tamura, M., Gu, J., Takino, T. & Yamada, K. M. Tumor suppressor PTEN inhibition of cell invasion, migration, and growth: differential involvement of focal adhesion kinase and p130Cas. *Cancer Res.* **59,** 442–449 (1999).
141. Muir, T. W., Sondhi, D. & Cole, P. A. Expressed protein ligation: a general method for protein engineering. *Proc. Natl. Acad. Sci. U. S. A.* **95,** 6705–6710 (1998).
142. Elleuche, S. & Pöggeler, S. Inteins, valuable genetic elements in molecular biology and biotechnology. *Appl. Microbiol. Biotechnol.* **87,** 479–489 (2010).
143. Ghosh, I. *et al.* Site-specific protein labeling by intein-mediated protein ligation. *Methods Mol. Biol. Clifton NJ* **705,** 87–107 (2011).
144. Ludwig, C. *et al.* Semisynthesis of proteins using split inteins. *Methods Enzymol.* **462,** 77–96 (2009).
145. Clark, K. M., van der Donk, W. A. & Lu, Y. Expressed protein ligation for metalloprotein design and engineering. *Methods Enzymol.* **462,** 97–115 (2009).

146. Schwarzer, D. & Cole, P. A. Protein semisynthesis and expressed protein ligation: chasing a protein's tail. *Curr. Opin. Chem. Biol.* **9,** 561–569 (2005).
147. Raghavan, R. & Minnick, M. F. Group I introns and inteins: disparate origins but convergent parasitic strategies. *J. Bacteriol.* **191,** 6193–6202 (2009).
148. Berg, O. G. *Interfacial enzyme kinetics*. (John Wiley & Sons, 2002).
149. Huang, C.-H., Mandelker, D., Gabelli, S. B. & Amzel, L. M. Insights into the oncogenic effects of PIK3CA mutations from the structure of p110alpha/p85alpha. *Cell Cycle* **7,** 1151–1156 (2008).
150. Kurumbail, R. G., Kiefer, J. R. & Marnett, L. J. Cyclooxygenase enzymes: catalysis and inhibition. *Curr. Opin. Struct. Biol.* **11,** 752–760 (2001).
151. Picot, D., Loll, P. J. & Garavito, R. M. The X-ray crystal structure of the membrane protein prostaglandin H2 synthase-1. *Nature* **367,** 243–249 (1994).
152. Ananthanarayanan, B. Membrane Targeting of C2 Domains of Phospholipase C-delta Isoforms. *J. Biol. Chem.* **277,** 3568–3575 (2001).
153. Singh, S. M. & Murray, D. Molecular modeling of the membrane targeting of phospholipase C pleckstrin homology domains. *Protein Sci.* **12,** 1934–1953 (2003).
154. Deems, R. A., Eaton, B. R. & Dennis, E. A. Kinetic analysis of phospholipase A2 activity toward mixed micelles and its implications for the study of lipolytic enzymes. *J. Biol. Chem.* **250,** 9013–9020 (1975).
155. Carman, G. M., Deems, R. A. & Dennis, E. A. Lipid signaling enzymes and surface dilution kinetics. *J. Biol. Chem.* **270,** 18711–18714 (1995).
156. Deems, R. A. & Dennis, E. A. Characterization and physical properties of the major form of phospholipase A2 from cobra venom (Naja naja naja) that has a molecular weight of 11,000. *J. Biol. Chem.* **250,** 9008–9012 (1975).
157. Roberts, M. F., Deems, R. A. & Dennis, E. A. Dual role of interfacial phospholipid in phospholipase A2 catalysis. *Proc. Natl. Acad. Sci. U. S. A.* **74,** 1950–1954 (1977).
158. Lin, Y. P. & Carman, G. M. Kinetic analysis of yeast phosphatidate phosphatase toward Triton X-100/phosphatidate mixed micelles. *J. Biol. Chem.* **265,** 166–170 (1990).
159. Hendrickson, H. S. & Dennis, E. A. Analysis of the kinetics of phospholipid activation of cobra venom phospholipase A2. *J. Biol. Chem.* **259,** 5740–5744 (1984).
160. Akbarzadeh, A. *et al.* Liposome: classification, preparation, and applications. *Nanoscale Res. Lett.* **8,** 102 (2013).
161. Allen, T. M. Liposomes. Opportunities in drug delivery. *Drugs* **54 Suppl 4,** 8–14 (1997).

162. Bernadó, P. & Svergun, D. I. Analysis of intrinsically disordered proteins by small-angle X-ray scattering. *Methods Mol. Biol. Clifton NJ* **896,** 107–122 (2012).
163. Mertens, H. D. T. & Svergun, D. I. Structural characterization of proteins and complexes using small-angle X-ray solution scattering. *J. Struct. Biol.* **172,** 128–141 (2010).
164. Blanchet, C. E. & Svergun, D. I. Small-angle X-ray scattering on biological macromolecules and nanocomposites in solution. *Annu. Rev. Phys. Chem.* **64,** 37–54 (2013).
165. Rambo, R. P. & Tainer, J. A. Bridging the solution divide: comprehensive structural analyses of dynamic RNA, DNA, and protein assemblies by small-angle X-ray scattering. *Curr. Opin. Struct. Biol.* **20,** 128–137 (2010).
166. Tsutakawa, S. E. *et al.* Solution X-ray scattering combined with computational modeling reveals multiple conformations of covalently bound ubiquitin on PCNA. *Proc. Natl. Acad. Sci. U. S. A.* **108,** 17672–17677 (2011).
167. Jacques, D. A. & Trewhella, J. Small-angle scattering for structural biology--expanding the frontier while avoiding the pitfalls. *Protein Sci.* **19,** 642–657 (2010).
168. Hura, G. L. *et al.* Robust, high-throughput solution structural analyses by small angle X-ray scattering (SAXS). *Nat. Methods* **6,** 606–612 (2009).
169. Jacques, D. A., Guss, J. M., Svergun, D. I. & Trewhella, J. Publication guidelines for structural modelling of small-angle scattering data from biomolecules in solution. *Acta Crystallogr. D Biol. Crystallogr.* **68,** 620–626 (2012).
170. Franke, D. & Svergun, D. I. *DAMMIF* , a program for rapid *ab-initio* shape determination in small-angle scattering. *J. Appl. Crystallogr.* **42,** 342–346 (2009).
171. Konarev, P. V., Volkov, V. V., Sokolova, A. V., Koch, M. H. J. & Svergun, D. I. *PRIMUS* : a Windows PC-based system for small-angle scattering data analysis. *J. Appl. Crystallogr.* **36,** 1277–1282 (2003).
172. Svergun, D. I. Determination of the regularization parameter in indirect-transform methods using perceptual criteria. *J. Appl. Crystallogr.* **25,** 495–503 (1992).
173. Volkov, V. V. & Svergun, D. I. Uniqueness of *ab initio* shape determination in small-angle scattering. *J. Appl. Crystallogr.* **36,** 860–864 (2003).
174. Cotter, L. *et al.* Dlg1-PTEN interaction regulates myelin thickness to prevent damaging peripheral nerve overmyelination. *Science* **328,** 1415–1418 (2010).
175. Das, S., Dixon, J. E. & Cho, W. Membrane-binding and activation mechanism of PTEN. *Proc. Natl. Acad. Sci. U. S. A.* **100,** 7491–7496 (2003).

176. Bodanszky, M. *Principles of peptide synthesis*. (Springer-Verlag, 1993).
177. Gutte, B. *Peptides synthesis, structures, and applications*. (Academic Press, 1995). at <http://site.ebrary.com/id/10254663>
178. Howl, J. *Peptide synthesis and applications*. (Humana Press, 2005).
179. Stawikowski, M. & Fields, G. B. Introduction to peptide synthesis. *Curr. Protoc. Protein Sci. Editor. Board John E Coligan Al* **Chapter 18,** Unit 18.1 (2012).
180. Chong, S. *et al.* Single-column purification of free recombinant proteins using a self-cleavable affinity tag derived from a protein splicing element. *Gene* **192,** 271–281 (1997).
181. Southworth, M. W., Amaya, K., Evans, T. C., Xu, M. Q. & Perler, F. B. Purification of proteins fused to either the amino or carboxy terminus of the Mycobacterium xenopi gyrase A intein. *BioTechniques* **27,** 110–114, 116, 118–120 (1999).
182. King, L. A. *The baculovirus expression system: a laboratory guide*. (Chapman & Hall, 1992).
183. Gropengiesser, J., Varadarajan, B. T., Stephanowitz, H. & Krause, E. The relative influence of phosphorylation and methylation on responsiveness of peptides to MALDI and ESI mass spectrometry. *J. Mass Spectrom.* **44,** 821–831 (2009).
184. Klemm, C. *et al.* Evaluation of the titanium dioxide approach for MS analysis of phosphopeptides. *J. Mass Spectrom.* **41,** 1623–1632 (2006).
185. Zhu, X. & Papayannopoulos, I. A. Improvement in the detection of low concentration protein digests on a MALDI TOF/TOF workstation by reducing alpha-cyano-4-hydroxycinnamic acid adduct ions. *J. Biomol. Tech.* **14,** 298–307 (2003).
186. Myasein, K. T. *Methods for peptide analysis of sub-microliter biological samples using.* (Proquest, Umi Dissertatio, 2011).
187. Carter, S. G. & Karl, D. W. Inorganic phosphate assay with malachite green: An improvement and evaluation. *J. Biochem. Biophys. Methods* **7,** 7–13 (1982).
188. Geladopoulos, T. P., Sotiroudis, T. G. & Evangelopoulos, A. E. A malachite green colorimetric assay for protein phosphatase activity. *Anal. Biochem.* **192,** 112–116 (1991).
189. Ikenoue, T., Inoki, K., Zhao, B. & Guan, K.-L. PTEN acetylation modulates its interaction with PDZ domain. *Cancer Res.* **68,** 6908–6912 (2008).
190. Besenicar, M., Macek, P., Lakey, J. H. & Anderluh, G. Surface plasmon resonance in protein-membrane interactions. *Chem. Phys. Lipids* **141,** 169–178 (2006).

191. Besenicar, M. P. & Anderluh, G. Preparation of lipid membrane surfaces for molecular interaction studies by surface plasmon resonance biosensors. *Methods Mol. Biol. Clifton NJ* **627,** 191–200 (2010).
192. Dufourcq, J. & Faucon, J.-F. Intrinsic fluorescence study of lipid-protein interactions in membrane models. Binding of melittin, an amphipathic peptide, to phospholipid vesicles. *Biochim. Biophys. Acta BBA - Biomembr.* **467,** 1–11 (1977).
193. Van Paridon, P. A., Visser, A. J. W. G. & Wirtz, K. W. A. Binding of phospholipids to the phosphatidylinositol transfer protein from bovine brain as studied by steady-state and time-resolved fluorescence spectroscopy. *Biochim. Biophys. Acta BBA - Biomembr.* **898,** 172–180 (1987).
194. Sabatino, P., Choudhury, R. P., Schönhoff, M., Van der Meeren, P. & Martins, J. C. NMR investigation of exchange dynamics and binding of phenol and phenolate in DODAC vesicular dispersions. *J. Phys. Chem. B* **116,** 9269–9276 (2012).
195. Sommer, L. A. M., Schaad, M. & Dames, S. A. NMR- and CD-Monitored Lipid-Binding Studies Suggest a General Role for the FATC Domain as Membrane Anchor of Phosphatidyl-Inositol-3 Kinase-Related Kinases (PIKKs). *J. Biol. Chem.* (2013).
196. Vazquez, F. Tumor suppressor PTEN acts through dynamic interaction with the plasma membrane. *Proc. Natl. Acad. Sci.* **103,** 3633–3638 (2006).
197. Bligh, E. G. & Dyer, W. J. A rapid method of total lipid extraction and purification. *Biochem. Cell Biol.* **37,** 911–917 (1959).
198. Gao, X. *et al.* PI3K/Akt signaling requires spatial compartmentalization in plasma membrane microdomains. *Proc. Natl. Acad. Sci. U. S. A.* **108,** 14509–14514 (2011).
199. Plant, P. J. The C2 Domain of the Ubiquitin Protein Ligase Nedd4 Mediates Ca2+-dependent Plasma Membrane Localization. *J. Biol. Chem.* **272,** 32329–32336 (1997).
200. Wang, J. *et al.* Calcium activates Nedd4 E3 ubiquitin ligases by releasing the C2 domain-mediated auto-inhibition. *J. Biol. Chem.* **285,** 12279–12288 (2010).
201. Plant, P. J. Apical Membrane Targeting of Nedd4 Is Mediated by an Association of Its C2 Domain with Annexin XIIIb. *J. Cell Biol.* **149,** 1473–1484 (2000).
202. Fine, B. *et al.* Activation of the PI3K pathway in cancer through inhibition of PTEN by exchange factor P-REX2a. *Science* **325,** 1261–1265 (2009).
203. Leslie, N. R. P-REX2a driving tumorigenesis by PTEN inhibition. *Sci. Signal.* **2,** pe68 (2009).

204. Sicheri, F., Moarefi, I. & Kuriyan, J. Crystal structure of the Src family tyrosine kinase Hck. *Nature* **385,** 602–609 (1997).
205. Xu, W., Harrison, S. C. & Eck, M. J. Three-dimensional structure of the tyrosine kinase c-Src. *Nature* **385,** 595–602 (1997).
206. Wang, D. Substrate Conformational Restriction and CD45-catalyzed Dephosphorylation of Tail Tyrosine-phosphorylated Src Protein. *J. Biol. Chem.* **277,** 40428–40433 (2002).
207. Rosen, M. K. *et al.* Direct demonstration of an intramolecular SH2—phosphotyrosine interaction in the Crk protein. *Nature* **374,** 477–479 (1995).
208. Lu, W., Gong, D., Bar-Sagi, D. & Cole, P. A. Site-Specific Incorporation of a Phosphotyrosine Mimetic Reveals a Role for Tyrosine Phosphorylation of SHP-2 in Cell Signaling. *Mol. Cell* **8,** 759–769 (2001).
209. Zhang, Z. The Role of C-terminal Tyrosine Phosphorylation in the Regulation of SHP-1 Explored via Expressed Protein Ligation. *J. Biol. Chem.* **278,** 4668–4674 (2002).
210. Edman, P., Högfeldt, E., Sillén, L. G. & Kinell, P.-O. Method for Determination of the Amino Acid Sequence in Peptides. *Acta Chem. Scand.* **4,** 283–293 (1950).
211. Edman, P. & Begg, G. A protein sequenator. *Eur. J. Biochem. FEBS* **1,** 80–91 (1967).
212. Allaire, M. & Yang, L. Biomolecular solution X-ray scattering at the National Synchrotron Light Source. *J. Synchrotron Radiat.* **18,** 41–44 (2010).
213. The PyMOL Molecular Graphics System, Version 1.5.0.4 Schrodinger, LLC.
214. Chung, W. K. *et al.* Investigation of protein binding affinity and preferred orientations in ion exchange systems using a homologous protein library. *Biotechnol. Bioeng.* **102,** 869–881 (2009).
215. Hou, Y., Hansen, T. B., Staby, A. & Cramer, S. M. Effects of urea induced protein conformational changes on ion exchange chromatographic behavior. *J. Chromatogr. A* **1217,** 7393–7400 (2010).
216. Coulter-Mackie, M. B. & Lian, Q. Partial trypsin digestion as an indicator of mis-folding of mutant alanine:glyoxylate aminotransferase and chaperone effects of specific ligands. Study of a spectrum of missense mutants. *Mol. Genet. Metab.* **94,** 368–374 (2008).
217. Malkin, L. I. & Rich, A. Partial resistance of nascent polypeptide chains to proteolytic digestion due to ribosomal shielding. *J. Mol. Biol.* **26,** 329–346 (1967).
218. Schumann, J., Richter, M. L. & McCarty, R. E. Partial proteolysis as a probe of the conformation of the gamma subunit in activated soluble and membrane-bound chloroplast coupling factor 1. *J. Biol. Chem.* **260,** 11817–11823 (1985).

Curriculum Vitae

David M Bolduc
715 N. Charles St. Baltimore, MD 21201
dbolduc1@jhmi.edu

Education

Johns Hopkins University, Baltimore MD **June 2008 – September 2013**

Doctor of Philosophy (candidate): Pharmacology and Molecular Sciences
Advisor: Dr. Phil Cole, MD PhD
Dissertation: *The Phosphorylation Induced Conformational Changes of PTEN Revealed by Protein Semisynthesis*

University of Connecticut, Storrs CT **August 2004 – May 2008**

Bachelor of Science: *Major:* Chemistry, *Minor:* Molecular and Cellular Biology
Magna Cum Laude

Research Experience

Johns Hopkins University, Graduate Student **June 2008 – September 2013**

- **Project Goal**: Gain a detailed mechanistic understanding of how phosphorylation modulates the tumor suppressor PTEN's structure and function.
- Utilized expressed protein ligation, a method of protein engineering, to generate semisynthetic PTEN with different posttranslational modifications.
- Developed assays to characterize the enzymatic activity of semisynthetic PTEN proteins with vesicle embedded lipid substrate as well as water soluble substrates.
- Developed vesicle based binding assays to examine PTEN binding ability modulated by posttranslational modifications.
- Developed a strategy using a variety of biochemical and biophysical techniques to characterize the protein conformational changes of PTEN induced by posttranslational modifications.

- **Additional Projects**

- Assay development for a high-through put screen to identify potential PTEN activators.
- Developed a cell based assay to study the applicability of kinase inhibitors for modulating PTEN phosphorylation levels and subsequently its cellular activity.
- Developed enzymatic assays and fluorescent based binding assays to characterized cancer derived mutant forms of PI3-Kinase.
- Elucidated the mechanism of PTEN regulation by p85, the regulatory subunit of PI3-Kinase, using enzymatic and binding assays.
- Engineered semisynthetic CTP Synthase to study its posttranslational regulation.

- Developed an improved, hybrid method of protein engineering utilizing subtiligase in conjunction with inteins as a tool for protein semisynthesis.

University of Connecticut, Research Assistant **September 2005 – May 2008**

- Synthesized several natural products including the anti-cancer drug pancratistatin and analogs of lipid ceramides involved in the pathogenesis of gingivitis.

Loctite®, Division of Henkel Corp, Intern **May 2007 – August 2007**

- Synthesized compounds to be used as catalysts for the polymerization of anaerobic glues.

Skills and Techniques

- Protein expression (*E. coli*, Baculovirus/insect cells)
- Protein purification (affinity column, HPLC, FPLC – anion/cation exchange, gel filtration, HIC)
- Enzymatic assay development applicable to HTS (radioactive endpoint, continuous spectrophotometric, fluorescent, colorimetric, direct and enzyme coupled assays)
- Experienced in steady-state enzyme kinetics and subsequent application to enzyme, ligand and inhibitor characterization (determination of steady state constants: K_m, K_d, K_i, k_{cat}, IC_{50})
- Enzymatic characterization of interfacial enzymes as well as enzymes following standard Michaelis-Menten kinetics
- Mammalian cell culture (drug treatment, transfection, western blot analysis, immunoprecipitation)
- Molecular biology techniques (PCR, sub-cloning techniques, mutagenesis, sequencing analysis, transfection)
- Western blot, SDS-PAGE, native gel
- Binding assays (vesicle and lipid binding, fluorescence quenching, immunoprecipitation)
- *Fluorimetry*
- UV-Vis spectroscopy
- Peptide synthesis and purification (HPLC)
- Protein engineering (expressed protein ligation, native chemical ligation, protein labeling/tagging)
- Mass spectrometry (MALDI-TOF, ESI)
- Lipid and vesicle handling, formulation and purification
- Small angle X-ray scattering (SAXS)
- Crystallography

Mentoring Experience

- Supervised six graduate and undergraduate students, often concurrently, demonstrating the ability to multitask, manage a small group and focus on key technical details of multiple projects simultaneously.
- Trained graduate students and postdocs in areas of technical expertise.
- Graduate student tutor employed by the Department of Pharmacology.
- Volunteer tutor for city high school students.

Publications

Bolduc D, Rahdar M, Tu-Sekine B, Sivakumarin SC, Raben DM, Amzel LM, Devreotes PN, Gabelli SB and Cole PA. (2013). Phosphorylation-mediated PTEN conformational closure and deactivation revealed by protein semisynthesis. *eLIFE.* 2013;2:e00691 Doi:10.7554/elife.00691

Bolduc D, Brower E, Tu-Sekine B, Devreotes PN, Vogelstein B, Raben DM, Amzel LM, Gabelli SB and Cole PA. Biochemical analysis of the PTEN – p85 interaction. *In preparation*

Miller M, Schmidt-Kittler O, **Bolduc D**, Amzel LM, Gabelli SB. Structural basis of PIP_2 binding to lipid kinases. *In preparation*

Professional Awards

Granquist Scholarship Recipient (2008)
Anti-Cancer Drug Development Fellow (2008-present)
Schienberg Travel Award Recipient (2011)

References

Dr. Phil Cole
Professor, Director of the Department of Pharmacology and Molecular Sciences
Johns Hopkins University
410-614-8849
pcole@jhmi.edu

Dr. L. Mario Amzel
Professor, Director of the Department of Biophysics and Biophysical Chemistry
Johns Hopkins University
410-955-3955
mamzel@jhmi.edu

Dr. Peter Devreotes
Professor, Director of the Department of Cell Biology
Johns Hopkins University
410-955-3225
pnd@jhmi.edu

Dr. Sandra Gabelli
Assistant Professor, Department of Biophysics and Biophysical Chemistry
Johns Hopkins University
410-614-4145
gabelli@jhmi.edu